MEASUREMENT AND MODELLING OF BUBBLE SIZE IN FLOTATION FROTHS

Eric Mukendi Tshibwabwa

MSc Eng (Wits)

A thesis submitted to the Faculty of Engineering and the Built Environment, University of the Witwatersrand, Johannesburg, in fulfilment of the requirements for the degree of Master of Science in Engineering

Johannesburg, August 2018

Declaration

I declare that this thesis is my own, unaided work. It is being submitted for the Degree of Masters of Science to the University of the Witwatersrand, Johannesburg. It has not been submitted before for any degree or examination in any other University.

Eric Mukendi Tshibwabwa

………… day of ……………………………. year ……………..

Synopsis

The flotation process is widely used for upgrading valuable minerals in the field of mining. Many diverse minerals, including most of the world's base and precious metals are processed by flotation process. Most valuable products produced by flotation pass through the froth phase of the flotation process. The froth phase has attracted more research in recent times because of its significant role in determining the mineral grade and recovery achieved from a flotation operation. The complex processes that occur in the froth phase – detachment, re-attachment, coalescence of bubbles, and competition for attachment sites, mixing and transport all combine to affect the net transfer of mineral particles into the concentrate.

Bubbles are formed at different sizes in the pulp phase and coalesce at different rates and as a result the bubble size distribution varies from point to point in the froth phase. Substantial coalescence gives rise to loss of bubble surface area and hence loss of recovery. Competition for attachment sites gives rise to an increase in grade.

No method for measuring the variation of froth bubble size distribution (FBSD) was available until Bhondayi and Moys developed one. The method measures the intrabubble impact distance in the froth using a probe dropped at known height through the froth. The average of these intra bubble impacts was considered to be a proxy for froth bubble size distribution; this was calibrated using FBSD. However the measured in the laboratory using photographs taken through the transparent wall of a laboratory cell. A 31 % of error was found and compared to the photographic method, which indicated that the technique over-estimates the actual froth bubble size distributions. This is due to the use of an average IID (proxy) as an estimate of the bubble.

In response to the known of actual froth bubble size distribution FBSD in order to quantify the complex processes in the froth phase, an application of a stereological technique/model was developed and tested to obtain estimates of the actual froth bubble size distribution FBSD in lab flotation and Mintek pilot rougher cells as a function of froth height, frother dosage and superficial gas velocity. The model was first validated for a system of flotation with variable froth height in a transparent Wits lab flotation cell. The two-parameter normal distribution model FBSD was considered to fit the model-predicted intrabubble impact distance distribution IIDDs to measured intrabubble impact distance distribution IIDDs. The model was seen to accurately

predict the FBSD compared to actual FBSD data obtained from above-mentioned conventional photographic method using a calibration scale attached to the transparent flotation cell wall, wherein the experimental IIDDs were accurately fitted by the model-predicted IIDDs. Similar estimation of froth bubble size distribution were also found with the inversion matrix technique. Secondly, the model was then evaluated for flotation condition with variable frother dosage in the Mintek pilot plant rougher cell. The model was seen to estimate the actual FBSD, wherein the IIDDs were precisely predicted compared to experimental IIDDs. Finally, the model validity was then tested for various systems of flotation conditions with variable superficial gas velocity. The model was seen to estimate the actual FBSD for these cases compared to both model-predicted IIDD and experimental IIDDs. The performance of the present model for these systems of flotation was seen to estimate froth bubble size in froth phase from measured IIDD information. Froth bubble size increases with increasing in froth height, and decreases with increasing in frother dosage and superficial gas velocity. Froth height, frother dosage and superficial gas velocity have a strong effect on froth bubble size distribution.

Dedications

To all my family members

Publication

Paper accepted for publication as a conference paper (Mineral Engineering International Conference: Flotation'17) on the contents of this thesis:

Eric Tshibwabwa, M. Moys and C. Bhondayi. Measurement of bubble size distribution in the flotation froths. Mineral Engineering International 2017- reviewed and accepted for publication.

Other paper

C Bhondayi, M Moys, Eric Tshibwabwa, 2018. Relationship between froth bubble size estimates and flotation performance in a semi-batch lab cell. Mineral Processing and Extractive Metallurgy Review. Vol. 31(2018).

List of Presentations on the contents of this thesis

Date	Name and place	Presentation type
13 November 2017	8th International Flotation Conference, Cape town, South Africa	Oral
07 November 2017	Peter King event, Peter King Laboratory, Richard Ward Building, School of Chemical and Metallurgical Engineering, Wits University	Poster
26 October 2017	8th Cross Faculty Postgraduate Symposium, Auditorium, School of Public Health, Education Campus, Wits University	Poster
28 September 2017	School of Chemical and Metallurgical Engineering Research Day, Mineral processing lab Richard Ward Building, School of Chemical and Metallurgical Engineering, Wits University	Poster

Acknowledgements

I would like to pay particular tribute to the following key persons who have worked closely with me in various ways during this period. You have made me who I am.

My supervisors, Prof. Michael, H. Moys and Dr. Murray Bwalya for their inspiring guidance and support throughout this MSc study.

Dr. Clayton Bhondayi for many insights he formulated during experiments and write-up. This work would not be what it is without his insights.

The Lonmin; Mintek and the School of Chemical and Metallurgical Engineering at University of the Witwatersrand for their financial and technical support of this research project.

Workshop staff, Mr. Theo Prassinos, Mr. Rhod McRae-Samuel and Phathu Sikhwari for their technical input in the construction of the electrical conductivity probe and repair of flotation cell, setting up and modifying the experimental apparatus used in this work. It wasn't easy. I am grateful.

Prof Frank Kienhofer for offering the data logger SCXI 1520 data acquisition device used during bubble size measurements.

Mr. Kelvin from Mintek (South Africa, Johannesburg, South Africa) for his assistance during the measurements of froth bubble size in pilot plant rougher flotation bank.

I owe more thanks to family. Words cannot express how grateful I am to my mother and father for all the sacrifices that you have made on my behalf. Also I would like to thank my brothers and sisters for their endless support. I would like also to thank my wife Vanessa Mushiya Tshibwabwa for her endless love and support.

Lastly to God, for all things are possible with his grace.

Table of contents

List of Figures

List of Tables

List of Symbols

A: Cross sectional area of flotation cell

C: Decay constant

C_i:material concentration of species i in the froth phase

D_i or D_b: Diameter bubble

D_i : Representive size of class

D_{32} : Sauter mean bubble diameter

D_i , D_{i+1}: Boundaries of size class

ε_g: Gas holdup

h_f: Froth height

f: Probability of the probe hits a bubble

J_g: Superficial gas velocity

L_j: Intrabubble impact distance or chord length

L_j , L_{j+1}: Boundaries of intrabubble impact distance class

M: Number of size classes (diameter class)

Q_i: Number of the bubbles in the i^{th} class

n : Corresponds to the number of bubbles per second passing through cell area A

N: Number of intrabubble impact distance classes

$N_{d_{2,t}}$: Numbers of bubbles at the top and bottom

$N_{d_{2,b}}$: Numbers of bubbles at bottom of a foam

P L_b D_b : Cumulative distribution that a random drop of the probe measures an intra bubble impact distance IID having its distance less than or equal to L_j

p L_b D_b : Probability density that a random drop of the probe measures an intra bubble impact distance IID having its distance between L_j and L_{j+1}

p D_i : Probability density function of bubble size distribution

p L_j : Intrabubble impact distance distributions

P_A: is the probability of attachment (adhesion) given that the particle has collided

P_C : is the probability of bubble particle collision

P_D: Probability of detachment given that the particle has attached

q: Probability of the probe misses a bubble

r_b: Bubble radius

S: Average surface area per bubble

t_0: Time at which a probe enters a bubble from the top,

t_b : Time at which a probe comes out of a bubble from the bottom

Δt_p: Duration time for a probe to cut a bubble

V_b: Velocity of probe at top lamella of bubble

V_b: Velocity of probe at bottom lamella of bubble

ΔV_p: Average velocity of a probe

Z_{in} : Position of the probe at bubble to surface

Z_{out} : Position of the probe at bubble bottom surface

μ: Average

δ: Standard deviation

List of abbreviations

AFBSD: Actual froth bubble size distribution

BSD: Bubble size distribution

CL: Chord length

CLD: Chord length distribution

IID: Intrabubble impact distance

IIDD: Intrabubble impact distance distribution

IMT (IM): Inversion matrix technique

FBSD: Froth bubble size distribution

LSR: Least square regression

SMBD: Sauter mean bubble diameter

Chapter 1

Introduction

1.1 Background and motivation

Froth flotation is a method for selectively separating a valuable mineral from waste materials by means of the air bubbles dispersed in pulp phase. The flotation process is widely used for upgrading valuable minerals in the field of mining and mineral processing. Many diverse minerals, including most of the world's nickel, copper, zinc, cobalt and lead are processed by flotation process (Zhang, 2009). It has also been stated by Seungwoo Park (2009), the flotation process has been used to remove the contaminant compounds from waste water in the water treatment industries, ink removal from paper fibres in the paper industries as well as the bitumen oil sands in the petroleum industries.

In the flotation process, its success in separating minerals is based on physico-chemistry of the mineral particle surfaces. This is achieved by rendering desired mineral particle surfaces to be hydrophobic by absorption of collectors. While, this happens; the unwanted material particles keep their properties of being hydrophilic. The air bubbles are injected into pulp zone with purpose to select the hydrophobic mineral particles by forming a bubble-particle aggregate. The bubble-particle aggregates rise upward through the pulp phase because of buoyancy forces, and then form a layer of froth phase on the pulp-froth surface at a level in the flotation cell.

The hydrophobic mineral particles are recovered as concentrate, if the attachment of bubble-particle aggregates travels the whole height of froth phase without detachment and attaining its top surface. The target is to recover desired mineral particles from the low grade ores as much as possible.

During their rise in the froth, bubbles can coalesce with other bubbles and become larger diminishing the available surface area of froth bubbles. Accordingly, detachment of desired mineral particles from bubbles in the froth (Li et al., 1990) take place, provoking decrease in mineral recoveries (Yianatos et al., 1986). Reattachment of desired mineral particles can take place in the froth phase if there is availability of bubble surface area, which results in mineral upgrading (Moys, 1979). The froth phase plays an important role in the process of froth flotation, aiming to improve the grade and recovery of mineral particles.

Bubble size is one of the variables that should be controlled in the flotation process (Moys and Finch, 1988). Liu et al. (2005) reported that froth bubble size is the major feature used by the operators to assess the status of the process at the Laronde plant. The effectiveness of the flotation process is significantly related to the size of bubbles in the froth phase. Bubble size distribution is an indicator of sub-processes occurring within the froth phase (Cilliers and Sandr-Kazemi, 1997; Moys, 1979). The control of froth bubble size distribution in the flotation process is expected to be relevant to flotation efficiency. It determines the surface area flux of the bubbles into the concentrate stream which determines the mineral grade and recovery. Therefore, froth bubble size needs to be controlled during the flotation process.

The sub-processes occurring in the froth phase are not well understood and have not been quantified adequately yet due to the lack of adequate methods to measure froth bubble properties such as diameter, rate of coalescence etc. Many measurement techniques have been developed to measure bubble size in the process of flotation. Bulchholz and Schugerl, 1979, classified the bubble size measurement technique into electrical conductivity probe, conventional photographic and light scattering. Finch, 2001 investigated both methods based on (a) drift flux calculation and (b) on equivalent volume cylinder formed when bubbles are drawn into a capillary (UCT technique). These, have been applied in the pulp bubble size measurements at laboratory scale. However, they present disadvantages on froth bubble size measurement, due to the complicated nature and structure of froth phase. Ata, Ahmed & Jameson (2003) performed a photographic method to estimate froth bubble size from transparent flotation cell wall. This cannot be applied at industry scale because it requires transparent flotation cell walls to allow froth bubble photography.. A few researchers have developed electrical conductivity probe methods; Neethling and Cilliers (2004) method consists of fixing the probe tip in the flowing foam and calculating the chord length from known bubble velocities. Bhondayi and Moys, 2014 recently developed a novel electrical conductivity probe (Wits Bubble sizer). It gives several advantages of estimating froth bubble size in non-transparent flotation cell walls (e.g. industrial flotation cell) and can quantify the variation of froth bubble size distribution. The measurement technique consists of randomly dropping a conductivity probe tip through the froth phase. When the conducting tip impacts the top and bottom of bubble surface lamellas, the electrical signals are produced and assessed to obtain the experimental intra bubble impact distances IIDs (chord length, CL). In the previous work, comparison of the technique to the photographic method indicated that the technique over-estimates the Sauter mean bubble diameter D_{32} or actual froth bubble size distribution AFBSD with 31 % error.

However, froth bubble size studies described in this thesis focuses on development of a stereological technique/model to estimate froth phase bubble size distribution FBSD from experimental intra bubble impact distance distributions IIDDs using Wits-BubbleSizer developed by Bhondayi and Moys (2014).

1.2 Thesis objectives

The present work is focused on measurement and modelling of froth bubble size distributions. To achieve and validate the above, the following sub-objectives are set:

- To measure the intra-bubble impact distance distributions (IIDDs) in froth phase using conductivity probe technique (Wits Bubble-sizer) at Wits lab and Mintek pilot plant scales;

- To develop a model to derive intrabubble impact distance distribution from bubble with known diameter distribution;

- To develop an application of stereological techniques to obtain estimates of actual froth bubble size distribution from measured intrabubble impact distance distributions using Wits-BubbleSizer.

To test the model under diverse experimental flotation conditions 1) as a function of froth height in transparent Wits lab flotation cell; 2) as a function of frother dosage in Mintek pilot plant rougher cell and 3) as a function of superficial gas velocity in transparent Wits lab flotation cell.

The major drive of this dissertation is to understand complex processes that take place in the froth phase such as coalescence which has a negative impact on flotation performance. Away of estimating the actual froth bubble size distribution can be developed using the probe technique (Wits-BubbleSizer).

1.3 Thesis layout

This dissertation is organised into 6 Chapters, Chapter 1 provides the background and motivation to the study as well as its importance to the mineral processing industry. The Chapter also highlights the objectives and work scope which will be addressed.

Chapter 2 reviews the literature on flotation froths that is relevant to this work. It starts with comminution. The Chapter includes fundamental basics on flotation froth principle, pulp and froth phases. It highlights the importance of the gas dispersion and hydrodynamic parameters. It assesses the advantages and disadvantages of past and current measurement methods of bubble sizes in flotation process. Emphasis is placed on measurement methods of bubble size distribution in the froth phase applied in Lab, Pilot and Industrial flotation cells. Wits-BubbleSizer is briefly described in this Chapter. The parameters that influence the bubble size distributions in the froth phase are reported. The discussions of the sub - processes occurring in the froth phase are also covered.

Chapter 3, describes the experimental methods that were used in performing the study. It includes the description of the Wits lab and Mintek pilot cells and flotation experiment conditions. The Chapter also describes the design of the probe and its accessories as well as the measurement conditions. The experimental set-up used in both lab and pilot are also presented in this Chapter.

Chapter 4 is dedicated to a development of a model for estimating froth bubble size distribution from measured intra bubble impact distance distribution. The Chapter begins with some assumptions in order to derive the equations. It provides an illustration of geometrical probability of hitting a single spherical bubble in a cubical box model by dropping probes into the box. Chapter also describes the derivation of the intrabubble impact distance distributions from a single bubble and extended to a mixture of bubbles. It describes the stereological technique to estimate the froth bubble size distributions from measured intrabubble impact distance distributions. It also offers the transformation backward inversion matrix method to convert the experimental IIDD distributions into bubble size distributions.

Chapter 5 is dedicated to an analysis of the froth bubble size distribution from data (intra bubble size distribution) as a function of frother height, frother dosage and air flowrate in Wits lab and Mintek pilot cells. The chapter presents application of stereological schematic description algorithm for froth BSD. It also gives the results and discussion on the estimates of froth bubble size distributions obtained with the stereological technique.

Chapter 6 offers the overall conclusions of the work in this thesis and revisits the objectives highlighted in Chapter 1 to evaluate if all goals were achieved. It provides the contribution of the work to the knowledge and finally, this chapter explores further investigation studies.

Chapter 2

Literature review

2.1 Comminution

Metal production process is widely applied technology. Metals are found in two forms, firstly in the form of native elements, e.g. copper and more frequently as minerals contained in ore in the earth crust. The mined ore is the mixture of valuable minerals (i.e. galena, chalcopyrite, etc) and gangue minerals (i.e. silica, calcium carbonate, etc). The recoveries of metals from the ores can be achieved by two methods i.e, pyrometallurgical and hydrometallurgical routes. However, due to high consumption of acid from gangue materials during the leaching of metals (Hydrometallurgical process) and to high energy of smelting both metals and gangue materials (pyrometallurgical process), it is economically important to decrease the amount of gangue materials in the ore which is destined to the leaching and smelting processes. This demands that the ore get concentrated before the chemical extraction methods.

It is apparent that the technology of mineral processing involves two fundamentally different types of processes, which are liberation and separation. The challenging task in mineral processing is to yield a concentrate which contains the majority of the valuable minerals (Weimeng Hu, 2014). The high degree of liberation is the first important prerequisite for a successful mineral-beneficiation operation. If the degree of liberation is insufficient, the mineral particles should be broken into smaller fragments so that better liberation is achieved. This is done by the comminution or size reduction process. Generally there are two major objectives for comminution in mineral beneficiation; the first objective is liberation. Liberation is the process used to unlock composite minerals in the raw ore into more independent particles, without it we cannot collect the wanted components only. In this process, the ore from the mine is subjected to a series of crushing processes in order to liberate the unlocked valuable minerals as shown in figure 2.1 and obtain suitable sizes for further downstream processes.

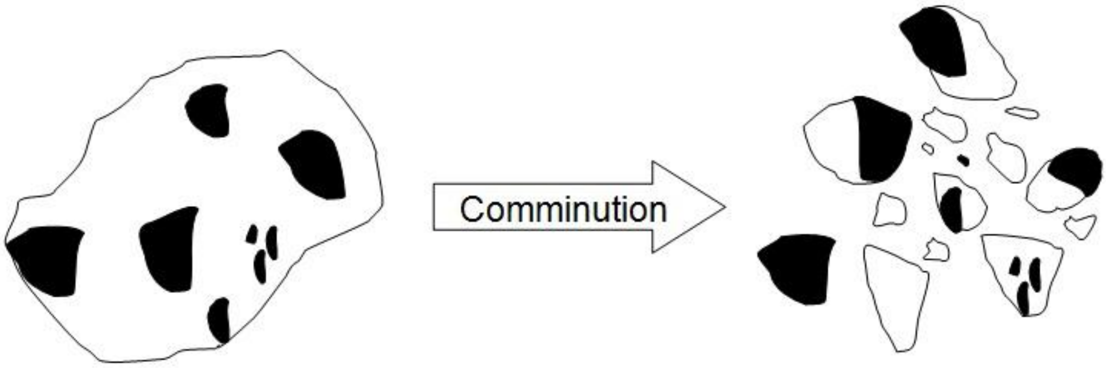

Figure 2.1: Crushing of ore to smaller particles. The valuable mineral particles are indicated by shaded surface area (Weimeng, 2014).

The second objective of comminution in is to adjust the size of mineral particles to adapt to the requirement size for the successive separation process. The crushed ore is mixed with water to form the pulp and then milled to find a particle size distribution, for example minus 100μm. The optimal size distribution for flotation process is predefined, for example 80% of milled ore should be finer than a predetermined size for suitable separation process. This is specially achieved by using classification processes such as hydrocyclones, or a series of screens.

2.2 Froth flotation review

2.2.1 Introduction

Froth flotation has been used for over a century and it is used on a large scale to upgrade ores containing valuable minerals. The flotation process, which is versatile, can separate minerals as great as 3.3 millimetres (6 mesh) and minimum as a 5 microns and can handle minerals with specific density as high as 19 (gold) and as low as 1.5 (vermiculite) (National Research Council (U.S.), 2002). Flotation is a major separation method for metals, coal, and industrial minerals. Most sulphides can be economically recovered by the flotation process.

2.2.2 Fundamentals of flotation froth behaviour

The main goal of flotation operation process is to maximise the solid particles attachment that are suspended within a pulp, to bubbles and form a stable bubble-particle cluster.

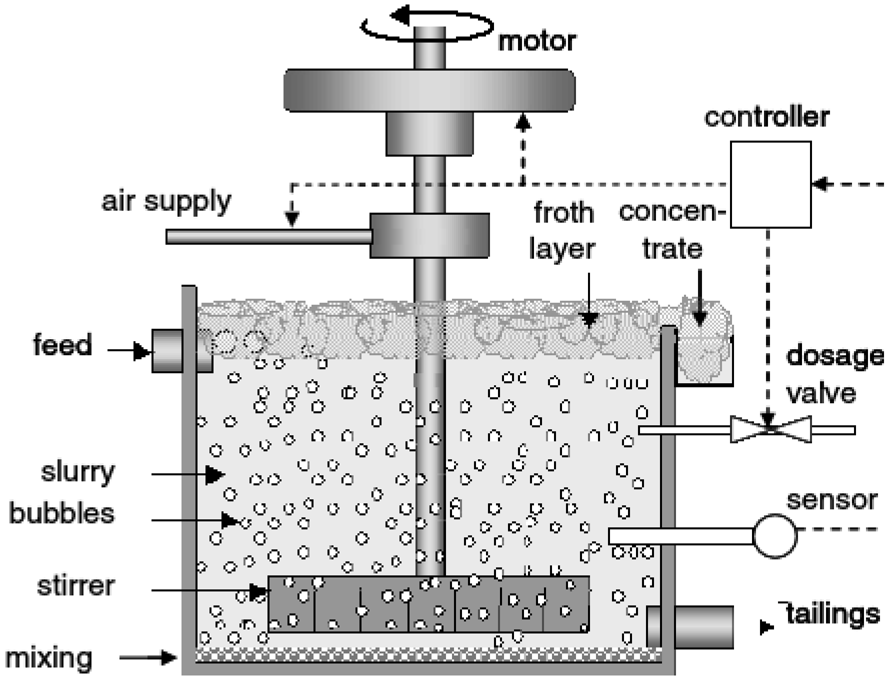

Figure 2.1: Picture showing the flotation operation process in mechanical flotation cell (Kramer et al., 2012)

This is promoted by adding reagents that can change mineral surface properties or modify slurry properties as mentioned in Fuerstenau et al. (2007) into the pulp. The reagent chemicals are divided into three classes namely; frother, collectors and modifiers (depressants, regulators and activators). Each of them promoting particular behaviour of a contained mineral or change the slurry properties. These reagents and theirs functions serve are listed below as obtained from Bulatovic (2007).

• **Collectors** are used to render hydrophobicity on a mineral surface. This is needed since there exists only a few minerals that are hydrophobic by nature.

• **Activators** enhance flotation in the existing of collectors by interaction with the minerals surface and the collector.

• **Depressants** are used to depress one of the ore minerals in the pulp, without affecting the properties of desired minerals. This promotes the selectivity of a component.

• **Frothers** are added to contribute to the production of a froth phase which holds the floating particles until the froth is removed. Frothers should also and promote bubble dispersion.

• **Regulators** are added to the suspension to maintain a specific pH or Eh field or control the stability of the slurry.

In batch flotation there is a conditioning stage (mixing) which is conducted prior to flotation to allow reagents to interact with particles. In an operational plant separate conditioners are available in line before flotation machines. Chemical adsorption of the reagents generates hydrophobic surface properties on selected minerals, whilst agitation and aeration increase collision probability between bubbles and particles (Clark et al., 2006).

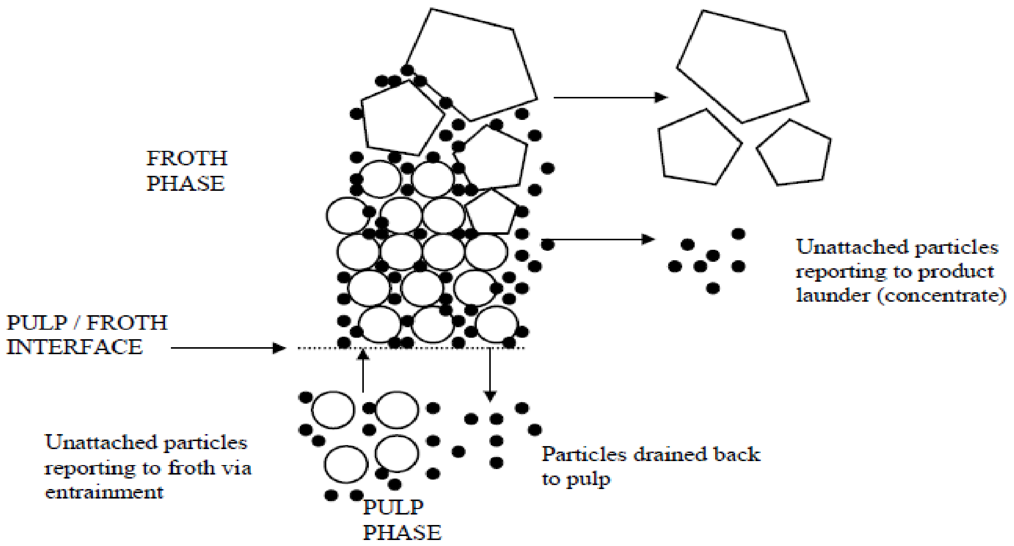

Figure 2.2: Schematic of Model of the froth phase for particles attached to bubbles (Schwarz, S., 2014).

In the next stage gas is dispersed at the lower part of the flotation cell. The gas is injected into the lower part of the flotation cell as displayed in Figure 2.2 and broken into small bubbles by shear action of impeller. The bubbles will attach to the hydrophobic particles in the cell and transport these aggregates from the liquid suspension to the froth phase indicated in Figure 2.3. The froth is built up on top of the slurry and allowed to overflow the cell. The froth phase removal is achieved and forms the concentrate (final flotation product). The hydrophilic mineral particles are wetted by the available water and will stay in suspension and flow out of the flotation cell to the flotation tailing stream as shown in Figure 2.2. The transition of mineral particles from the water suspension into the froth can occur by several mechanisms. True flotation is the main mechanism for flotation, where bubble-particle aggregates form by means of selective collector attachment stimulating hydrophobicity of the mineral surface. The density difference between slurry and aggregate will transport the aggregate to the froth layer. But there are other mechanisms that enhance flotation. Entrapment of particles is described as 'the particles that get physically trapped between bubble-particle clusters rising through the slurry or that are already adjacent in the froth. Entrapment of particles is described as 'the particles which are trapped between bubble-particle clusters rising through the slurry or that are already adjacent in the froth'. Entrainment is the transport of particles together with the water and froth that overflows into the launder. Both entrainment and entrapment are non-selective and are very much influenced by particle size, coarse particles are much more likely to get trapped or drained with the water. These mechanisms recover gangue and therefore decrease concentrate grade. To achieve an adequate separation and reduce entrainment and entrapment, the froth can be sprayed with water to wash unwanted entrapped particles from the froth. This is described in Drzymala (2007).

2.2.3 Collided, attached and detached particle-bubble mechanism

Collision of solid particle-bubble and interaction of attachment in froth flotation process have been described in Figure 2.4. A particle probability of being extracted by a gas bubble in the slurry phase of a flotation cell can be found by:

$$P_c = P_c P_a (1 - P_d) \qquad 2.1$$

Where P_c is the particle-bubble collision probability, P_a is the probability of attachment given that the particle has collided, P_d is the detachment probability given that the solid particle has attached (Yoon, 2000).

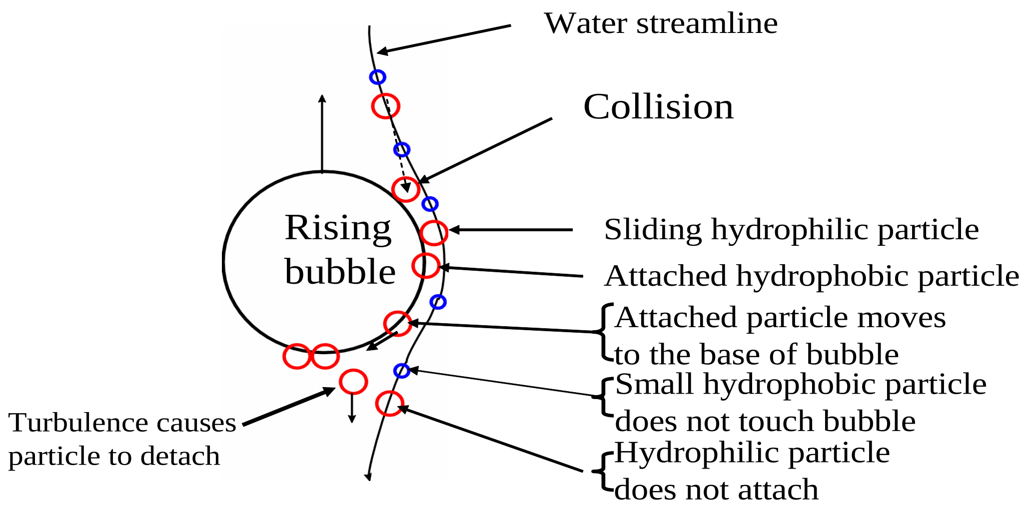

Figure 2.3: Particle and bubble interaction (Moys, 1996)

The attachment of particle-bubble is primarily controlled by surface tension forces, which are characterized by the forces of surface and water lamella breakage occured when the particle and the bubble are near to each other. The interaction force of surface between air bubble and a hydrophobic solid particle are strongly promoted by hydrophobic forces, van der Waals , double layer.

2.2.4 Gas dispersion and hydrodynamic parameters

2.2.4.1 Surface area flux of bubble

In froth flotation process, hydrophobic mineral particles are selectively extracted and lifted by air bubbles from the slurry into the froth phase. The performance of the flotation process is strongly influenced by the bubble sizes (Jameson, 1985; Finch, 1986; Yoon and Luttrell, 1986). Therefore, the capability to controlling the formation of air bubbles with purpose to yield a suitable range of size within a flotation cell is more attractive. Concerning this aim, estimations of bubble size in industrial cells have to be made. Bubble size distribution is often expressed by a mean D_{32} (Sauter mean bubble diameter) derived by the following:

$$D_{32} = \frac{{}_{i=1}^{i=n} {D_i}^3}{{}_{i=1}^{i=n} {D_i}^2} \qquad 2.2$$

Where D_i diameter of bubble with is spherical shape and n is total number of estimated spherical bubbles.

Sauter mean diameter is the diameter giving the same volume/interfacial area ratio as the bubble distribution of interest. This is the appropriate metric for calculating the surface area flux (S_b) of bubble. Typical bubble size range is 0.5 – 2.5 mm in the pulp zone (Gorain et al., 1995). Coalescence is considered the mechanism which reduces air dispersion efficiency (Harris, 1976). The bubble size distribution depends on the balance between coalescence and rupture phenomena (Grau and Laskowski, 2005); Gorain et al., 1995). There are many factors that influence bubble size includes frother sorts and dosage, gas flor rate and air bubble sparger.

2.2.4.2 Air holdup

Air holdup (ε_g) within a liquid is meant as the contained fraction of air volumetric:

$$\varepsilon_g = \frac{V_{bubbles}}{V_{bubbles} + V_{liquid}} 100 \qquad 2.3$$

Air holdup is depended on the frother sorts and dosage and superficial gas velocity. The superficial gas velocity has a direct effect, and measuring ε_g as a function of Jg can be employed to determine the effective range of operation of a flotation machine as well as troubleshoot for operational and maintenance problems (Dahlke et al., 2005).

2.2.5 Complex processes in froth phase

2.2.5.1 Bubble coalescence

The principle cause for coalescence of froth bubble is the breakage of thinning water films which separates two attached froth bubbles. The breakage occurred when the content of water within the froth zone drops below a critical value. Mineral particles and surfactants are known to have a strong effect on the breakage of water film. The breakage of water film behaviour of film has been experimentally investigated. Almost of these investigations have been conducted in two phase (Sharma and Ruckenstein, 1987). The oscillation of froth bubble and vibration were investigated to be the cause of bubble coalescence. The work done by Ireland was performed within a wetting froth phase, where the water content in the froth phase was ranging from 0.25 to 0.6. The high water fraction a part of pulp-froth interface zone in the mineralised froth phase and is located below the injection of washwater, if the addition washwater has been done.

The hydrophobic minerals particles can also cause the coalescence of froth bubble.

2.2.5.2 Detachment and reattachment of hydrophobic particles

There are many causes for the hydrophobic particle detachment from the froth phase. The relevant cause is the bubble coalescence. Coalescence bubble often happens in froth phase specifically at the pulp-froth interface and the froth phase surface. Bubbles coalesce in froth phase as their lamellae raptures (Ata, 2012). Floatable mineral particles separate from the bubble surfaces in froth phase. Detachment of mineral particle particles will drain back to the pulp phase or reattach to available surfaces. The detachment and reattachment subprocess forms a flow inside between the slurry and froth phases that can largely diminish the performance of flotation reactor. In the other side, when the detachment subprocess is selected with regards to the degree of hydrophobicity and particle size, the purity of concentrate produced can be effectively ameliorated. Particles that detach may reattach to available surfaces in the froth phase. Froth selectivity happens when froth preferentially rejects previously attached particles based on some particle property such as particle size, density or hydrophobicity (Seaman et al., 2006). This selective reattachment or rejection of before adhered mineral particles in the flotation froths results in additional upgrading of the concentrate (Moys, 1979; Cutting et al., 1981). Although a number of researchers have reported this kind of froth selectivity (Young, 1982; Ata, 2002) others found only apparent selectivity with regards to mineral particle size distribution (Vera et al., 1999). A high bubble coalescence rate can produce a froth phase overload at a target place where further hydrophobic mineral particle transfer to the concentrate launder cannot be possible. Large capacities of carrying are globally discovered within column flotation cell reactors as they possess a great froth phase depth and a smallest specific surface area/unit volume of capacity than the mechanical flotation cell reactors. Mineral particle detachment because of not sufficient surface area is expecting to be significant within a froth overloading. Research on the particle detachment in froth flotation has been done by many workers (Falutsu and Dobby, 1992).

It has been observed by Seaman et al. (2006) that the particle detachment at the pulp-froth interface can be effective within a plant flotation cell. Interface of pulp-froth locates within the “calm divers” no hydrodynamic zone than the zone of pulp (Yianatos et al., 1986). As the attached particles-bubbles within the pulp lift towards the interface of froth-pulp they necessarily come to take rest by losing the momentum because of the velocity difference between both phases. Interface of froth-pulp is a zone where air bubbles lifting from the beneath of pulp begin to come together in a crowd. Bubbles strongly coalesce in this zone.

Coalescence of bubbles leads to particle rejection which happens just above the pulp froth interface where bubbles begin to crowd (Yianatos et al., 1988). Measurement of bubble coalescence as change in froth bubble size above the interface of pulp-froth showed that coalescence is strongly dependent on attached mineral. Understanding coalescence in the froth is thus very important in understanding and optimizing the froth phase. Modelling of the bubble coalescence exists in flotation literature e.g. Neethling and Cilliers (2003) but actual size measurement of the froth bubbles above the interface within non-transparent cells is impossible.

2.2.5.3 Drainage of solid

The main froth role within flotation process is to transport desired mineral particles towards the flotation cell lip with lower loss, while at the same time rejecting gangue minerals which have come in the froth phase by entrainment. As the air bubbles move up into the froth phase, the water flows towards the pulp zone because of the difference in density between the water and the air. The drained water principally composes unwanted mineral particles and is regarded to be one of the key subprocesses within froth phase impacting both concentrate grade and recovery. Cutting and co-workers conducted research on drainage subprocesses taking place in the froth phase and will be briefly discussed here. Cutting and Devenish (1975) used an equilibrium flotation cell, in which the froth is not withdrawn but allowed to come to a dynamic equilibrium with the pulp. This sort of flotation cell was primarily performed by Watson et al., (1973) and utilised by Moys, (1978) in the modelling of froth phase behaviour. Two different functions of the mechanism of drainage within such a flotation cell reactor (Cutting and Devenish, 1975) are discussed. Firstly, the drainage of bubble film within which mineral particles and liquid drain between the bubbles in froth phase. This takes place within the entire volume of froth zone. Secondly is drainage of column, within which material descends rapidly at single vertical locations within the froth zone. In other work, Cutting, (1981) described a third mechanism of drainage that can uniquely be seen within a large-scale flotation cell. The solid drainage resulting from solid accumulations on the top of the froth phase surface, where they generate clumps that achieve a unstable mass and descend quickly. The drainage of solid behaviour is significantly affected on key parameters such as the properties of mineral particle, the degree of hydrophobicity and froth viscosity. The content of water of the froth phase, however, assures an important role in the subprocess of drainage of froth phase.

Gangue mineral and slight adhered particles are repulsed quickly at the heavier wet froth area that coincides to the lower part (base) of froth zone (Falutsu and Dobby, 1992; Moys, 1978).

2.2.6 Influence of key process parameters on froth bubble size and flotation performance

Investigating of the correlation between the variation of bubble size in froth as well as the parameters of metallurgical perfomance is of relevant for these purposes of process control. According to the results presented by several investigators, the operating process parameters froth height; frother concentration and superficial gas velocity affect the froth bubble size.

2.2.6.1 Superficial gas velocity

Froth bubble size decreases with augmenting suprficial gas velocity. It could be because of the lewer chances for the bubble to be coalesce, most probably because of smaller times of air bubbles in the froth phase (Seungwoo Park, 2015). The air bubble size in froth phase increases and mineral recovery augments with an increase in the suprficial gas velocity. Highest recoveries is related to improved surface area flux of bubble and bigger bubbles occured in increasing coalescence of bubble as well as the decrease in bubble breakage. The suprficial gas velocity was found to possess a strong effect on froth bubble size (Nesset et al., 2006). The true bubble size augmented with increase suprficial gas velocity over an optimum range of work conditions studied.

2.2.6.2 Frother concentration

The influence of frothers on size of air bubble has been extensively investigated (Laskowski, 2003; Grau et al., 2005). The continuous decrease in the Sauter mean bubble diameter with the concentration of frother can be caused by diminishing surface tension that prevents coalescence subprocess of bubble. The influence of frother on size of bubble results from its character to hinder coalescence of bubble. The ability of coalescence phenomena diminishes with augmenting the dosage of frother and at a target dosage for a frother reagent, it achieve uncoalescence environment. Coalescence of bubbles is controlled by the concentration of frother, which reduces interfacial surface tension and stabilises the froth. The value of CCC appeared to be distinct for each frother sort. It was found that augmenting frother dosage, size of air bubble diminished until the value of CCC is achieved. At dosage over CCC value, no additional bubble size variations were seen. The results from Aldrich and Feng (2000) showed the sauter mean diameter within the slurry phase is smaller compared to froth phase, and the diverse deceleration rate in coalescence of bubble combined with diverse frother sort and dosage affect the size of bubble in slurry and froth phases.

2.2.6.3 Froth height

The mean diameter augments in size of bubble as the height of froth phase from the interface augments. Bhondayi and Moys (2014) found the distribution of large froth bubble size in sections near to the froth phase surface, while the smaller one at base of froth interface. Similar results were observed by Seungwoo Park (2015) in a mechanical flotation cell. It has been seen that the bubble size ratio augmented with increase froth height, as given as by Eq.(2.4).

$$N_{d_{2,t}} = N_{d_{2,b}} exp \quad -C \frac{Y_{t=t_{cr}}}{h_f} \qquad 2.4$$

Where C is the decay constant, h_f is the froth height, and Y is the distance from the base of froth. $N_{d_{2,t}}$ and $N_{d_{2,b}}$ are the bubble numbers at the top and bottom of a foam, respectively, and $d_{2,t}$ and $d_{2,t}$ are the corresponding bubble sizes.

As a bubble rises along the y direction in a froth phase, the number of bubbles decreases due to bubble coalescing as clearly shown Figure 2.5. The reason is simply that bubbles will have a longer time to coalesce in a taller froth height (Bhondayi and Moys, 2014, Seungwoo Park, 2015).

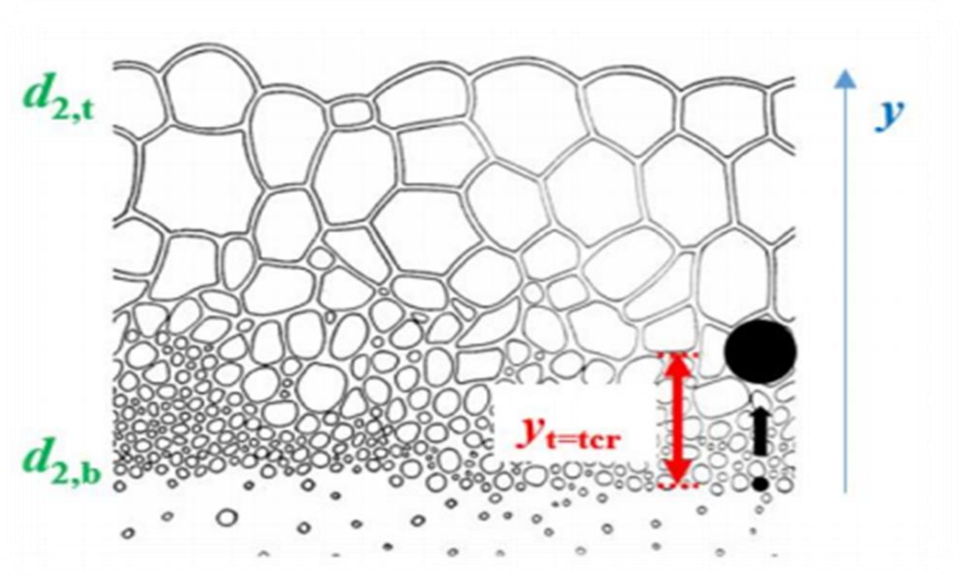

Figure 2.4: Bubbles get longer along the y direction in froth phase by coalescing (Seungwoo Park, 2015).

2.3 Measurement technique of bubble size

2.3.1 Relevance of froth bubble size

Complex process in froth phase such as coalescence of bubble result in augmenting the size of bubbles above the pulp-froth interface (Yianatos et al., 1988). This causes hydrophobic particles detachment from the bubbles (King, 2001). If the detached hydrophobic particles in froth phase reattach to the disposal surface area of bubble based on floatability then further cleaning action takes place (Moys, 1979). Seaman et al., 2006 stated that further action of cleaninig subprocess may occurs in the froth phase balk as hydrophobic particle rejected from froth bubbles due to coalescence (Seaman et al., 2006). Accordingly the rate at which coalescence of bubble takes place within the flotation froths is important to examine and optimize flotation recovery across `the froth phase.

2.3.2 Briefing on methods employed to estimate the size of bubble

Many techniques have been performed to estimate bubble size over the decades, that can be categorised based on their functioning principles. Fibre optics, capillary (UCT technique), laser, analysis of photographs or video images and probes. These were used in various fields such as pharmaceutics, mineral processing, petroleum, etc. Variable “Bubble size” in the process of flotation assures a greater role in mineral recovery. Thus, Saxena et al. (1984) utilised cinematographical technique, Tucker (1994) employed UCT Bubble-sizer, Atkinson, (1988) employed pressure probes, Grau (2002) used Helsinki University of Technology (HUT) Bubble-sizer sampler, Hemandez-Aguilar et al., (2002), Rodrigues (2003) employed LTM-Bsizer method and Burgess (1987) estimated with a laser, Hemandez-Aguilar et al., (2002) investigated McGill bubble size analyzer, Yianatos (2001) used USM bubble size sampler.

Most of above techniques were developed to measure bubble size in pulp phase. Some of them cannot work in froth phase because of their limitations due to complicated structure and nature except conventional photographic method. However, few works have been done on froth phase.

2.3.3 Measurement technique of froth bubble size

The conventional photographic method is the most utilised technique to determine size distributions of froth bubble in lab froth phase (Ata et al. 2003).

Figure 2.5: SmartFroth camara installations for froth surface bubble size (Forbes, G., 2007)

Many researchers have used conventional photographic methods to measure bubble sizes on the froth surface. The camera is placed on above the froth phase in such a way that it is observing the top view area of froth which is representative of the cell as shown in Fig.2.6. The images are processed using different algorithms. Wang et al., 2000 present a set of image processing algorithms to determine froth surface bubble size distribution. They initially categorize an image based on a calculation on the white spots of the image, and then proceed to delineate individual bubbles using a valley edge detection algorithm. Watershed algorithm was used for bubble size measurement of froth surface (Liu, 2015; Sadr-Kazemi et al., 1997; Wright, 1999; Botha, 1999) indicates the machine vision segmented bubbles. Francis, 2001, discusses various preprocessing techniques that can be used to improve the results from the bubble segmentation algorithms. These typically take the form of various non-linear filters. Botha, 1999 identifies the problem of segmenting flotation froth bubbles which have both large and tiny bubbles present. Forbes, 2007 correlated the size of bubbles at the surface of the froth with grade of concentrate. But, according to Murphy et al. (1998) statement found from observing the surface of the froth is not enough. This method, suffers from some limitations. It gives only the information of bubble size on the froth surface and complicated algorithm is needed. The use of surface of the froth bubble sizes has been limited for reliable and industrially applicable method to measure bubble sizes within the froth.

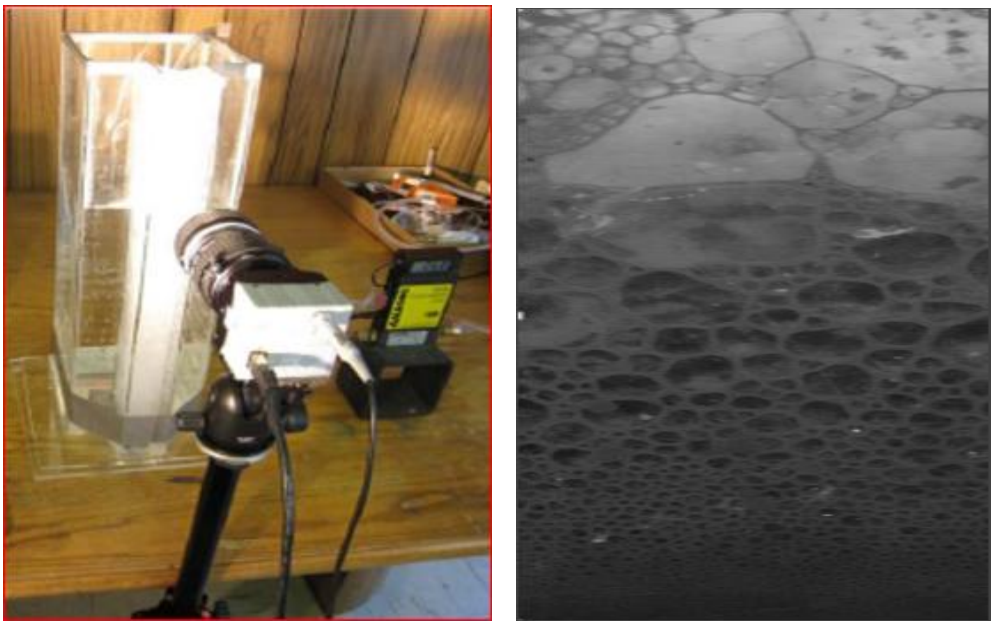

(a) (b)

Figure 2.6: (a) Experiment employed to quantify bubble size within foam (Seungwoo, 2015) (b) Variation of bubble sizes with height (Bhondayi and Moys, 2014).

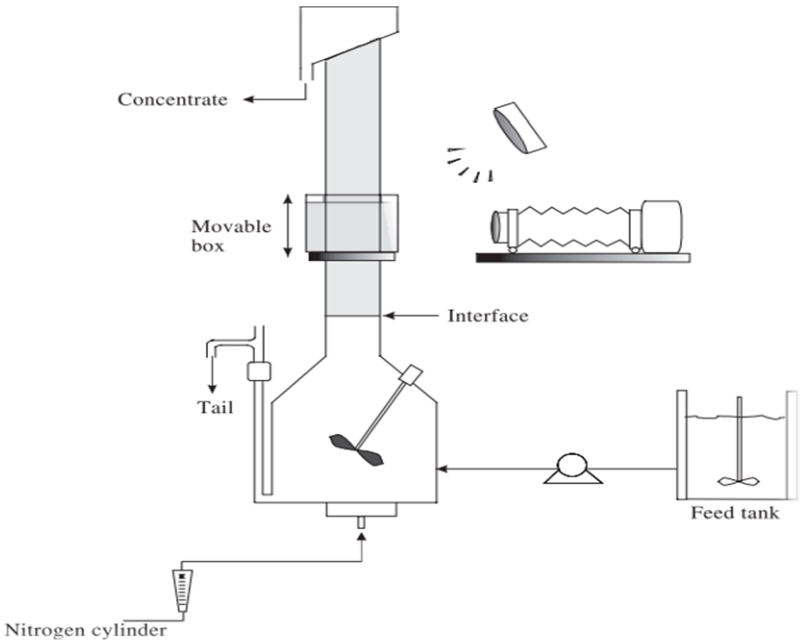

Figure 2.7: Froth flotation cell employed to estimate size of bubble within froth phase (Ata, 2003).

Quantification of size of bubble within the froth phase and a comprehension of the rate at which froth bubble sizes vary in the froth can offer numerical information which will help comprehension of froth subprocesses particularly coalescence of bubble. Few works have been done on froth bubble size measurement through transparent flotation cell from interface using photographic technique (Ata S., et al., 2003 and Seungwoo P., 2015). In this method, the camera is placed in manner that it captures the side view of the froth part as shown in Figure 2.7a and 2.8. It has a capability of quantifying the variation of size distribution of froth bubble and represented by true bubble size as illustrated in Figure 2.7b. Its utilization in plant flotation cells is limited as it needs the flotation machine windows to be transparent to allow clear photography.

Unfortunately techniques that may be used to measure the variation of bubble sizes with froth depth above interface in flotation froths produced in non-transparent flotation cells was not yet in the literature until Bhondayi and Moys, 2014. Bubble coalescence results in an overall augment of bubble sizes in froth from the interface of pulp-froth to the froth surface resulting in decrease in available bubble surface area.

2.3.4 Wits-BubbleSizer (Bhondayi and Moys, 2014)

The probe (Figure 2.9) was constructed out of a copper wire with various diameters that is insulated while allowing only the probe tip to conduct the electricity. The diameter of the tip was chosen to be thin to allow measurements of smaller bubble fraction in the froth phase.

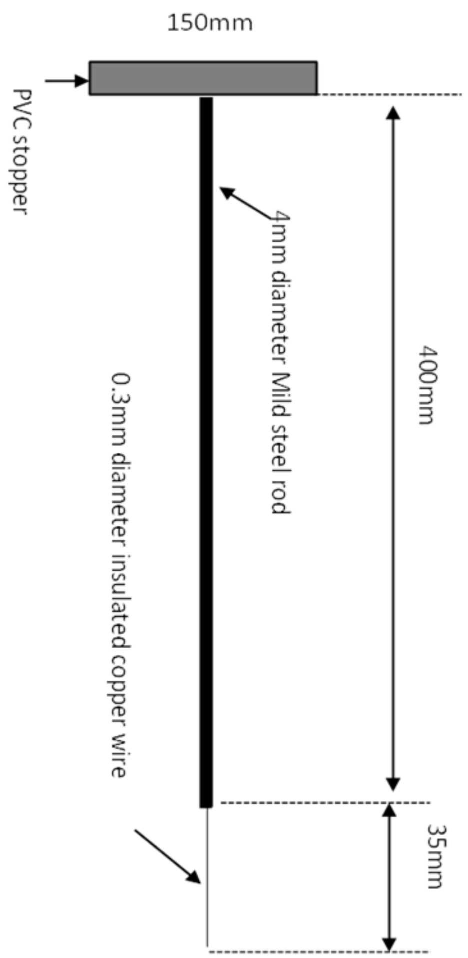

Figure 2.8: Schematic of the electrical probe, displying the mill steel rod, the PVC stopper and insulated copper wire (Bhondayi and Moys, 2014)

In a flotation cell, properties of froth bubble can be quantified using electroconductivity probes. Bhondayi and Moys, (2014) investigated the froth bubble properties in a column flotation cell employing a single electroconductivity probe tip. This had a single electrical tip point (Figure 2.9) and the conductivity difference between the air and liquid phases in froth phase and slurry phase was detected by releasing the conductivity probe tip into the froth phase from given height of 0.5 m. It is expected that when the tip of probe comes into contact with air and liquid as it moves from the froth surface towards pulp-froth interface, the voltage brusquely changes from high to low, respectively as displayed in Figure.2.8. The voltage output electrical signal is described mathematically by Eq. (2.5).

$$V_{out} = \frac{R_f}{R_f + R_1} V_{in} \qquad 2.5$$

Where V_{out} is output voltage, V_f froth resistance,R_1 is fixed resistance and V_{in} is the input voltage. Electrical signals recorded were utilised to determine the chord length which are related to froth bubbles.

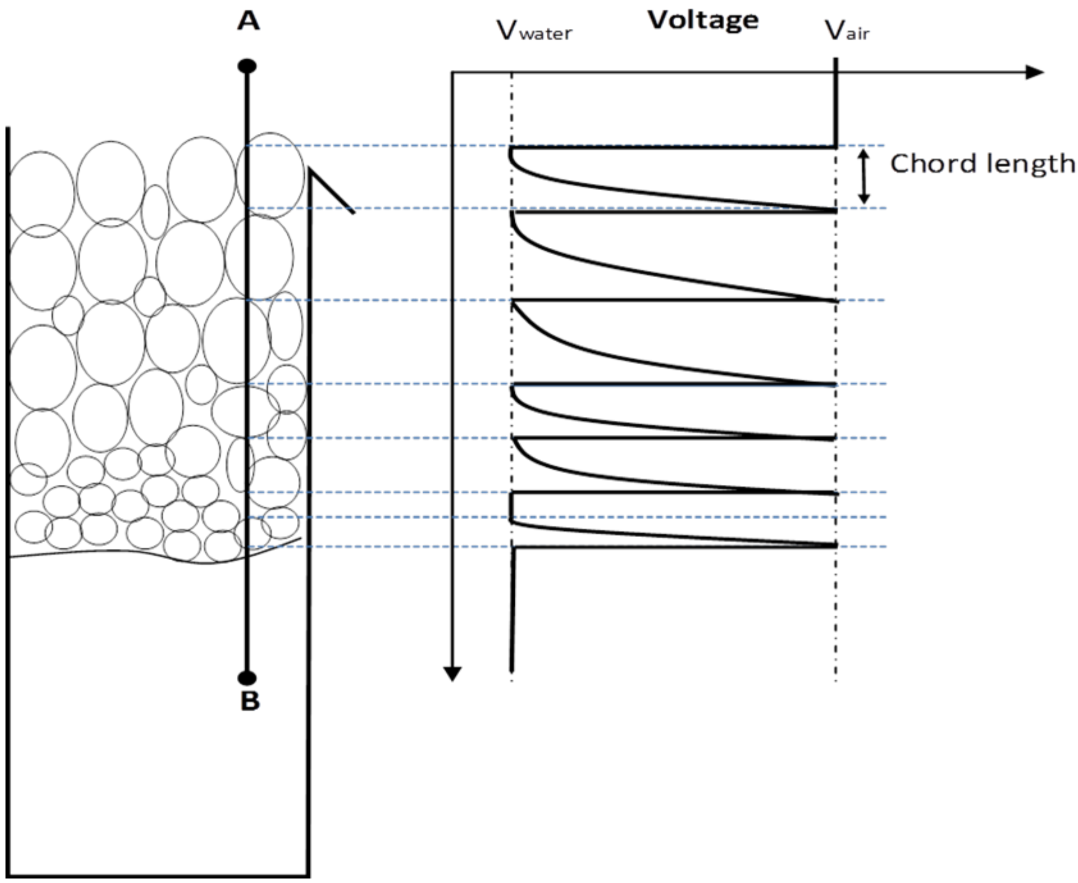

Figure 2.9: Example of the output electrical signal that is found when an electrical needle cross through froth height (Bhondayi and Moys, 2014).

Therefore, intrabubble impact distance IID is described as the length between the consecutive significant impact points. The conductivity probe crossing the whole froth height with an increasing velocity as governed by Newton's laws. The residence time of probe taken to cross the consecutive significant impact points and velocity at which the probe is crossing through the froth bubbles are utilized to determine the intra bubble impact distance by

$$IID = L_j = \frac{V_t + V_b}{2} \quad \frac{t_t + t_b}{2} = \Delta V_p \ \Delta t_p \qquad 2.6$$

Where V_t is velocity of probe at top lamella of bubble, V_b is velocity of probe at bottom lamella of bubble, $t_0$is the time at which a probe enters a bubble from the the top of a bubble, t_b is the time at which a probe enters a bubble from the bottom of a bubble. ΔV_p is the average velocity of a probe, Δt_p is a duration time for a probe to cut a bubble and L_j is vertical length of the bubble chord.

NB: In overall, this approach consists of randomly dropping a probe several times from a known height into flotation cell by cutting the whole froth height. The electrical signal from measurement is sent to a computer via data logger. The signals are assessed using Matlab to obtain the intra bubble impact distance. This technique does not directly give froth bubble size distribution due to random measurements because, the probe can intercept the bubble anywhere. Therefore, IID does not provide froth bubble diameter. Consequently, this work is focused on developing a method for deducing froth bubble size distributions FBSDs from Wits Bubble-sizer measured intra bubble impact distance distributions IIDDs.

Chapter 3

Equipment and experimental description

3.1 Introduction

Experimental work was done both at the Wits laboratory and Mintek. The equipment, equipment set-up and experimental procedures are presented in this Chapter. The two first sections give respectively the description of Lab and Mintek pilot flotation cells as well as their flotation conditions. The following section describes the design of the probe and its accessories. Final section gives the equipment set up description used to measure froth bubble size in both wits lab and Mintek pilot flotation cells.

3.2 Flotation equipment and experiments

3.2.1 Lab flotation experiments

In this work, a transparent rectangular flotation cell of 20 Liters was used. This cell was designed by Bhondayi and Moys, 2014 and its main characteristics are respectively variable depth and variable rotor position as shown in Figure 3.1. The air sparger with diameter 2 mm is located above the impeller at the lower part of the flotation cell through which gas is fed into the cell. Slurry feed and discharge are located across from one another, the concentrate is recovered at the cell top surface, while the unwanted mineral port is situated towards the lower of the flotation cell. Figure.3.2 contains the pictures of the experimental setup used in this study. It is composed of 85 Liters mixing tank used to feed the flotation cell, a peristaltic pump, an air compressor and rotameters (BAILEY) used to measure the air into the flotation cell. Flotation experiment was carried out in steady state mode. The concentrate and tailings of the flotation cell flow back to mixing tank as shown Figure 3.2.

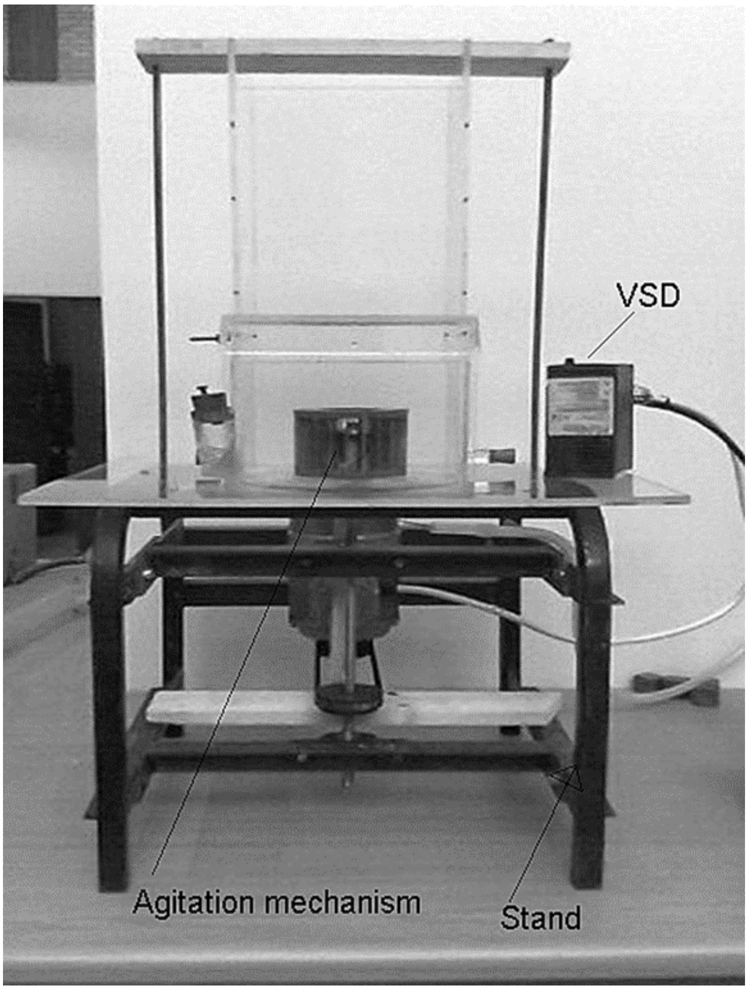

Figure 3.1: Picture of flotation cell, showing stand and VSD (variable speed drive) and stator (Bhondayi and Moys, 2014)

Flotation experiments were performed utilising an artificial ore with contents of 20% limestone and 80% silica regarded as respectively gangue and floatable minerals. The flotation was carried out in two series of conditions. Firstly, superficial gas velocity of 0.97 cm/s was utilized in whole experiments, with the feed to the flotation cell containing a solid content of 15%. The impeller speed was fixed at 1200 rpm and Oleic acid and Dowfroth were added respectively at rate of 30 g/ton of limestone and 0.30 mg/ per liter of water. In these experiments, firstly, froth height was considered to variable with 0-2 cm, 2-4 cm, 4-6 cm, 6-8 cm and 8-10.5 cm and secondly, superficial gas velocity was considered as a variable with 0.33 and 0.75 cm/s respectively with froth height 10.5 cm and 17 cm.

Figure 3.2: Picture of the pseudo-steady state flotation experimental equipment in the Mineral Processing laboratory at University of the Witwatersrand.

3.2.2 Mintek pilot plant rougher flotation experiments

Experiments were carried out on liquid-gas phases in the rougher bank of the secondary flotation circuit at the Mintek pilot plant, Johannesburg, South Africa. The flotation bank has 6 rectangular cells in series (each 30 × 40 cm long) as shown in Fig.3.3. The gas flow rate was injected from the bottom of each cell through a pipe. The water level was controlled by an interface controller. The experiments were operated in closed circuit. This means that both liquid tailings and froth streams drain back into the batch sump. In turn, it is pumped into the first cell. The water flow rate, airflow rate, liquid-froth interface and impeller speed were operated at constant values through all the experiments, respectively 1500 rpm, 50% and 20 cm. The variable manipulated during the study was frother concentration (MIBC). Three diverse sets of operating conditions were utilized; 3 ppm, 6ppm and 12 ppm. All changes and measurements were done on the second cell of the rougher bank.

Figure 3.3: Mintek pilot plant, showing secondary rougher bank which consists of 6 cells and installation of probe for froth bubble measurement.

3.3 Measurement equipment and experiments

3.3.1 Design of probe and its accessories

Figures 3.4 and 3.5 show probe release mechanism.

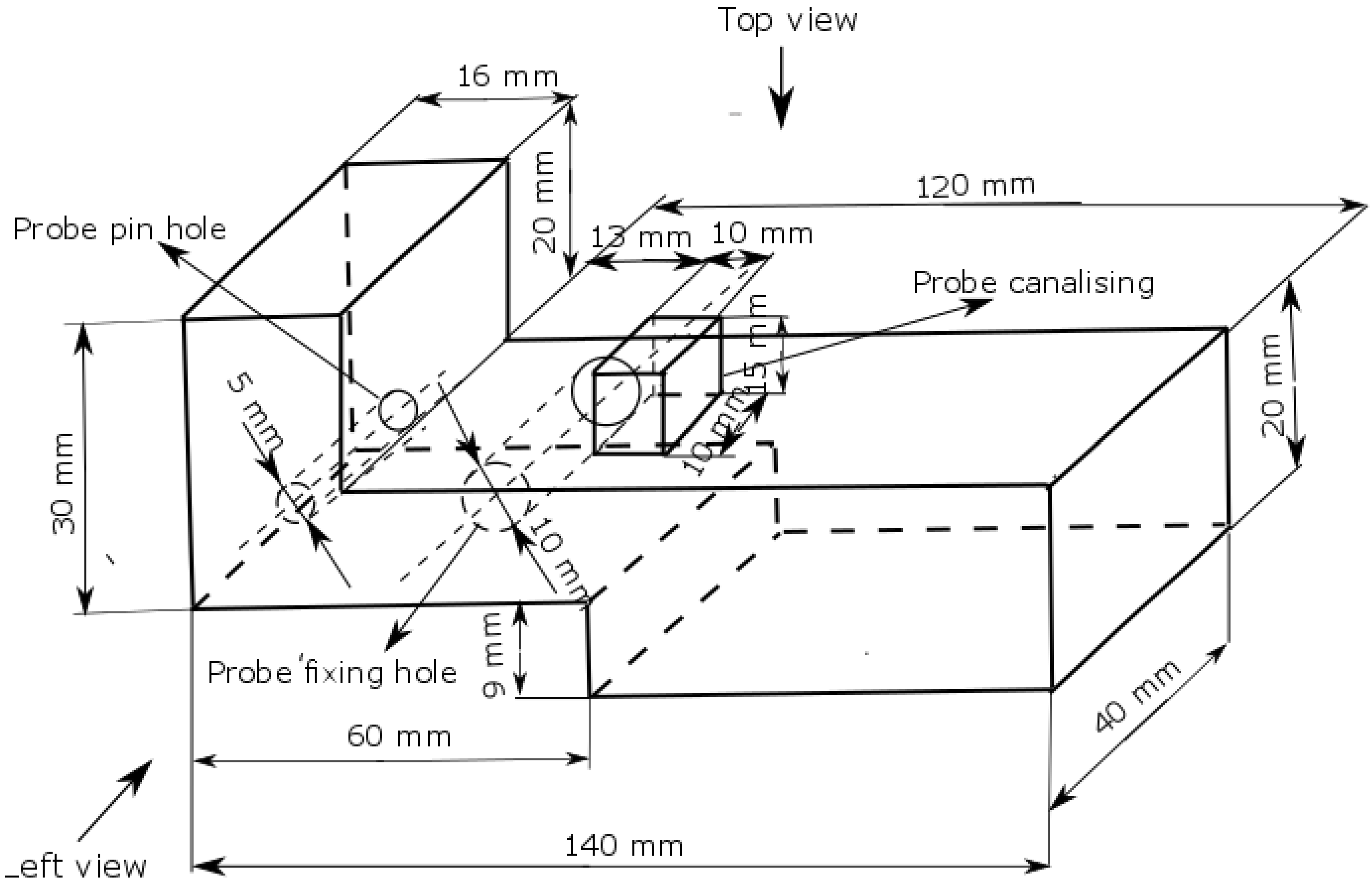

Figure 3.4: Sketch of probe release mechanism design with its dimensions. See Figure 3.7 (A)

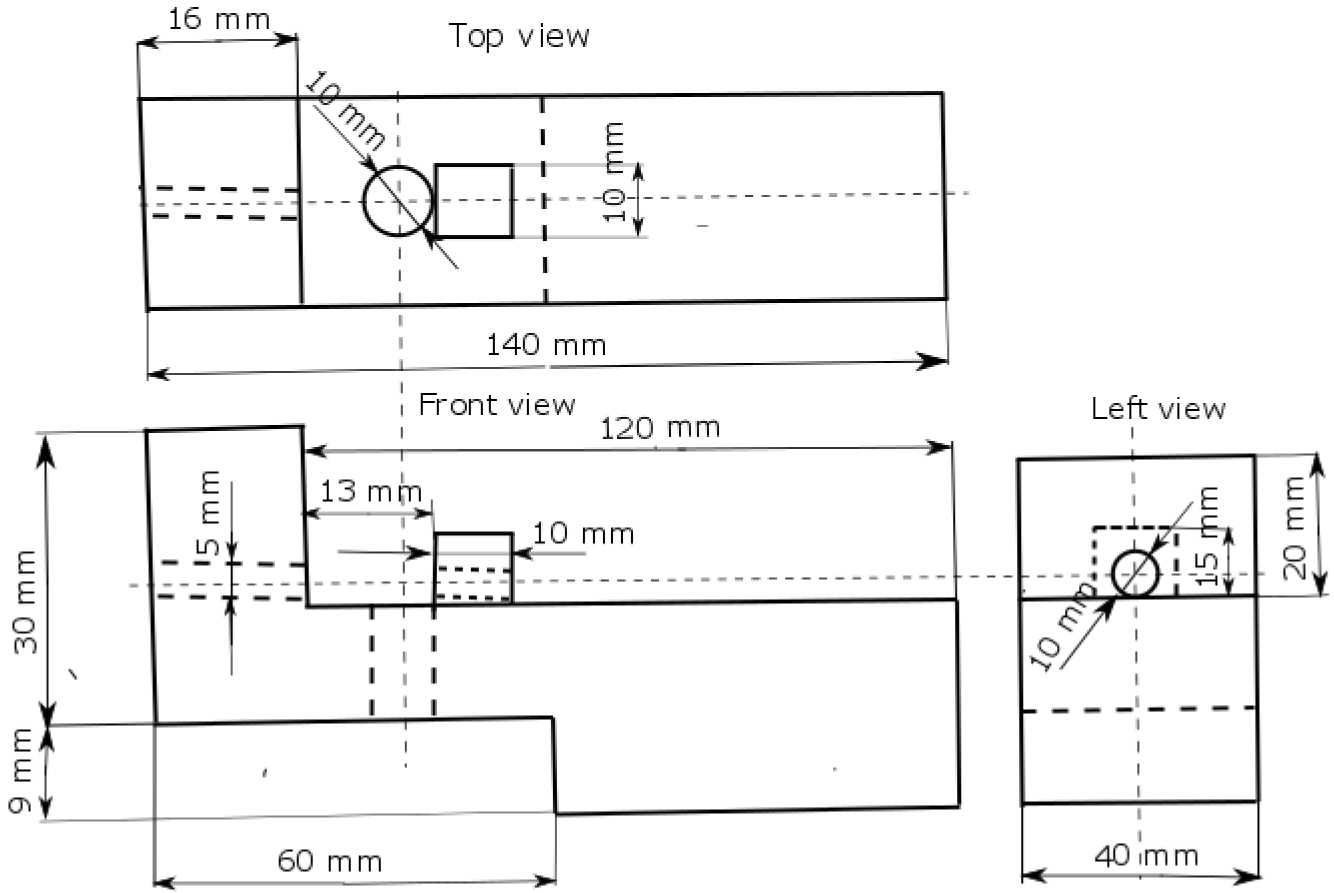

Figure 3.5: Front, top and left view representations of probe release mechanism.

The penetration depth of the tip of the probe was controlled by adjusting the position of the stopper shown in Figure 2.9. The drops of the probe were carried out with variable-drop-height probe release. The probe release was designed with an insulted materiel to avoid the electrical conductivity. The probe release (Figure 3.4) was designed in such a way that it drops a probe by pulling the electrical pin. This design enabled to fix the probe at a given height from the froth surface. The probe release was also designed in such a way that the probe could be dropped vertically from release mechanism. This required the probe release core to be designed with a material that cannot be electrical conductive. Figure 3.5 is a side view of the probe release showing the front, top and left views. The probe release is made from black PVC 39 mm thick, with length 140 mm and 40 mm width. Figure 3.6 is a picture of the probe release.

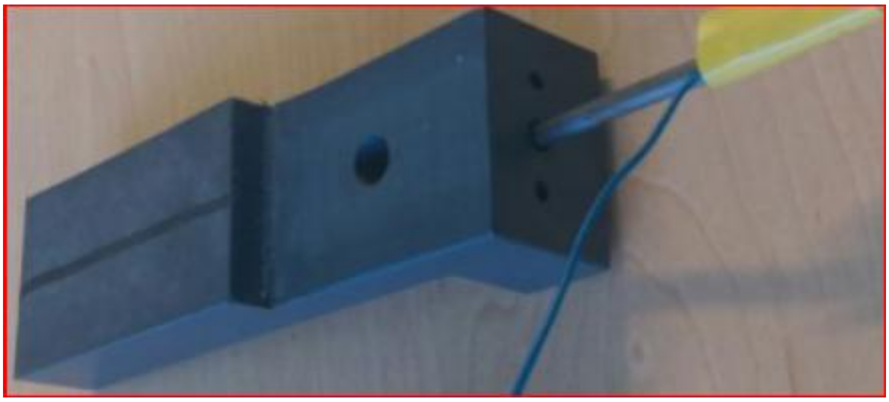

Figure 3.6: Picture of probe release, showing probe and pin holes.

The measurement experiment work was carried out using the electrical conductivity probe. The probe was designed with a bottom electrical sharp tip to allow the penetration of froth bubbles without breakage. The probe was designed in such a way that it has a sufficient weight to fall vertically into the flotation cell at a rate governed by Newton’s law. This design enables studies of the estimation of froth bubble size with depth. The probe was also designed in such a way that the probe head can be conductive and core to be no conductive. This required the probe head to be designed with steel that can also be connected to electrical pin. Figure 3.7 shows a side view of the probe showing its accessories such as the tip, electrical pin, nut, groove, head, and insulated body.

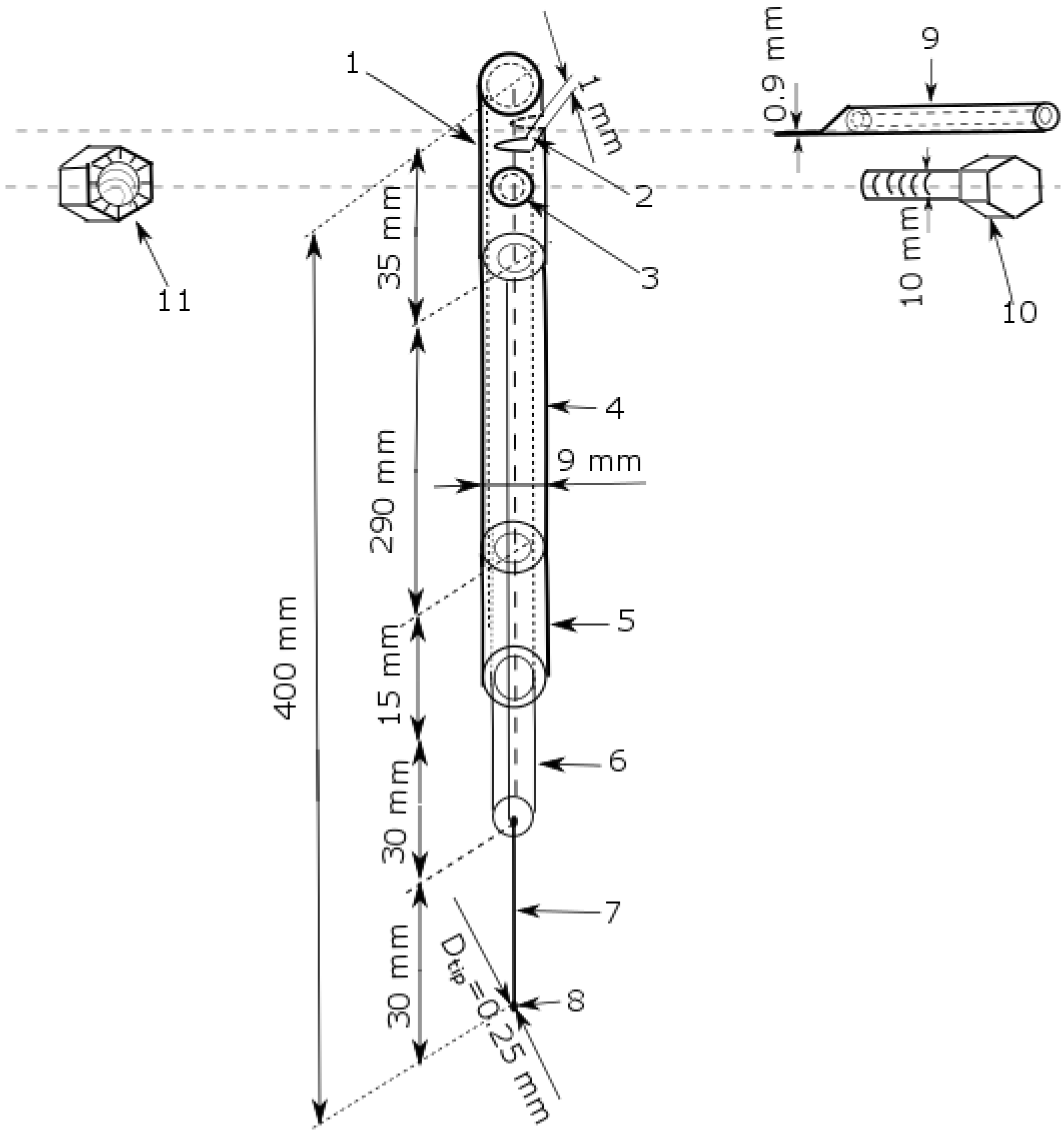

Figure 3.7: Detail drawings of the probe and their dimensions (1: probe head, 2: pin groove, 3: screw hole, 4: Rigid plastic tube, 5: PVC, 6: wire support (insulated part), 7: copper wire, 8: conductive probe tip, 9: Electrical pin, 10: bolt and 11: nut. See Figure 3.8

The probe is made from transparent perspex tube of diameter 9 mm. Both extremities of probe tube are designed to be connected by pieces of cylinder metal (probe head) of length 35 mm in steel and a cylinder of PVC (probe bottom) of length 15 mm with the same diameter as probe tube. The insulted rigid wire is made to be sealed into cylinder PVC (probe bottom) upon which an electrical wire of smaller diameter is carried. The electrical wire of probe tip can be changed based on how small or large the bubbles are in a froth phase. For example, the probe tip should have a diameter smaller than smallest bubble size in the froth phase in order to measure them$(i.e. probe\ \ tip\ \emptyset = 0.35\, mm)$. The hole and groove are made at probe head to carry a nut and an electrical pin, respectively. Figure 3.8 is a picture of the probe.

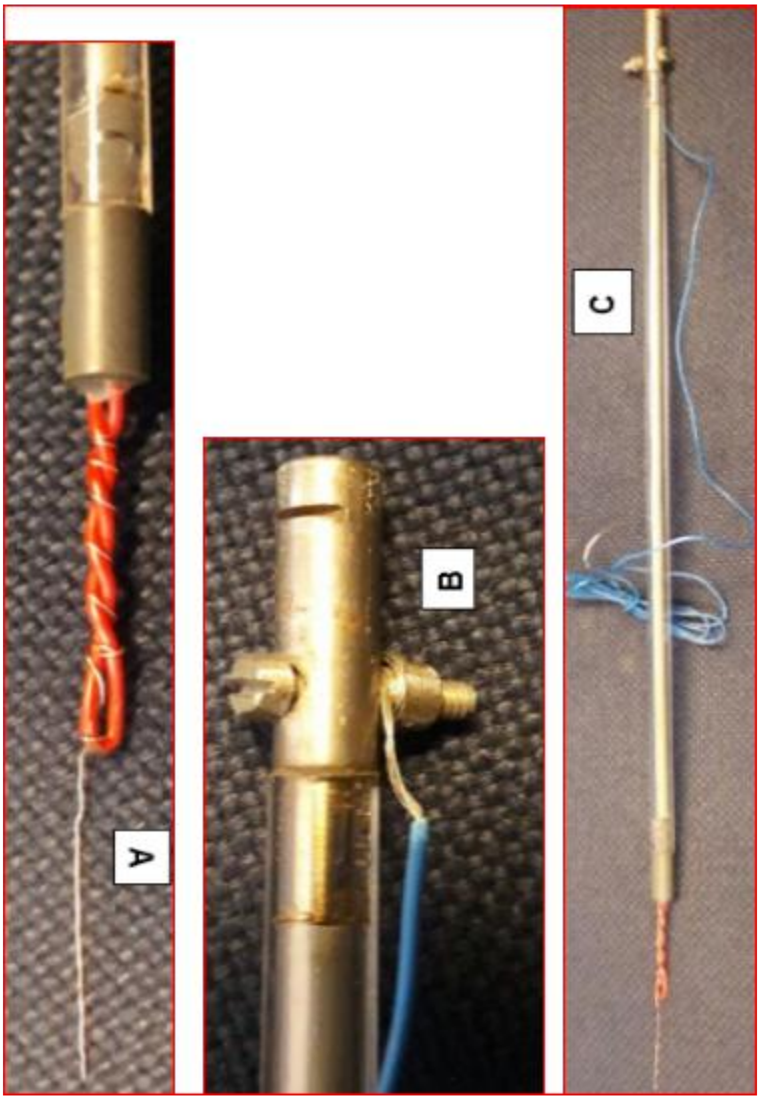

Figure 3.8: Picture of the assembled flotation cell. (A) Probe bottom, (B) probe top and (C) Entire conductivity probe.

3.3.2 Wits lab experimental setup

Under steady state flotation conditions, the measurement of intrabubble impact distances IIDs were performed using conductivity probe and camera in lab flotation cell as showed schematically in Fig.3.9. The column was a 200 x 200 mm cross-section and 400 mm high,

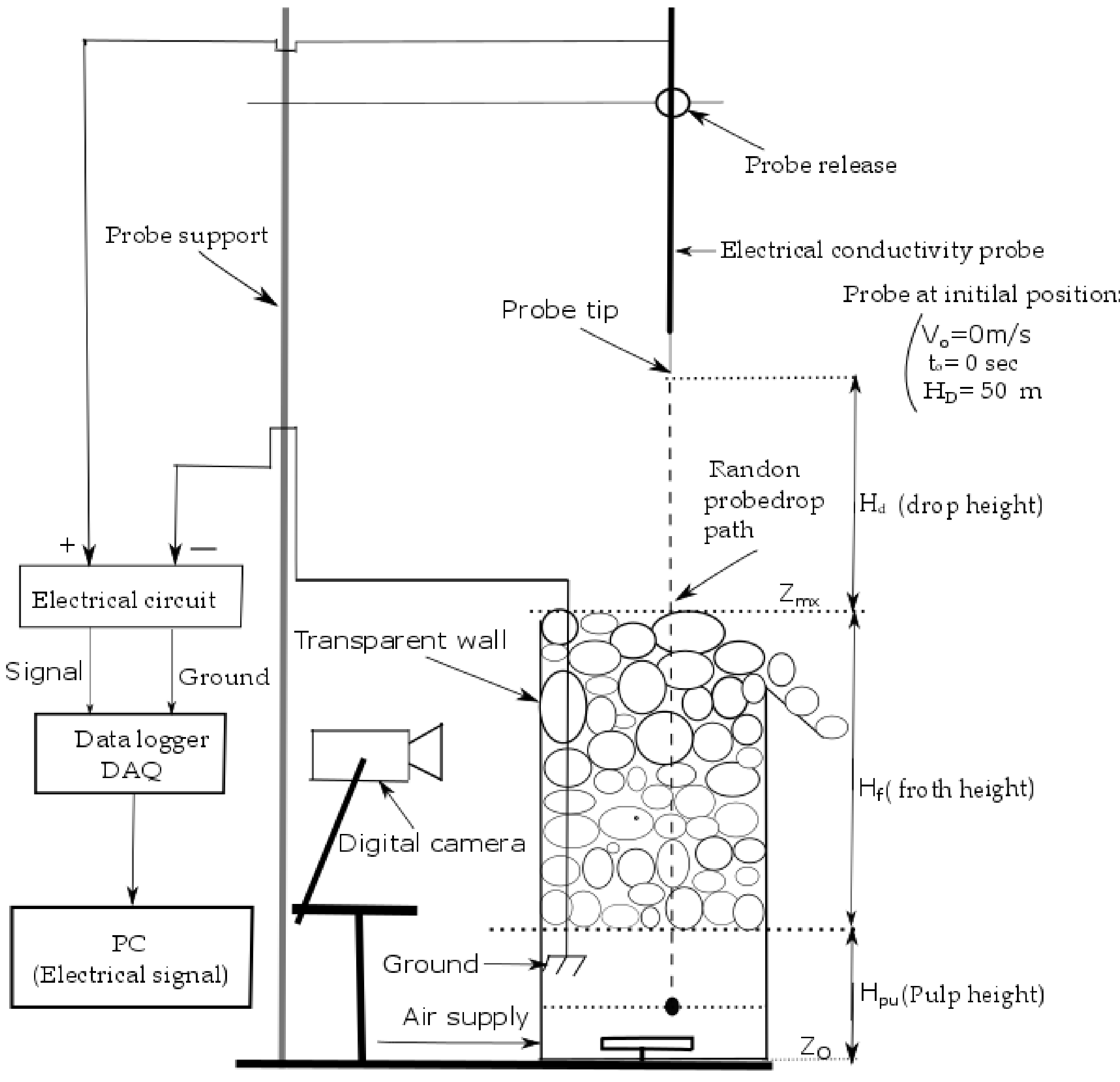

Figure 3.9: Schematic of the flotation experimental setup in the Wits lab for measuring froth bubble size distribution in froth phase.

made of clear perspex walls that had flat surfaces. One wall was chosen to possess a ruler from pulp-froth interface up to concentrate weir. This approach was made to set the scale for the accurate calculation of the actual bubble size (sauter mean bubble diameter). Then images of different froth phase sections in the cell were captured by high-speed digital camera. Good quality images of bubbles were then analyzed manually to obtain the froth bubble sizes. At the same time, intrabubble impact distances IIDs were also measured by electrical conductivity probe technique. According to this method, the probe was dropped at a given height of 50 cm through the froth phase. Sudden changes in output signal occur due to the successive contacts of probe tip and bubble lamellas as the probe moves through the froth bubbles. The output signal possessing information of froth bubble size is transferred into voltage signal through conductivity probe, and amplified via the data logger to output electrical signals as shown in Figure 3.9. The electrical signals are recorded by an analogue data acquisition-card. A specially written program based on Newton's equations has been performed to analyze the data of electrical signal to find the intrabubble impact distances IIDs. Results are kept into a file of data in a PC. In Mintek pilot plant, the intrabubble impact distances IIDs were measured in the secondary rougher bank of the flotation circuit. Conductivity probe unit was installed over the secondary rougher bank, just on top of impeller motor cover as seen in Figure 3.10 (A), (B). Same measurement procedure and conductivity probe were used in Minek pilot plant rougher cell. Direct measurement of probe bubbles could not be measured by the photographic technique because its random drops.

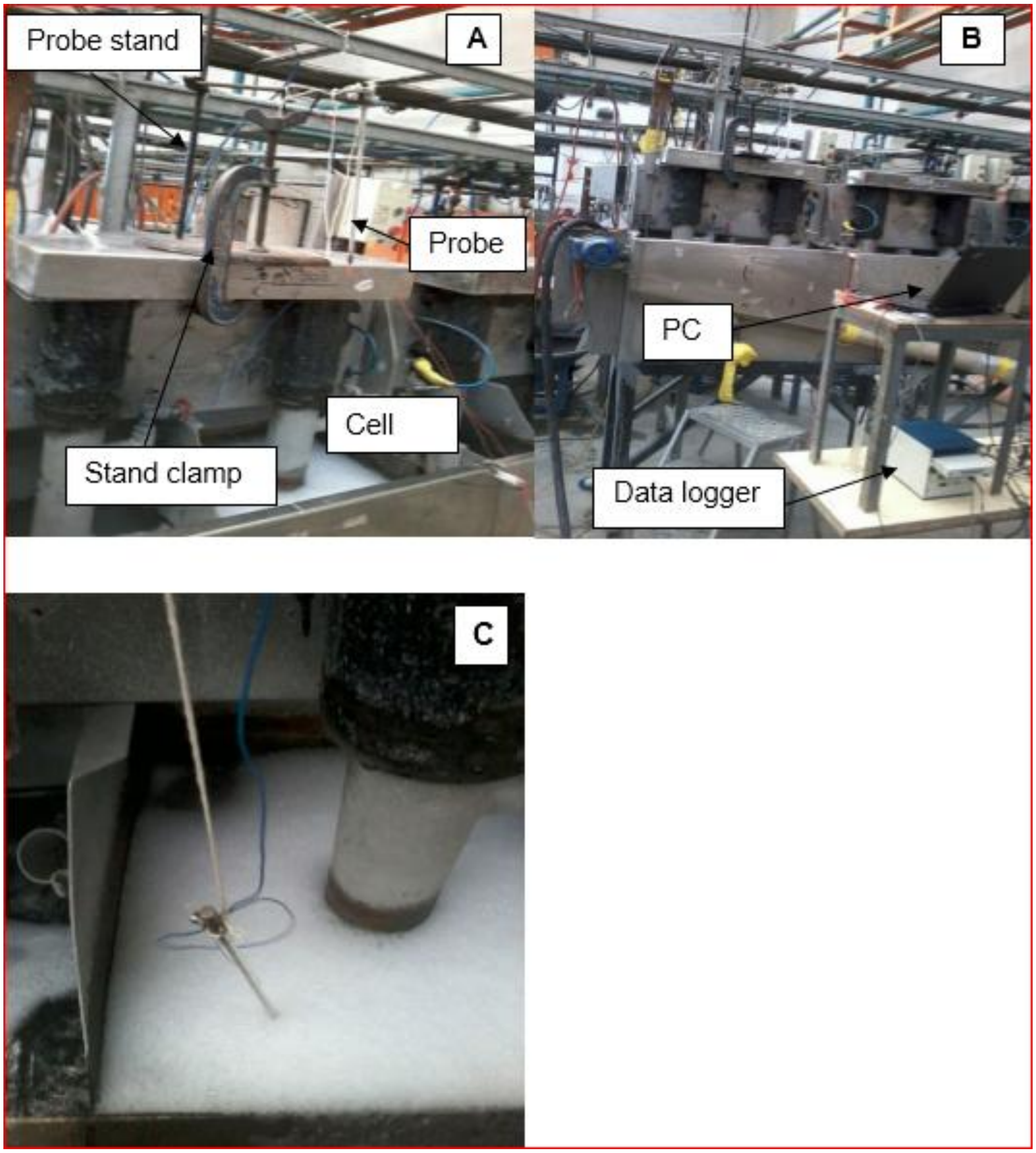

Figure 3.10: (A) Before measurement, probe at release, (B) Equipment (C): After measurement, probe in the froth phase.

After release of probe, it drops vertically into the cell towards the bottom. In these experiments, probe motion is managed using a strong cotton string to stop the probe tip between the pulp-froth interface and impeller zone (5 cm above the impeller zone), this is to avoid probe damage and other accidents. The probe is carried by a strong cotton string with an exact length to allow the probe to stop at desired level, see Figure 3.10 (C).

Chapter 4

Development of a model for predicting froth bubble size dristribution in the froth phase

Work in this Chapter and Chapter 5 was presented at the Mineral International Engineering Congress 2017 (Flotation 2017) in Cape Town, South Africa.

4.1 Introduction

In the previous work conducted by Bhondayi and Moys, (2014), a new method was developed to estimated bubble size distributions (FBSD) in the froth phase that can be compared to conventional photographic method for measuring FBSD. The measurement principle is dependent on the electrical conductivity of water and gas of the froth phase. The method was tested under different flotation conditions by recording the signals which have been successfully transformed into a proxy for froth bubble sizes. The proxy obtained was the average in order to represent the size of bubble due to random drop of the probe measurement technique.

The average IID was compared to actual froth bubble size obtained with photographic method. Hence, significant error of 31 % between the sizes obtained from the probe and photographic method. This is due to the fact that the random drop of the probe tip does not always cross the bubble through its centre. Therefore, the average IID does not relate the actual froth bubble size. This Chapter is focused on developing a method of estimating froth bubble size distribution FBSD from experimental measured intra bubble impact distribution IIDDs using the Wits Bubble-sizer.

4.2 Determination of intrabubble impact distance IIDD from bubble size distribution BSD

4.2.1 Assumptions

With the aim of deriving the intra bubble impact distance distributions IIDDs from bubble size distributions BSD, the following key basic assumptions are:

- Froth bubbles remain spherical
- The rise of froth bubbles are regarded to follow the vertical streamlines
- Froth bubbles are intercepted by a probe, they have random orientation
- A probe intercepts a bubble at random position with equal probability everywhere on projected surface area.
- The velocity of bubble in froth phase is negligible compared to a probe velocity.
- A probe path through a bubble is a vertical line
- When the probe crosses a bubble by intercepting two points, the distance between both points is the chord length of intra bubble impact IID.
- The probability of hitting a bubble in a cell is proportional to its equatorial surface area
- The probe tip travels through the bubble without breaking a bubble
- Probe tip diameter (0.35 mm) is extremely smaller than the bubble.
- The above assumptions are reasonable in order to derive the intra bubble impact distance IID from the model.

4.2.2 IIDD for a single bubble

As aimed early, the primary challenge that requires to be presented as follows: For a single bubble of size D_i 1) what are the positions of probe at both bubble top and bottom positions? 2) What is the cumulative distribution that a random drop of the probe measures an intra bubble impact distance IID having its distance less than or equal toL_j $(where\ \ L_j < D_i)$? and 3) What is the probability density that a random drop of the probe measures an intra bubble impact distance IID having its distance between $L_j\ and\ L_{j+1}(whereL_j\ and\ L_{j+1} < D_i)$?

It is relevant to mention that the key parameter within the problem is the intrabubble impact distance IID estimated by drop of the probe and identify a specific random IID itself. The IID of a random drop of the probe can be determined by the following sections.

4.2.2.1 Illustration of hitting a bubble by a random drop of the probe

Considering a case of spherical bubble of radius r_b and with its centre C at $X_c, Y_c\ and\ Z_c$ is contained in a cubical box with sides $2r_b$. Probes are randomly dropped into the cubical box as shown in Figure 4.1. The probability that a single probe hits a bubble is determined by the flowing equations as

$$f = \frac{S_{bubble}}{S_{box}} \tag{4.1}$$

Where S_{bubble} and S_{box} represent respectively the equatorial surface area of spherical bubble and cross sectional area of cubical box, given respectively as

$$S_{bubble} = \pi {r_b}^2 \tag{4.2}$$

$$S_{box} = (2r_b)^2 = 4{r_b}^2 \tag{4.3}$$

By substituting Eq.(4.2) and (4.3) into Eq.(4.1), Eq.(4.1) becomes

$$f = \frac{\pi {r_b}^2}{4{r_b}^2} = \frac{\pi}{4} \tag{4.4}$$

Eq. (4.4) is the probability of hitting a single bubble shown in Figure 4.1 with size r_b by a probe in box with side $2r_b$. The probability that a probe misses a bubble is found as

$$q = 1 - \frac{\pi}{4} \tag{4.5}$$

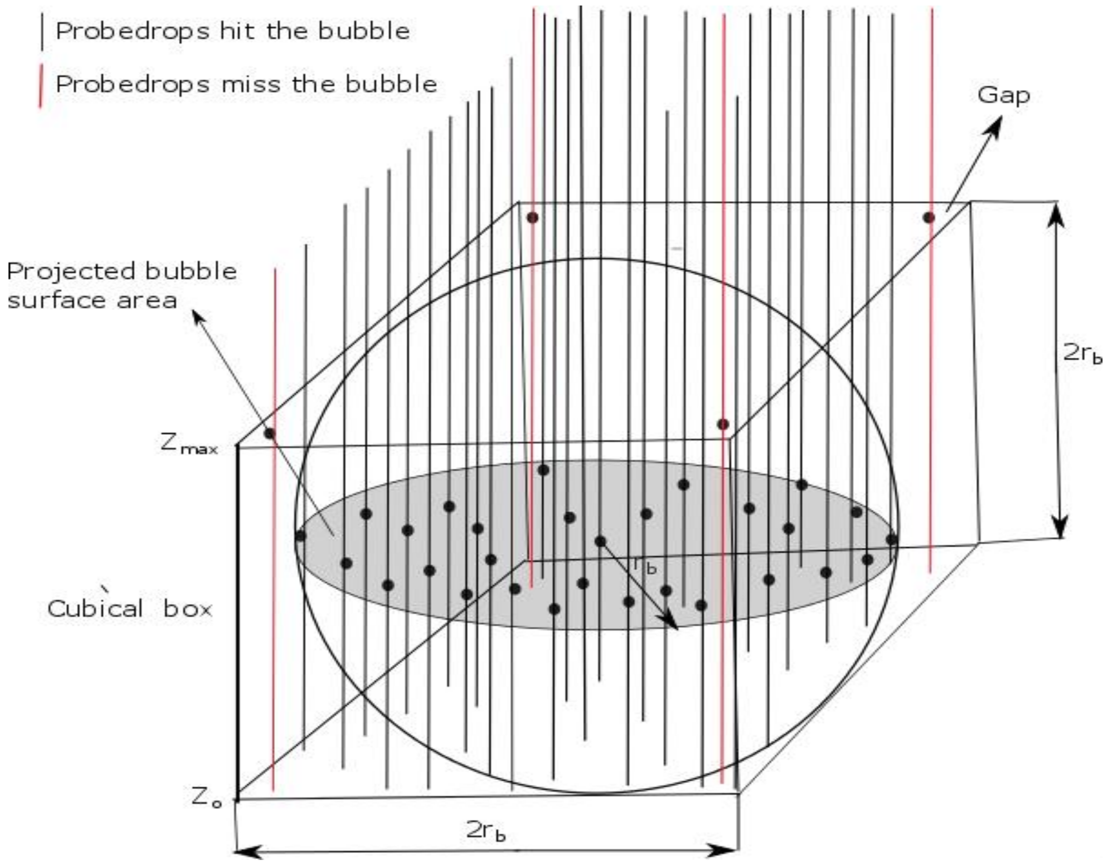

Figure 4.1: Illustration of representation of a single bubble in a cubical box with its probabilities of being hit and missed by random drop of the probe.

As we are discussing random measurements, the number of probes that hit a bubble inside the cubical box is variable after each series of drop of the probe. For example N number of series of 1000 drops of the probe will provide different number of probes hit the bubble due to random drop of the probe. The number of drops of the probe that hit the bubble will change at all times. But here we have early assumed that the number of drop of the probe that hit the bubble is proportional to its equatorial surface area of bubble. In this work, the number of drop of the probe should be significant in order to obtain enough number of IIDs. In practice, the number of random drop of the probe hitting the bubble will be approximately true with the calculated number of IIDs.

4.2.2.2 Probe position and bubble geometries in box

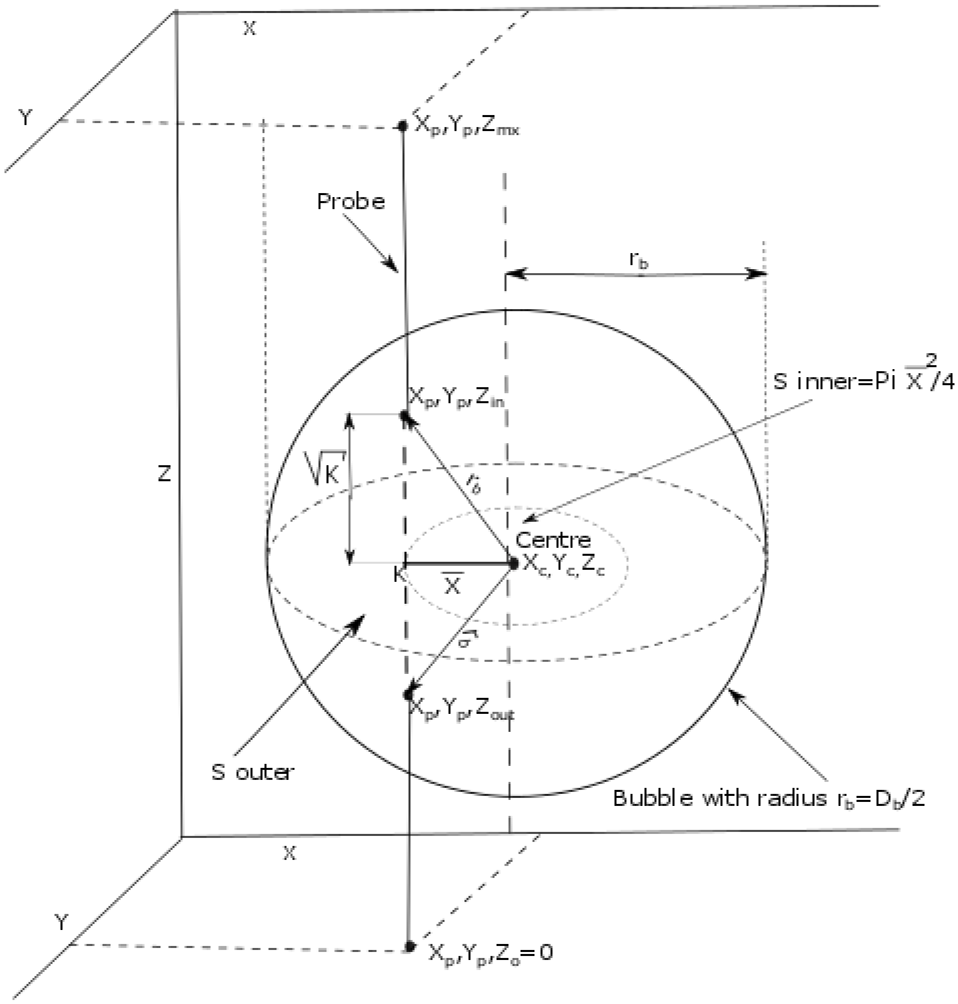

Figure 4.2: Representation schematic of geometric model of probe and bubble with radius r_b.(or r_i.) IIDs is generated by intercepting the both successive points of bubble films (top and bottom) at IID of $L_b\ or\ L_j = 2\ \ \overline{K}$.

Consider again a cubical box which is penetrated by random probe that is parallel to one of the lateral edges. Let us take a single bubble of diameter. D_i or $2r_i$and with its centre coordinates X_c, Y_c, Y_c would be hit by probe as illustrated in Figure 4.2. It is important to remind the reader that in this method, bubble is assumed to be a sphere. The Bubble is randomly cut by probe at two successive position points at Z_{in}, where the probe enters the bubble and Z_{out}, where the probe comes out of the bubble. The drop of the probe position Z_p can be deduced from the equation of a sphere given as

$$X_p - X_c\ ^2 + \ Y_p - Y_c\ ^2 + \ Z_p - Z_c\ ^2 = r_i{}^2 \qquad (4.6)$$

In Eq.(4.6), the only unknown factors are the positions of probe tips, at Z_p. The Eq.(4.6) can be rewritten as

$$(Z_p - Z_c)^2 = r_i^2 - \left[(X_p - X_c)^2 + (Y_p - Y_c)^2\right] \qquad (4.7)$$

Where $r_i^2 - \left[(X_p - X_c)^2 + (Y_p - Y_c)^2\right]$ can be replaced by K, Eq.(4.7) becomes

$$(Z_p - Z_c)^2 = K \qquad (4.8)$$

Therefore, the position can be found by equation below

$$Z_p = Z_c \mp \sqrt{K} \qquad (4.9)$$

Thus, the positions of probe-drop on top of bubble at Z_{in} can be determined as

$$Z_{in} = Z_c + \sqrt{K} \qquad (4.10)$$

And while on bottom of bubble at Z_{out} obtained as

$$Z_{out} = Z_c - \sqrt{K} \qquad (4.11)$$

Once the probe tip and bubble are geometrically known, the distance between two successive intersection points of bubble and probe can be found respectively at Z_{in} and Z_{out} generates an intra bubble impact distance IID shown in Figure 4.2:

$$IID = L_j = Z_{in} - Z_{out} \qquad (4.12)$$

Where $IID = L_j$ is the intra bubble impact distance (chord length).

It is clearly observed from Figure 4.2, the intra bubble impact distance IID, can also be found

$$IID = L_j = 2\sqrt{K} \qquad (4.13)$$

This can be written as

$$L_j^2 = 4K \qquad (4.14)$$

4.2.2.3 Cumulative distribution of intrabubble impact distribution IIDD

Let determine the cumulative distribution which described the way of finding an intra bubble impact distance IID less than or equal to L_j for defined bubble size D_j. Suppose that a single bubble with diameter D_i, is randomly intercepted N times of drops of the probe as indicated in Figures 4.2. From this, we can try to find the probability of IID less than or equal to L_j. The cumulative distribution function of IID, $P\ L_j$ is defined here as the number of intrabubble impact distances IIDs less than or equal to L_j over the total number of IIDs in bubble. It can be written as follows:

$$P\ L_j\ D_b \ = \frac{Number\ of\ IIDs\ less\ than\ or\ equal\ to\ L_j}{Total\ number\ of\ IIDs\ in\ bubble}$$

$$= \frac{S_{outher}}{S_{bubble}} \qquad (4.15)$$

Where S_{outher} is the surface area of outer ring and S_{bubble} is the surface area of bubble. These are well represented in Figure 4.2. The cumulative distribution is developed as

$$P\ L_j\ D_i \ = 1 - \frac{S_{inner}}{S_{bubble}} = 1 - \frac{\pi \overline{X}^2\ \ 4}{\pi r_i^2\ \ 4} \qquad (4.16)$$

The probe is seen in a 3-D projection of the bubble in Figure 4.2. Regarding the situation of a bubble with spherical shape of size D_i, the 2D projection of bubble gives a circle with the same size D_i. It must be mentioned that for any point in the circle, there is related with the point, a single IID for which the regarded point is the midpoint of the IID. Thus, choosing the random IID of a circle surface is the same to selecting a random point in the circle. A ring of the midpoints of the IID is a circle of dimensions as displayed in Figure 4.2. Any point on the bubble surface area coincides to an IID with length L_j and every IID with distance L_j. For an IID whose length is less than or equal to L_j it is important that its midpoint is the radius of inner area as a given in Figure 4.2. The probability of the probe tip that crosses a bubble at distance $\overline{X}$ from the centre of bubble could be modelled, once the probe tip position and bubble geometries are known as displayed in Figure 4.2 and represented by Eq.(4.9). Once the probe tip and bubble are geometrically defined, Pythagoras relationship relating the intra bubble impact distance (chord length) to the position of the drop of the probe with regards to bubble centre can be used. From Eq.(4.16), $\overline{X}$ can be found by Pythagoras using Figure 4.2 given as

$$\overline{X}^2 + \quad \overline{K} \ ^2 = r_i^2 \qquad (4.17)$$

Eq. (4.17), can also be written as

$$\overline{X} = 2 \ r_i^2 - \quad \overline{K} \quad ^{0.5} \qquad (4.18)$$

Substituting Eq. (4.18) into Eq.(4.16), yields

$$P \ \ L_j \ D_i \ \ = 1 - \frac{\pi \ \ r_i^2 - K \ \ \ 4}{4 \ \pi r_i^2 \ \ 4} \qquad (4.19)$$

After simplifying of Eq.(4.19), it gives

$$P \ \ L_j \ D_i \ \ = 1 - \frac{r_i^2 - K}{r_i^2} \qquad (4.20)$$

The arrangement of Eq.(4.20), produces

$$P \ \ L_j \ D_i \ \ = \frac{K}{r_i^2} \qquad (4.21)$$

By substituting Eq.(4.14) into Eq.(4.21), yields

$$P \ \ L_j \ D_i \ \ = \frac{L_j^2}{4 \ r_i^2} = \frac{L_j^2}{D_i^2} \qquad for \ \ 0 < L_j < D_i \qquad (4.22)$$

Since no IID larger than the size could be estimated: $L_j > D_i$

$$P \ \ L_j \ D_i \ \ = 0 \qquad for \quad \infty > \ L_j > D_i$$

Also the probability, that an estimated IID has a diameter less than or equal to the bubble diameter, is one $L_j = D_i$,

$P(L_j|D_i) = 1 \qquad for\ L_j = D_i$

Where Eq.(4.22) is the cumulative distribution function of IID, L_j is the intra bubble impact distance IID and D_i is the bubble size. Figure 4.5 illustrates the cumulative distribution of IID for single bubble. The intra bubble impact distance distribution IIDD for a single bubble is given as

$$P(L_j) = \sum_i P_{ij}(L_j, D_i) \qquad 4.23$$

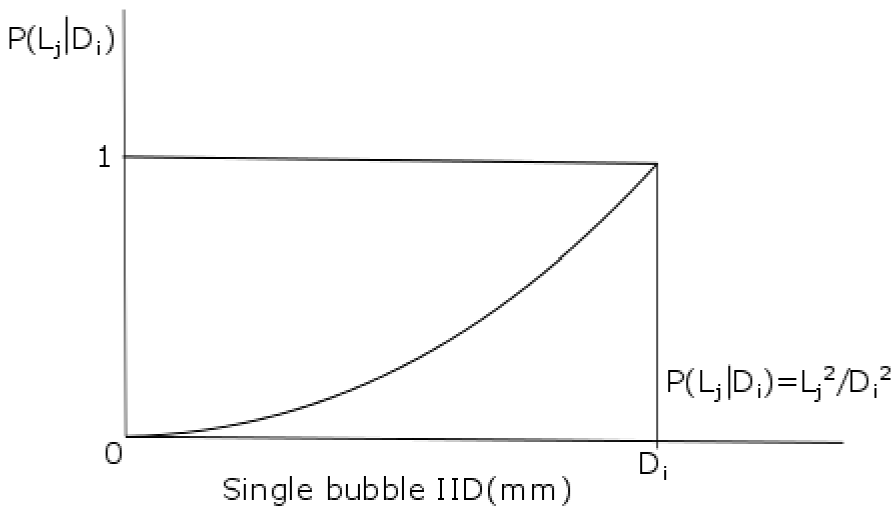

Figure 4. 3: Cumulative distribution of IID for a single bubble.

The curve of $P(L_j|D_i)$ for a single bubble responds as a parabolic function, which is illustrated in Figure 4.3. When the intra bubble impact distance L_j is equal to bubble diameter D_i, the cumulative probability $P(L_j|D_i)$ has a maximum value of 1.

4.2.2.4 Probability density function of intrabubble impact distribution IIDD

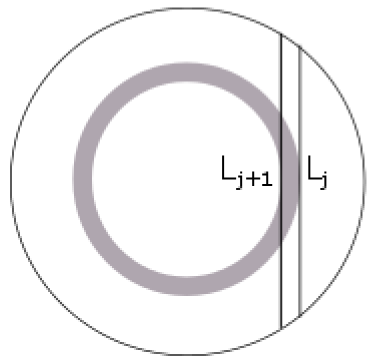

Figure 4.4: Representation of ring area regarded to estimate IID between L_j and L_{j+1}

The Probability density function of IID can be obtained by differentiating the above cumulative equation with respect to L_j as follows

$$p\ L_j\ D_i\ = \frac{dP\ L_j\ D_i}{dL_j} \qquad (4.24)$$

Replace Eq.(4.22) into Eq.(4.24), it gives

$$p\ L_j\ D_i\ = \frac{2\ L_j}{4\ {r_i}^2} \qquad (4.25)$$

Thus, the probability density function of IID, is found as

$$p\ L_j\ D_i\ = \frac{L_j}{2\ {r_i}^2} = \frac{2L_j}{{D_i}^2} \qquad for\ L_j < D_i \qquad (4.26)$$

Finally, $p\ L_j\ D_i$ is the probability of that the intra bubble impact distance is measured as a L_j when the probe intercepts a bubble of diameter D_i. The curve of $p\ L_j\ D_i$ for a single bubble responds as linear function, which is illustrated in Figure 4.5. When the intra bubble impact distance L_j is equal to bubble diameter D_i , the probability $p\ L_j\ D_i$ has a maximal value of $2/D_i$.

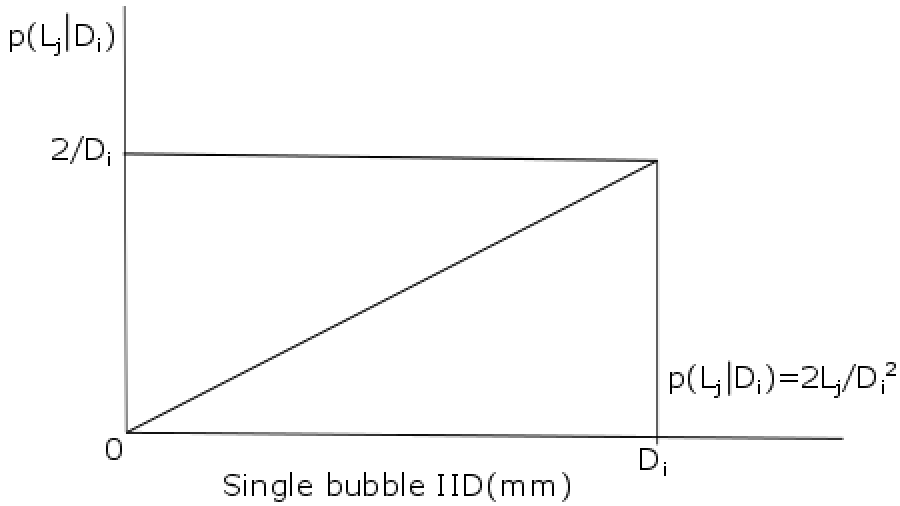

Figure 4.5: Probability density function of IID for a single bubble.

Eq.(4.26) is the probability density function $p\ \ L_j\ \ D_i$. Rather, the probability of estimating an IID with length between $L_j\ and\ L_{j+1}\ \ \ L_j\ <\ L_{j+1}$ leads to the ratio of the shaded region area to the total of projected bubble surface area given

$$p\ \ L_j\ \ D_i\ \ dL = P\ \ L_j + \Delta L\ \ D_i\ \ - P\ \ L_j\ \ D_i \qquad 4.27$$

The intra bubble impact distance distribution IIDD for a single bubble is given as

$$p\ \ L_j\ \ =\ \ {}_i\, p_{ij}\ \ L_j, D_i \qquad 4.28$$

4.2.3 Mixture of bubbles

In the previous section the problem of determining the positions of probes and calculating the probabilities of measuring an IID at specific size and within a particular size range, respectively was discussed. Let us extend the discussion to a cubical box within which the bubbles of different sizes are fully dispersed as illustrated in Figure 4.6. The probability of the fraction of the total number of bubbles which would be measured as having IIDs less than or equal to L_j and between sizes L_j and L_{j+1} is of interest. It is expected that the number of IIDs sampled by the drop of the probe are significantly high sufficient that the mentioned assumption is valid. Bubbles in any process system will have a certain size distribution. When an intra bubble impact distance, L_j is estimated by means of a probe, it will be from a certain bubble of diameter D_i larger than L_j, because a bubble of diameter smaller than L_j cannot provide the IID of L_j.

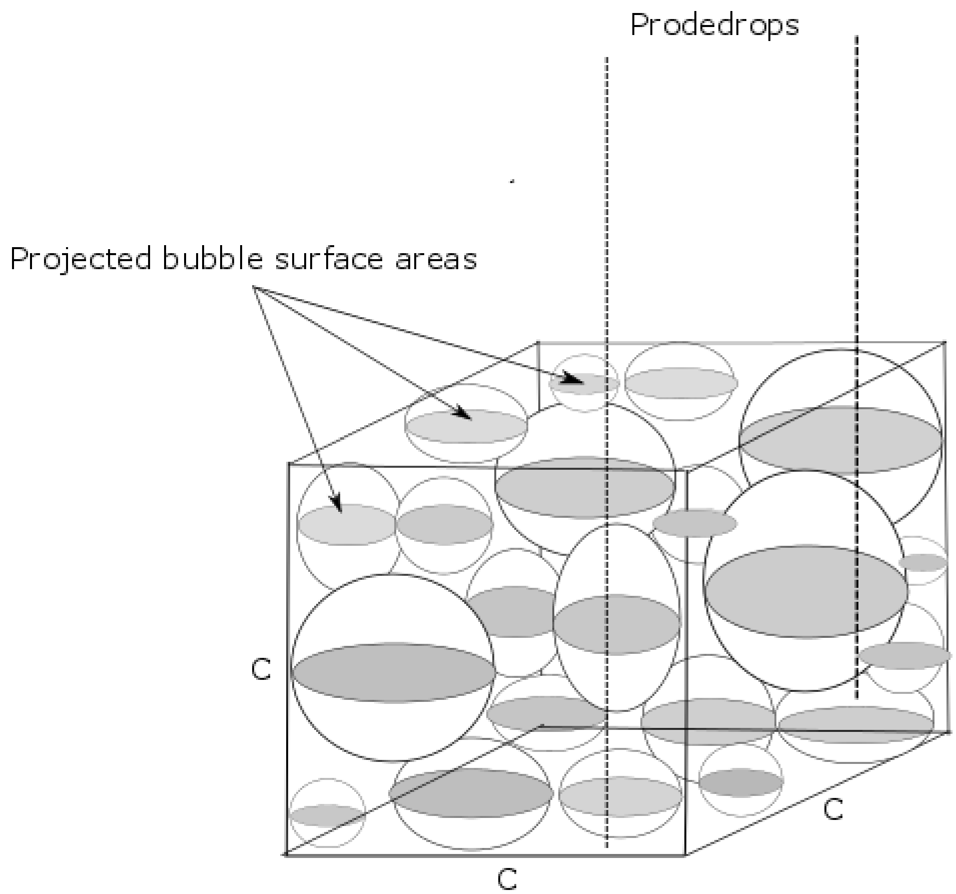

Figure 4.6: Illustration of realisation of bubbles located inside a cubical box in which is penetrated by random drop of the probe.

4.2.3.1 Prediction of bubble size distribution

The size distributions of bubble in the process system like froth flotation particularly in froth phase is not known. It may be predicted by analysis with some types of distribution models such as normal, Log normal, Weibull, uniform, etc. Typically, the size of bubbles or particles can follow a normal distribution or lognormal distribution, $p\ D_i$ with two parameters μ an δ (Guillermo et al, 2006; Brown and Pitt, 1972. Limpert, et al., 2001; Matsuura, 1984; Jillavenkatesa, 2001; Metti de Oliveira, 2003). A predicted bubble size distribution BSD represented in the form of two normal parameters is adopted. This assumption will be confirmed with the experimental results later in this work. It can be calculated as

$$p\left(D_i\right) = \frac{1}{\sigma\sqrt{2\pi}} e^{-\left(D_i-\mu\right)^2 / 2\delta^2} \qquad (4.29a)$$

Where $p\left(D_i\right)$ is the probability density function of diameter, D_i is the diameter, μ and δ are regarded as fitting parameters defining the model distribution respectively standard deviation and average. The average μ is the line perpendicular to diameter axis shown in Figure 4.7. We can see that the normal distribution is symmetrical about the mean value μ.

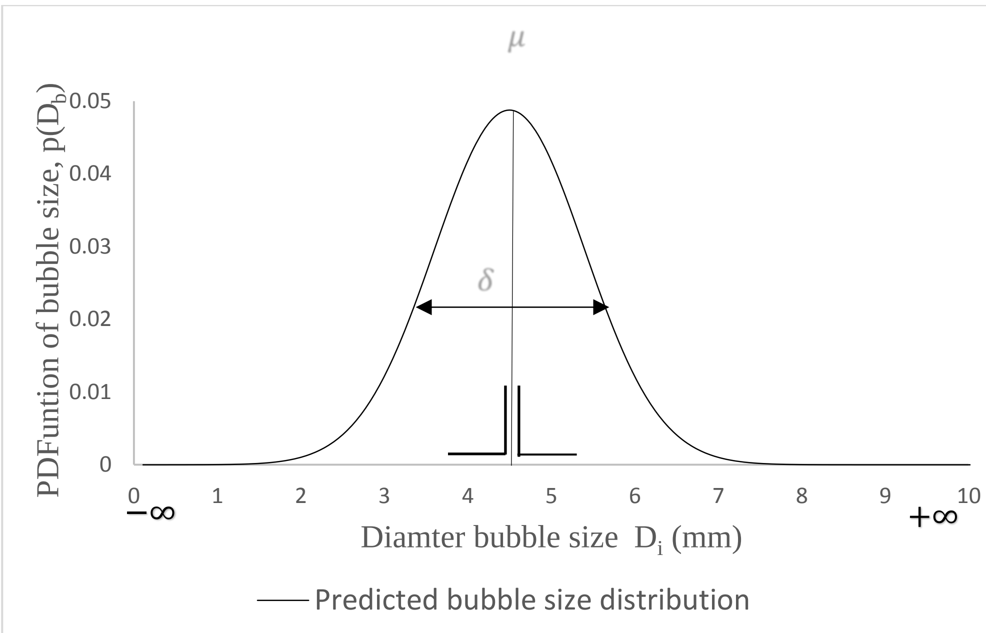

Figure 4.7: Predicted bubble size distribution curve by Normal – Distributions over continuous range of bubble diameters

Figure 4.7 was calculated from average diameter, $\mu = 4.5$ and standard deviation $\delta = 0.9$. The entire bubble population is distributed between $-\infty$ and $+\infty$. The area under the curve between $D_{-\infty}$ and $D_{+\infty}$ should be unity. If the parameter D_i is defined in terms of standard units, $D_i = \left(D_i - \delta\right)/\mu$, Eq.(4.29a) is substituted as follows

$$p\left(D_i\right) = \frac{1}{\delta\sqrt{2\pi}} e^{-\frac{1}{2}\mu^2} \qquad (4.29b)$$

The graph of normal distribution model depends on two factors, the average diameter and the standard deviation. The average diameter μ determines the location of the center of the data, and the standard deviation defines the spread of the data. When the standard deviation δ is larger, the curve is short and wide; when the standard deviation δ is small, the curve is tall and narrow (Spiegel, 1972)

4.2.3.2 Discretisation of bubble size

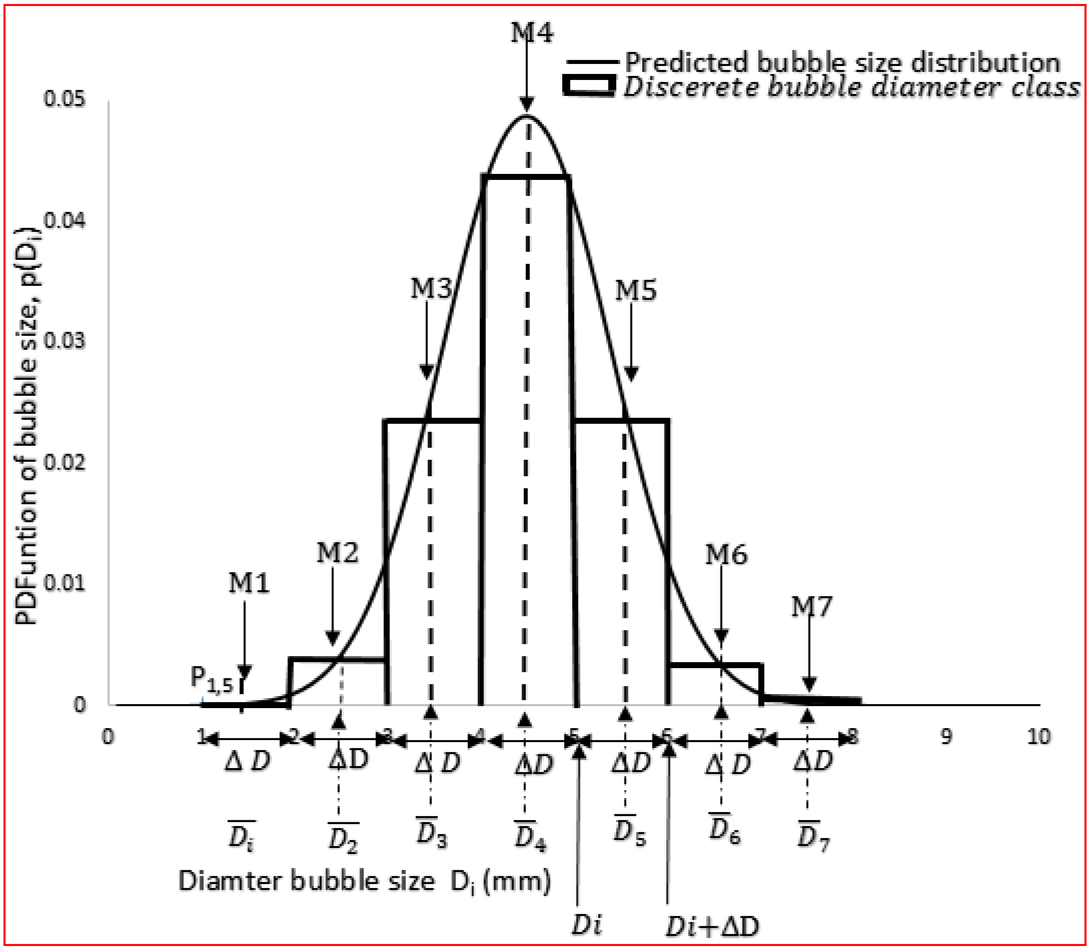

Figure 4.8: Discretization of bubble size class distributions and their characteristics.

The discrete (or histogram) form is helpful for practical analysis of actual data. The classes can be firstly constructed under the predicted size curve. The continuous range of the probability density distributions, from 0 to D_{mx} is divided into M diameter classes with equal width ΔD. The classes are assumed to be uniform in size with range equal to ΔD , $\Delta D = D_{mx}\ M$ and the domain regarded extending from 0 to D_{mx}. It is important to describe a size of representative, wherein, each froth bubble contained in the class could be assumed to be of the corresponding representative size. In this model, the bubble size here was taken as the average D_i of minimal and maximal boundaries. This is given as:

$$\overline{D}_i = \frac{1}{2} \quad D_i + \quad D_i + \Delta D \qquad (4.30)$$

The classes are constructed from the smaller to larger sizes. In the previous section, the challenge of calculating the probability of estimating the IID less than or equal to specific distance and the probability of measuring an IID in a specific size width with boundaries L_j *and* L_{j+1} was discussed. Now the number of bubbles is significant, the cumulative probability obtained for a single bubble may be applied to the amount of the total number of bubbles that can be measured with an IID less than or equal to L_j and can be measured as a distance between sizes L_j *and* L_{J+1}. In this work, it is expected that the number of IIDs recorded by the drop of the probe is sufficiently large enough to obtain an accurate size distribution.

Therefore, it is relevant to assume that all bubbles in the same diameter class with boundaries D_i *and* $D_i + \Delta D$ have the same characteristic diameter $\overline{D}_i$ as shown in Figure 4.8. Let us assume bubble size distribution can be either a histogram or a density function. Probability density function accurately shows how the bubbles are distributed at any size, whereas the histogram splits the whole range into classes and shows the number of bubbles in each bubble diameter class. Both are represented in Figure 4.8.

4.2.3.3 FBSD-IIDD of mixture of bubbles

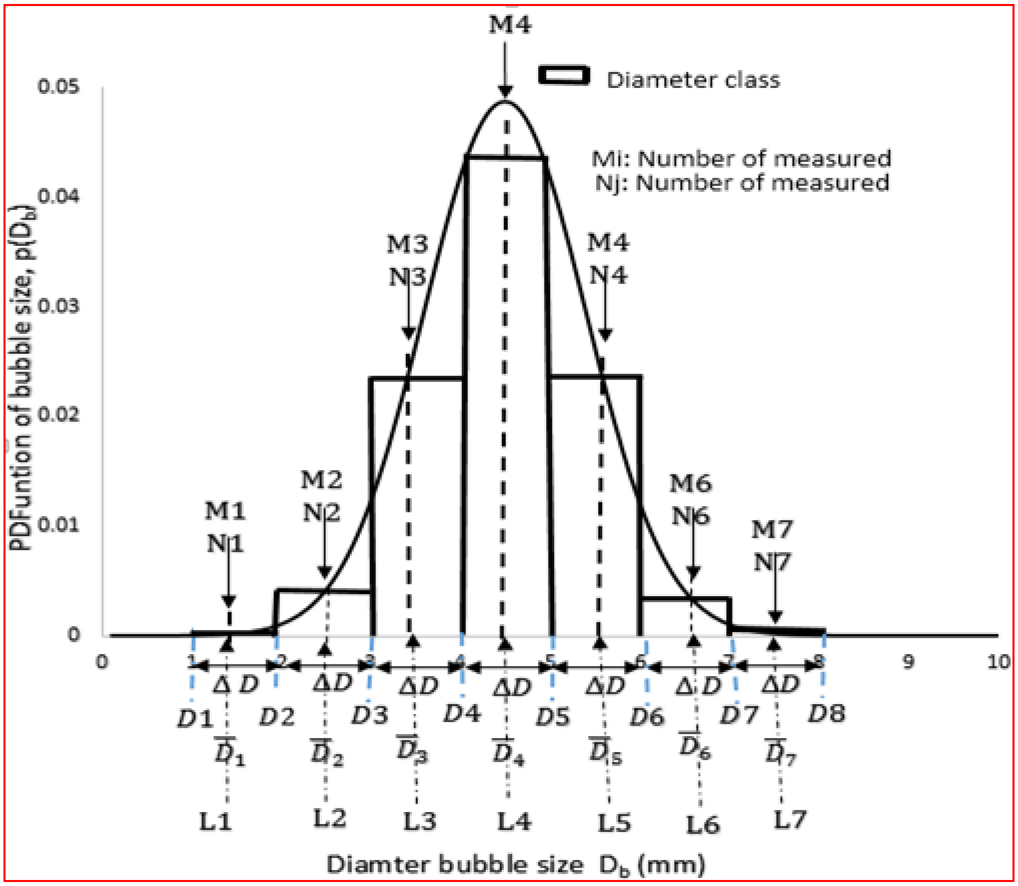

Figure 4.9: Developed technique for calculating intra bubble impact distance distribution IIDD from constructed discrete bubble size class distributions.

In this model, the size of the class $\overline{D}_i$ is considered to be equal to IID, L_j. The first and last size classes are obtained by adjusting the model parameters in order to fit the all range of experimental data. The class sizes are constructed by referring the whole experimental data range. Each class size can produce its own IID distribution as demonstrated in Figure 4.10. The distribution curve of IIDD in i^{th} class resemble to that obtained for single bubble. Let the number of bubbles measured in the i^{th} class for a general BSD be M_i and for a IID be N_i. Let the fraction of the total bubbles that contained in the i^{th} class estimated

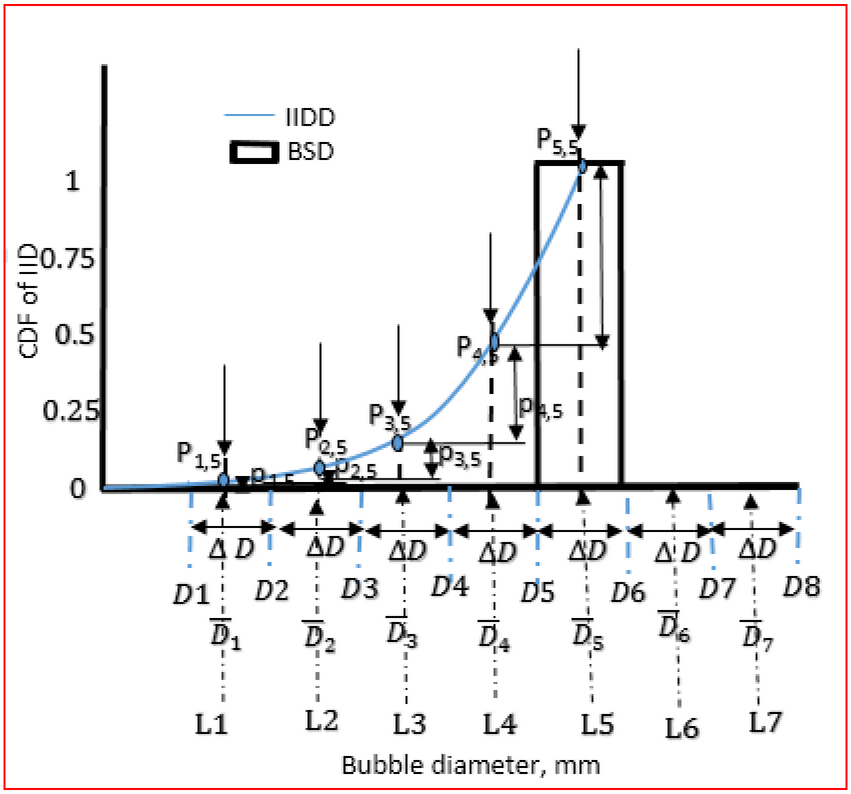

Figure 4.10: Illustration of constructing the IIDD distribution (blue line) the 5^{th} diameter class.

as having a specific IIDs of L_j, be denoted by $P\ L_j\ D_i$. As described in the previous section, the probability of estimating an IID in the j^{th} class for a bubble belonging to the i^{th} class can be written as $p\ L_j\ D_i$. Let the number of the bubbles in the i^{th} class be Q_i and represented by size D_i and the total bubble numbers estimated by a probe be Q_T. Theoretically, the probability density function of the intrabubble impact distance distribution IIDD obtained from bubble size distribution BSD, $p\ L_i$, can be described by following the expression:

$$p\ L_i\ = \int_0^{\infty} p\ L_j\ D_i\ p\ D_i\ dD_i \qquad (4.31)$$

Where $p\ L_j\ D_i$ is the conditional probability density function of obtaining an IID of size L_j from the bubble with size D_i. Typically, the bubble sizes can follow a normal distribution or lognormal distribution, $p\ D_i$ with two parameters μ and δ. The two model parameters could be optimized utilizing a least-squares technique such that the results of Eq.(31) offers a $p\ L_j$ that closely fits the measured intrabubble impact distance distribution obtained from the drop of the probe, $p\ L_j\ _{meas}$. However, a overalll analytical results to Eq.(31) is impossible, although this is exist for some particular cases (Liu and Clark,1095; Santana; 2000; Liu and Clark; 1996). A numerical procedure is then considered to estimate the integral in Eq.(31). This estimation may require the range of size of the size distribution of bubble $p\ D_i$. Since $p\ D_i$ is not known, a range of size wide sufficient to cover the whole $p\ D_i$ will require to be assumed. Additional approach is to consider that the range of of $p\ D_i$ is the same as that of $p\ L_j\ _{meas}$. M number of classes with width ΔD and midpoint sizes $\overline{D}_{1,\ldots,M}$ can be generated in the considereded range of $p\ D_i$. The intra bubble impact distance IIDD from BSD could then be estimated by

$$p\ L_j\ = \sum_{j=1}^{M} p\ L_j\ D_i\ p\ D_i\ \Delta D \qquad (4.32)$$

Thus, Eq.(4.32) can be utilized to determine the intrabubble impact distance IIDD in the j^{th} class for a population of bubbles. The Eq.(32) can also be written in the matrix form

$$[L]=[A_{ij}][D]\ \Delta D \qquad (4.33)$$

Where $[A_{ij}]$ is a $p\ L_j\ D_i$, [L] is $p\ L_j$ for a discrete interval of L and [D] is $p\ D_i$ for a discrete interval of D_i.

The overall IIDD for a population of bubbles may be obtained by summing the IIDD in each class in the IIDD. Eq.(4.32) can be applied in the i^{th} class (D class) for a general BSD.

Finally, the bubble size distribution BSD can be found utilising least-squares technique by optimizing the parameters of $p\ D_i$ such that the estimated $p\ L_j$ closely fits $p_{ex}\ L_j$. In this method, the intra bubble impact distance distributions IIDDs $p\ L_j\ _{pred}$ is predictted from the model bubble sizes distribution $p\ D_i$. This will be compared with experimental IIDD $p\ L_j\ _{meas}$ measured using probe.

Therefore, the difference between both $p(L_j)_{pred}$ and $p(L_j)_{meas}$ is considered as an error. The μ and δ of the bubble size distributions can be estimated by minimizing the error between the predicted IIDD $p(L_j)_{pred}$ and experimental IIDD $p(L_j)_{meas}$ in the form of sum squared error SSE using Least square regression, given as

$$SSE(\mu,\delta) = \sum_{j}^{N} \left(p(L_j)_{pred} - p(L_j)_{meas} \right)^2 \qquad (4.34)$$

Where $p_{Meas}(L_j)$ is the experimental IIDD, $p(L_j)_{pred}$ is IIDD predicted from the model, μ and δ are fitting model parameters average diameter and standard deviation, respectively.

The sum squared error SSE is performed by the Excel Solver tool to minimize the error between the experimental and model IIDDs. Graphical comparison between the model and experiment curves will be performed with purpose to assess the performance of the model. It is mentioned that the selection of N and M may influence the accuracy of results. It is obtained that a minimum number N of 20 is required to found an accurate results. Technically, $p(D_i)$ does not require to follow a specific distribution type. However, the optimization problem arises especially when the number of classes, M, in $p(D_i)$ is large. Nonetheless, the probability distribution function type utilized can still be specified basing on the application and system. The bubble size distribution BSD is also proposed to be obtained by Inversion Matrix technique. For the backward determination of the BSD, (D_i) from the IIDD, $p(L_i)$, which is given by the measured data, the bubble size distribution, (D), can be successfully computed via the Inversion of the square matrix of M=N as illustrated bellow

$$\begin{bmatrix} p(D_1) \\ p(D_2) \\ p(D_3) \end{bmatrix} = \begin{bmatrix} A_{1,1}{}^{-1} & A_{1,2}{}^{-1} & A_{1,3}{}^{-1} \\ 0 & A_{2,2}{}^{-1} & A_{2,3}{}^{-1} \\ 0 & 0 & A_{3,3}{}^{-1} \end{bmatrix} \begin{bmatrix} p(L_1) \\ p(L_2) \\ p(L_3) \end{bmatrix} \qquad (4.35)$$

Table 4.1: Probability of IIDDs obtained from Bubble size distribution BSD

$p\ \overline{D}_1$		$p\ L_1\ \overline{D}$	0	0	$\sum_{j}^{N} p\ L_j\ \overline{D}_1$	$p\ L_j, \overline{D}_1$
$p\ \overline{D}_2$		$p\ L_1\ \overline{D}$	$p\ L_2\ \overline{D}$	0	$\sum_{j}^{N} p$	$p\ L$
$p\ \overline{D}_3$		$p\ L_1\ \overline{D}$	$p\ L_2\ \overline{D}$	$p\ L_3\ \overline{D}$	$\sum_{j}^{N} p$	$p\ L$

It is important to underline that the number of IIDD classes, N, is not required to fit the number of bubble size classes M as reported by Bin Hu (2005). The Eq.(4.35) can be utilised to build the triangular matrix as indicated in Table 4.1. The triangularity forms due to A is zero when $i < j$, for example an IID L_j can only come from bubble of diameter D_i greater than L_j. Therefore, the matrix could be solved sequentially to obtain the unknown D_i . The triangular matrix is obtained because the intra bubble impact distance can be given from the diameter classes with diameter larger than IID class. It can be clearly shown in Table 4. 1.

4.3 Conclusion

In this Chapter a new model that can estimate the actual froth bubble sizes FBSD from intra bubble impact distance distribution measured by dropping of the probe in flotation froths has been developed. The model can predict the changes in bubble size along froth height as affected by any parameters such as frother concentration, gas flowrate, etc. Firstly, the concept of the method was been developed for a on single bubble. In this work, intra bubble impact distance distribution IIDD was derived from the BSD. Secondly, the case was extended to a mixture of bubbles. The model requires only two adjustable parameters to fit the experimental measured IIDD. This may be achieved using a least-squares method such that the solution of model intra bubble impact distance distribution that closely matches the experimental intra bubble impact distance distribution obtained from the drop of the probe. The inversion matrix method in the form of square matrix was also developed to convert the measured intra bubble impact distance distribution into bubble size distribution. The model is validated in the following Chapter.

Chapter 5

Froth bubble size distribution analysis from measured intrabubble impact distance distribution

Work in this Chapter and Chapter 4 was presented at the Mineral International Engineering Congress 2017 (Flotation 2017) in Cape Town, South Africa.

5.1 Introduction

A theoretical model developed in Chapter 4 is applied to determine froth bubble size distribution from measured intra bubble impact distance distributions IIDDs obtained from electrical signal analysis. In the present Chapter, the model is applied to different IIDD measured under different froth conditions.

5.2 Schematic algorithm for application of a stereological technique to obtain estimates of froth bubble size distribution.

Estimation of froth bubble size distribution is obtained by using the following schematic algorithm. This routine circuit consists of matching the experimental data with two model parameters.

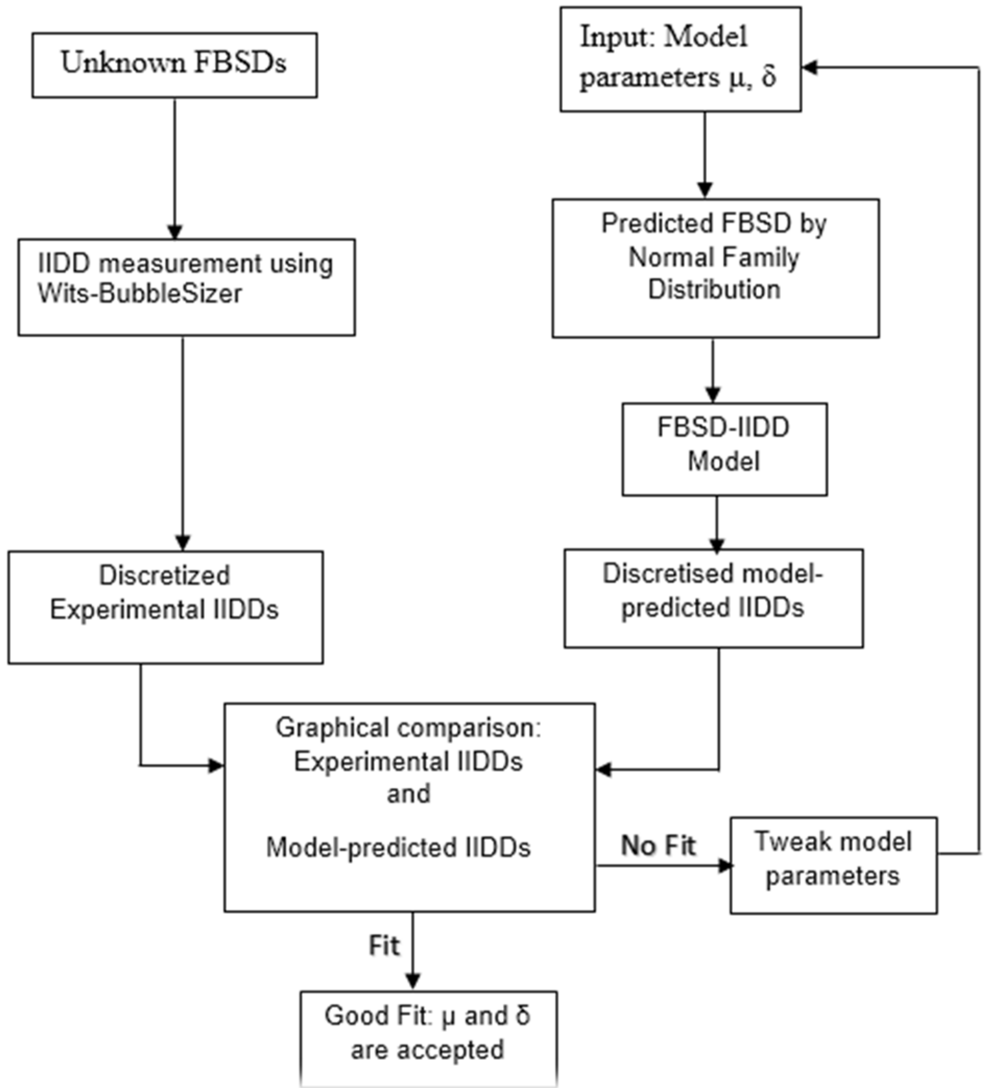

Figure 5.1: Schematic algorithm model for froth bubble size distribution (FBSD) analysis.

5.3 Results and discusions: Validation of the model

5.3.1 Determination of distribution model type

The process systems using air bubbles, have a certain distribution type which is unknown. The appropriate selection of distribution function model depends on the process system. Based on current information we identify a suitable distribution function for froth phase bubbles. The following are considered, a lognormal, normal, Gamma and Weibull distribution functions are commonly utilised to match the bubble size distributions. However, the chosen distribution function could not be the suitable distribution function to represent froth bubble size distribution FBSD in a system. Hence, the accuracy of the model is also evaluated theoretically when the chosen distribution function is not the same as the experimental intra bubble impact distribution IIDD.

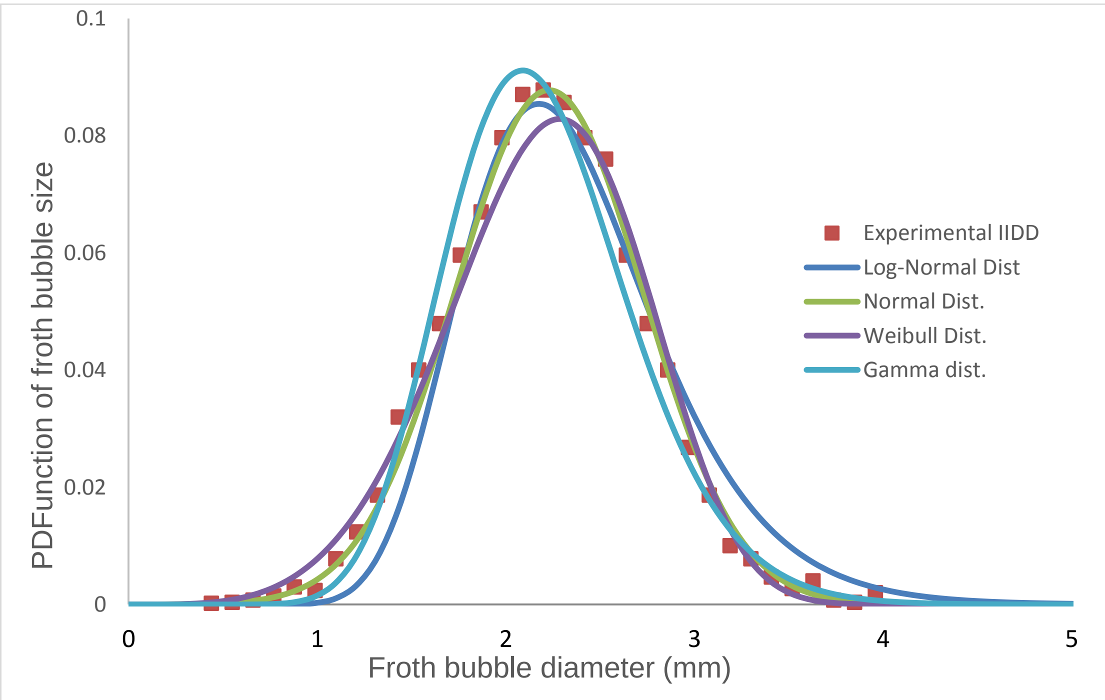

Figure 5.2: Comparison between the predicted IIDDs (Normal, lognormal Weibull and gamma distribution) and experimental IIDD.

A log-normal distribution, normal distribution, Gamma distribution, Weibull distribution functions are tested to predict froth bubble size distributions FBSDs by matching their IIDDs to the experimental IIDD as shown in Figure 5.1. In Figure 5.2, five curves show the probability distribution of intrabubble impact distance distributions. Among which the point represents the probability density of experimental IIDD in 0.11 mm intervals, e.g., the probability of IID from 0.33-0.44 mm is represented by the scatter labelled 0.385 mm. The last points indicates the probability of IID exceeding 3.96 mm.

The difference is large enough to make a clear distinction between the four distributions by fitting the experimental IIDD. The normal distribution provides the closest match to the experimental IIDD. Similar observations have been provided by Busciglio et al.,

2010. IIDD predicted from Weibull distribution function clearly indicates a deviation from smaller and middle IID ranges. The Weibull distribution does not show a good agreement with the experimental IIDD. Significant errors are present at the extremities when the Gamma distribution is used. Similar trends is observed with log normal distributions. According to log normal, Weibull and gamma do not gives better fit to experimental IIDD. Good fit is found with normal distribution in all range of IIDs. The experimental IIDD are found to follow a two-parameter normal distribution function. There is not sufficient evidence to show that the normal distribution is always preferred to other distributions. The main disadvantage of the normal distribution is that its range includes negative numbers. In only one case was there a significant probability for negative numbers.

5.3.2 Estimation of froth bubble size distribution as a function of froth height in transparent Wits lab flotation cell

The methodology proposed in this study was first validated for froth bubbles as a function of froth height in a Wits lab transparent flotation cell. Firstly, froth bubble sizes were obtained from images using a calibration scale at focusing transparent window by conventional photographic method.

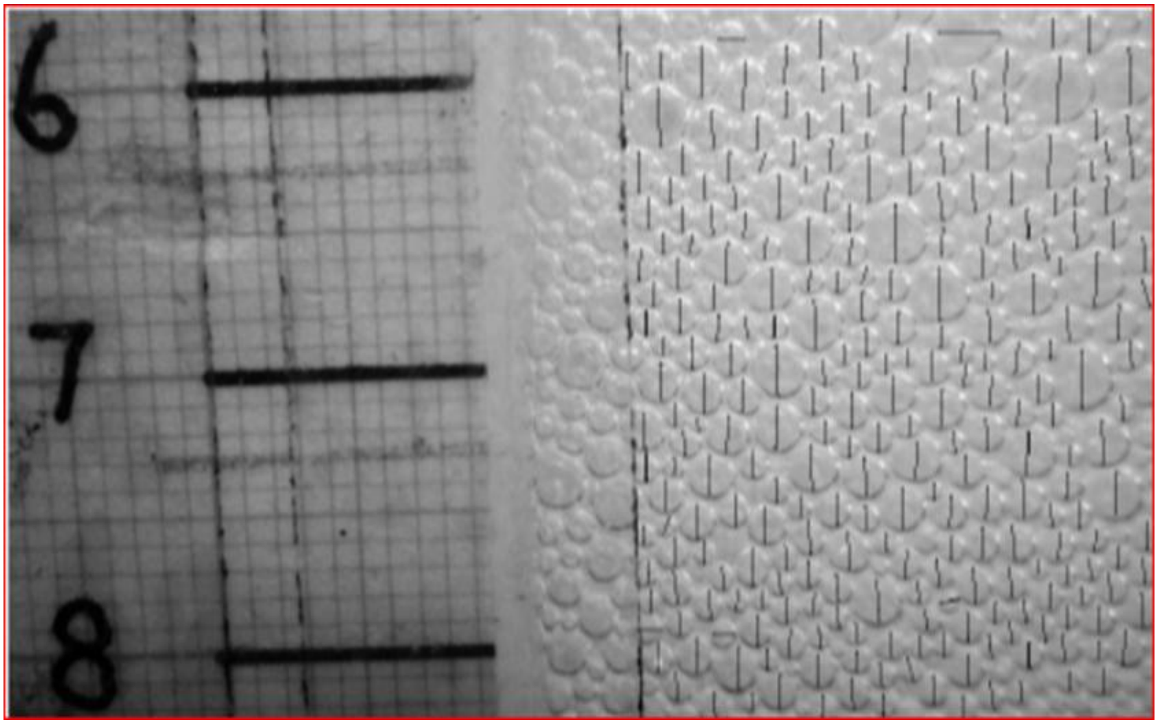

Figure 5.3: Illustration of manual bubble size measurement using ImageJ with lines indicating measured diameters (Bhondayi and Moys, 2014).

It is considered that froth bubbles are spherical based on image of froth bubbles as illustrated in Figure 5.3. The images captured by the digital camera, FBSD were prepared for measurement of the sauter mean diameters from image analysis. Actual FBSDs (data) were obtained from froth phase images with bubble numbers of 87, 129, 234,276 and 345 respectively in 5 froth segments with height 0-2, 2-4cm, 4-6, 6-8 and 8-10.5 cm. A probability density of FBSD was found by processing the data for each froth height class. The discretized FBSDs (experimental data) from 5 froth segments are displayed in Figure 5.4a and 5.4b.

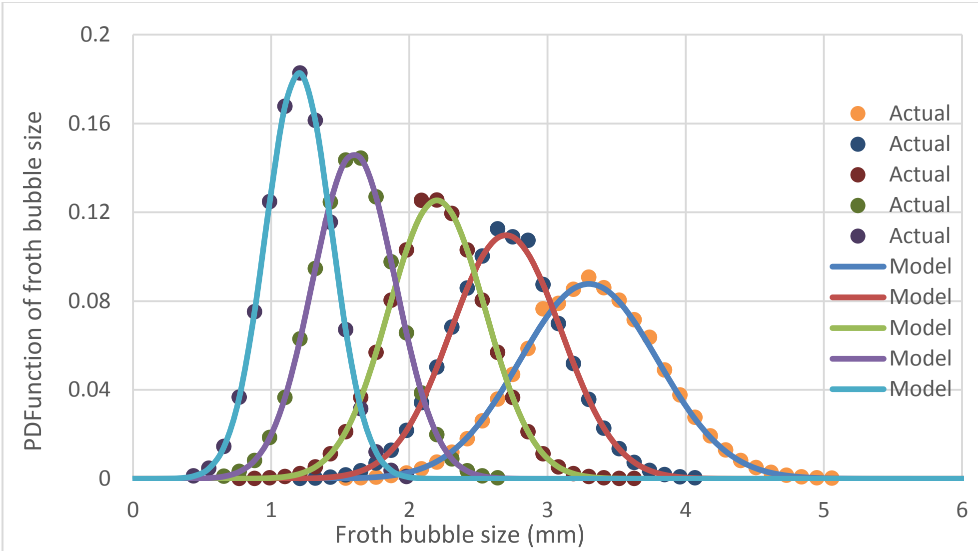

(a)

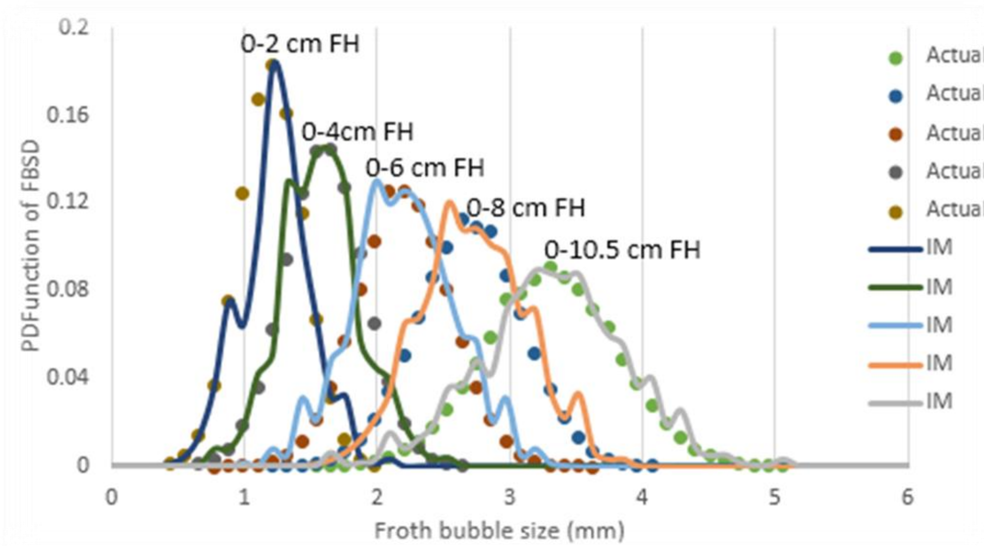

(b)

Figure 5.4: Estimation of FBSD from measured IIDD as function of froth heights FH, (a) Comparison of model predicted FBSD and actual (FBSD data) using photographic method (b) Comparison between the Inversion matrix technique (IM) and the model-predicted FBSD.

The actual FBSDs (data) measured by the photographic method in each froth segment were also measured as IIDDs using Wits-BubbleSizer (conductivity probe).. The experimental IIDDs were also discretized by dividing the IIDDs by the total number of IIDs. The present model was applied to invert the FBSD from the measured IIDD in each froth height segment. Segmentation of the froth into 2 cm high segments and determining experimental measured IIDD for each segment as follows

$$p\ L_j \ = \frac{Number\ of\ IIDs\ within\ size\ class\ L_j\ measured\ in\ a\ froth\ height\ segment}{Total\ number\ of\ IIDs\ measured\ in\ a\ froth\ height\ segment} \qquad 5.1$$

Figure 5.5 show the point plots of the experimental measured IIDDs of the ten drops per each segment above the pulp froth interface. A normal distribution was employed to predict the FBSD in each froth height segment. Uniform class size of 0.11 mm with total interval of 0-10 mm was corresponding to the type of data available from FBSD-IIDD measurements. The experimental IIDDs were discretized by dividing with regard to total number of froth bubbles or IIDs, as was important to facilitate comparison with the model-predicted IIDDs. Two parameters values, average and standard deviation were consider to predict the FBSDs. The FBSD in each froth segment is shown in Figure 5.4a was found by matching the discretized model-predicted IIDD to the measured IIDD data using the drop of the probe. Figure 5.5a and 5.5b show the comparison between the probability density and cumulative distribution functions of experimental and model-predicted IIDDs.

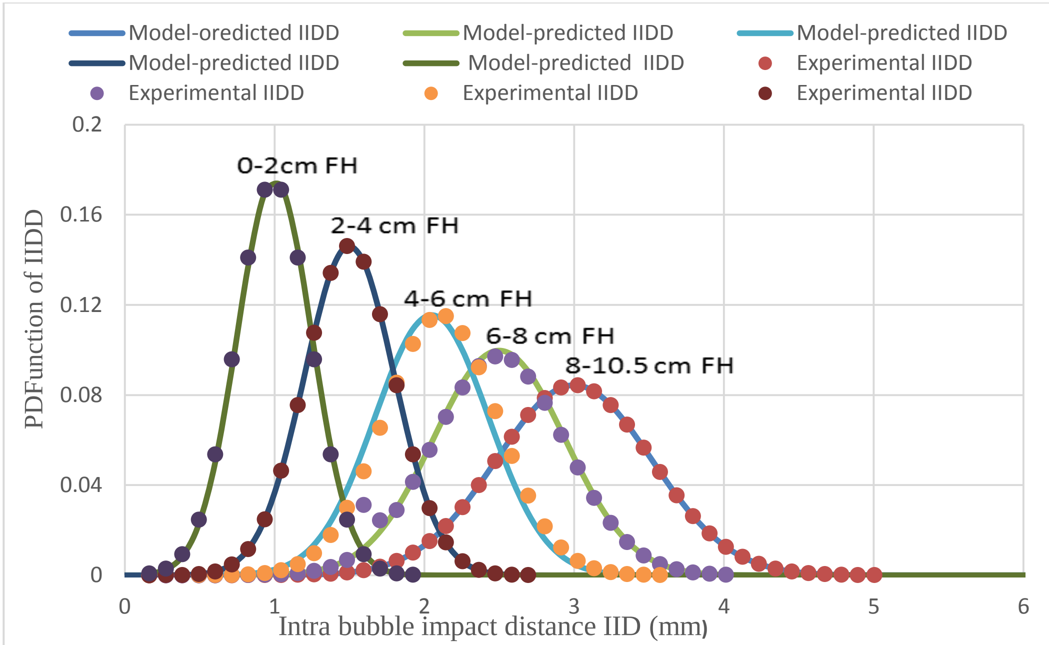

(a)

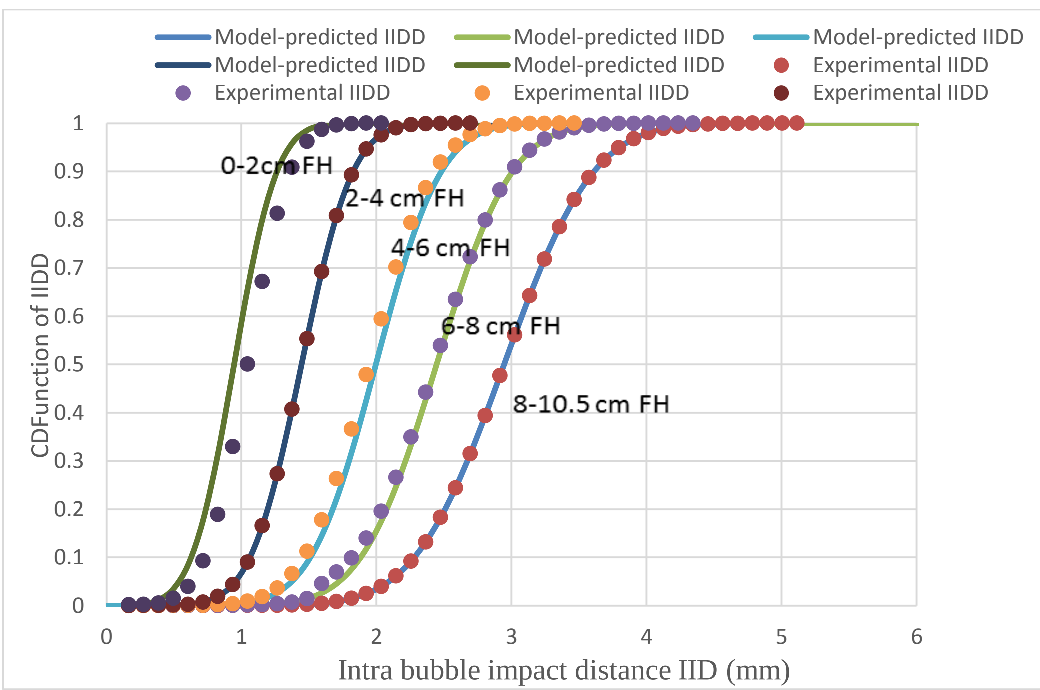

(b)

Figure 5.5: Comparison between model-predicted IIDDs with experimental measured IIDDs as a function of froth height segments FHS in the froth, respectively, (a) PDF of IIDD and (b) CFD of IIDD.

The optimal model parameters μ, δ in the 5 froth segments are respectively, 1.21 and 0.24; 1.65 and 0.301; 2.2 and 0.351; 2.75 and 0.401; 3.3 and 0.501 were with the sum square error SSE values 0.12, 0.23, 0.26, 0.46 and 0.53 in each froth height respectively from pulp-froth interface. As can be observed from the Figure 5.5a and 5.5b, there is a sufficient fit between the model-predicted IIDDs and the experimental measured IIDDs in all ranges of sizes. The comparison between the actual FBSD measured experimentally as a function of froth height and the discretized model FBSD using the model are displayed in Figure 5.4a. As may be observed in Figure, the model precisely predicts the actual FBSD data using just the IIDD information. Comparison of the results from the actual FBSD and inversion matrix technique is shown in Figure 5.4b. It is observed from the figure, the retrieved FBSDs obtained with inversion matrix technique, are in reasonable agreement with the measured actual FBSD data. Figure 5.4a and 5.4b also show that froth bubble size distribution increases with increasing froth height.

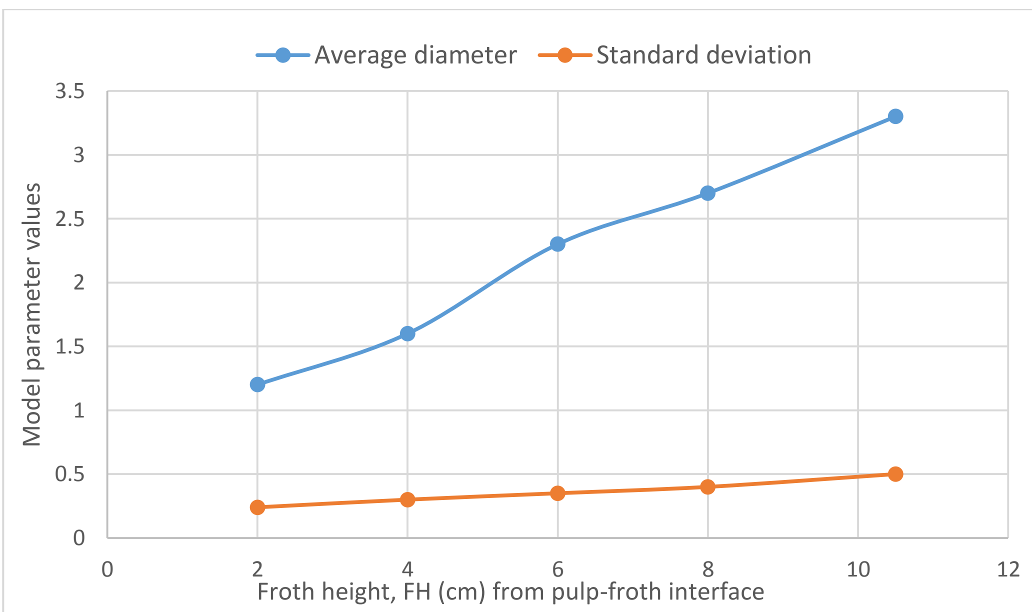

Figure 5.6: Model parameters as a function of froth height

Figure 5.6 shows that model parameters average diameter and standard deviation of FBSD increase with increase in froth height above the pulp-froth interface, which proves that froth bubble coalescence happens at point to point of froth height. The average has a strong dependency on froth height.

5.3.3 Estimation of froth bubble size distribution as a function of frother dosage in Mintek pilot plant rougher cell.

Secondly the model was applied to experimental data obtained with different frother dosages in Mintek pilot plant rougher cell. In this experiment, froth bubble images were not taken in the Mintek pilot plant rougher cell, due to absence of a transparent reactor wall. Only froth bubble size measurements by drop of the probe (Wits Bubble-sizer) were performed. This was used to test the suitability of IIDD size distribution models, using IID data from real flotation froth. Two parameter normal distribution function was considered to model the FBSD as function of frother dosages. The values of the two parameters for predicting the FBSD were determined by matching the discretized model-predicted IIDD to the discretized experimental measured IIDD obtained with each frother dosage. The model parameters, average and standard deviation were accepted where the sum square error SSE value are closest to zero. With different frother concentrations 3, 6 and 12 ppm of MIBC, optimized fitting model parameters μ, δ were respectively, 4.52 and 0.912; 3.55 and 0.651; 2.61 and 0.453 were found to give the SSE values 0.64; 0.54 and 0.24 corresponding to the match between the discretized experimental measured and discretized model IIDDs as shown in Figure 5.8a and 5.8b.

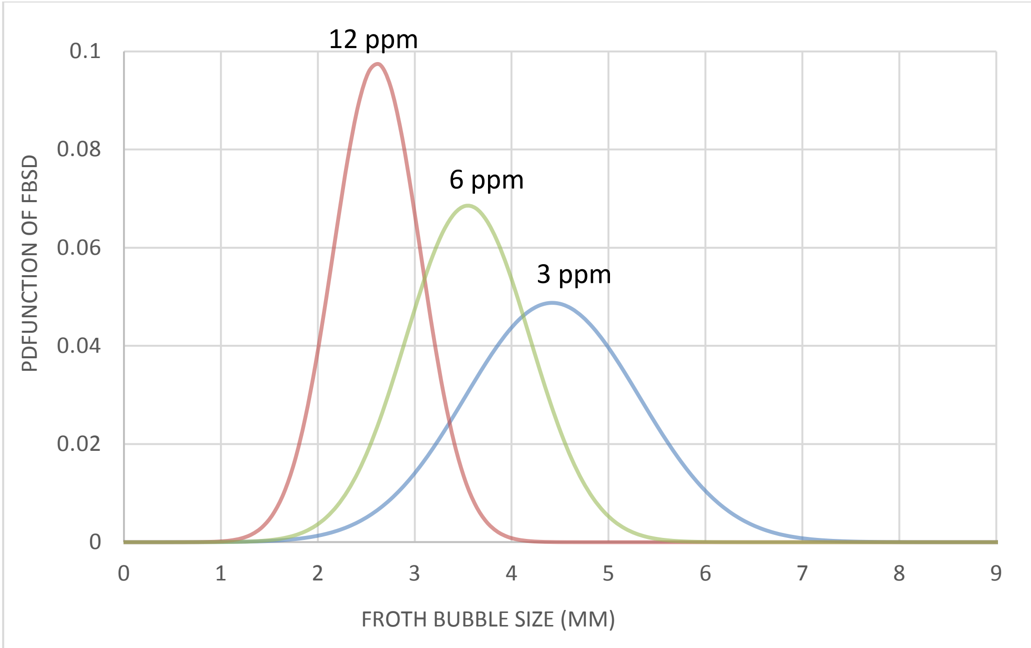

(a)

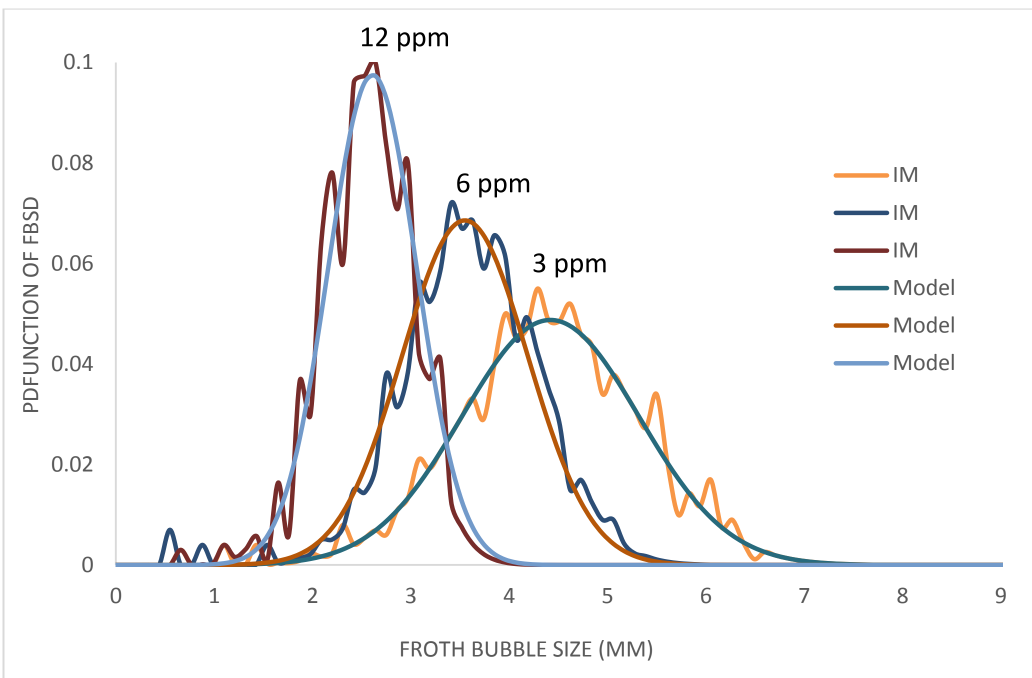

(b)

Figure 5.7: (a) Estimation of FBSD from measured IIDD as function of frother dosages (MIBC), 3; 6 and 12 ppm (b) Comparison of the Inversion matrix technique (IM) with the model-predicted FBSD.

From the figures, model-predicted IIDDs agree well with the experimental IIDDs in all range of sizes as clearly observed in Figures. A comparison between the present model FBSD obtained using least square regression LSR and inversion matrix technique are shown in Figure 5.7b. As can be seen from Figure, the FBSD obtained with LSR is in agreement with FBSD found through inversion matrix technique. Figure 5.7a shows that, froth bubble size increases with decrease in frother dosages.

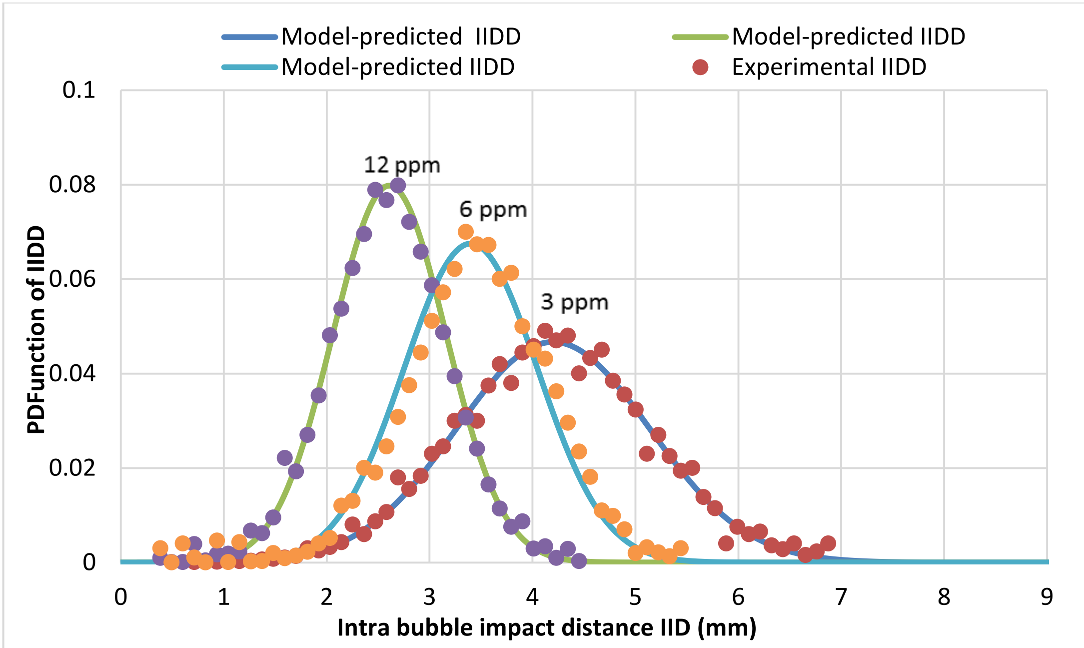

(a)

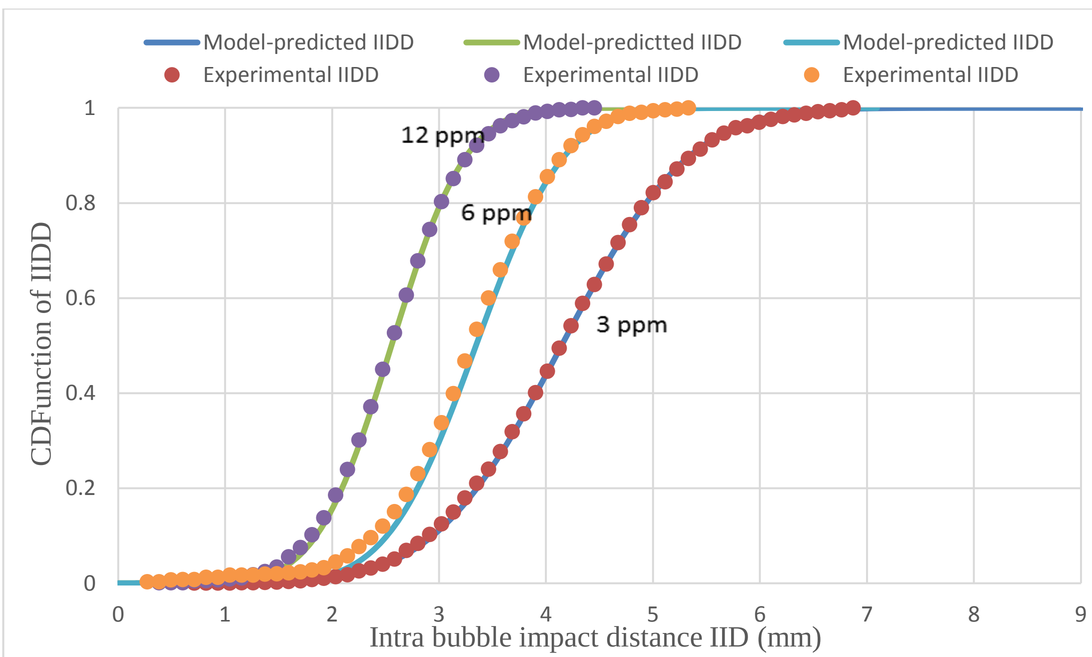

(b)

Figure 5.8: Comparison between model-calculated IIDDs with experimental measured IIDDs as a function of frother dosages 3; 6; and 12 ppm (MIBC), respectively, (a) PDF of IIDD and (b) CFD of IIDD.

The averages and standard deviations obtained for three frother dosages are presented in Figure 5.9. With increasing in frother dosages, the model parameters FBSDs decrease. The model parameters are strongly affected by the frother dosage.

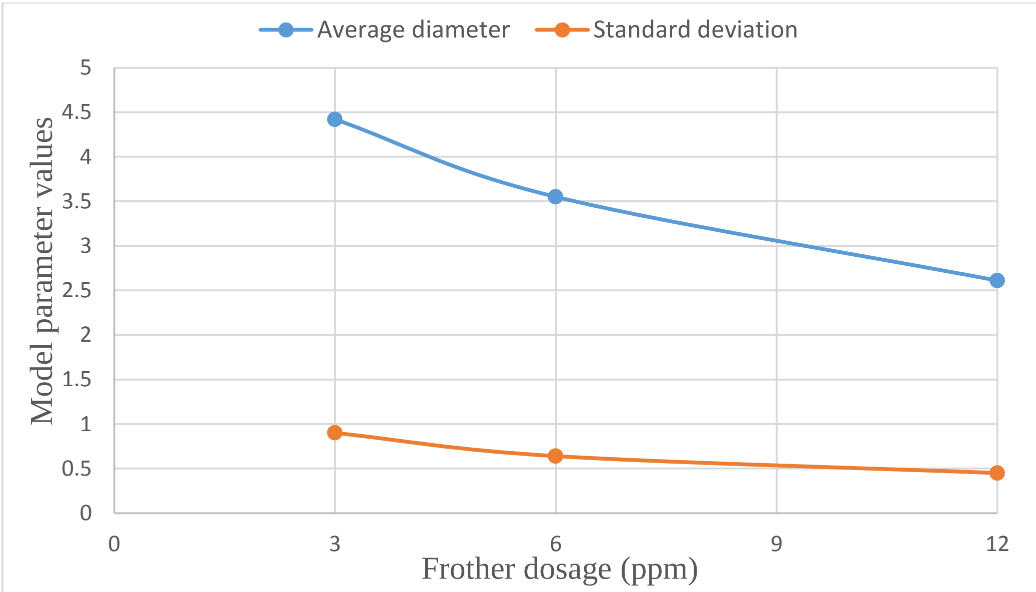

Figure 5.9: Model parameters as a function of frother concentration (MIBC).

5.3.4 Estimation of froth bubble size distribution as a function of superficial gas velocity in transparent Wits lab flotation cell

The validity of the present model was tested firstly in a system of froth height of 10.5 cm with two different superficial gas velocities Jg=0.33 cm/s and Jg=0.75 cm/s. A two parameters (average and standard deviation) normal distribution was used to model FBSDs as a function of superficial gas velocity. The froth bubble size distributions FBSDs for the current case were found by fitting the discretized model IIDDs with the discretized IIDD measured using Wits BubbleSizer such that the SSE values are closer to zero. The SSE values for this case were found to be 0.23 and 0.39 and the corresponding comparison between the discretized model IIDD and the discretized drop of the probe measured IIDD are shown in Figure 5.11a and 5.11b, respectively probability density and cumulative distribution functions. Each minimized SSE value provides the average μ and standard deviationδ, 2.86 and 0.42 with 0.33 c/s and 3.3 and 0.56 with 0.75 cm/s.

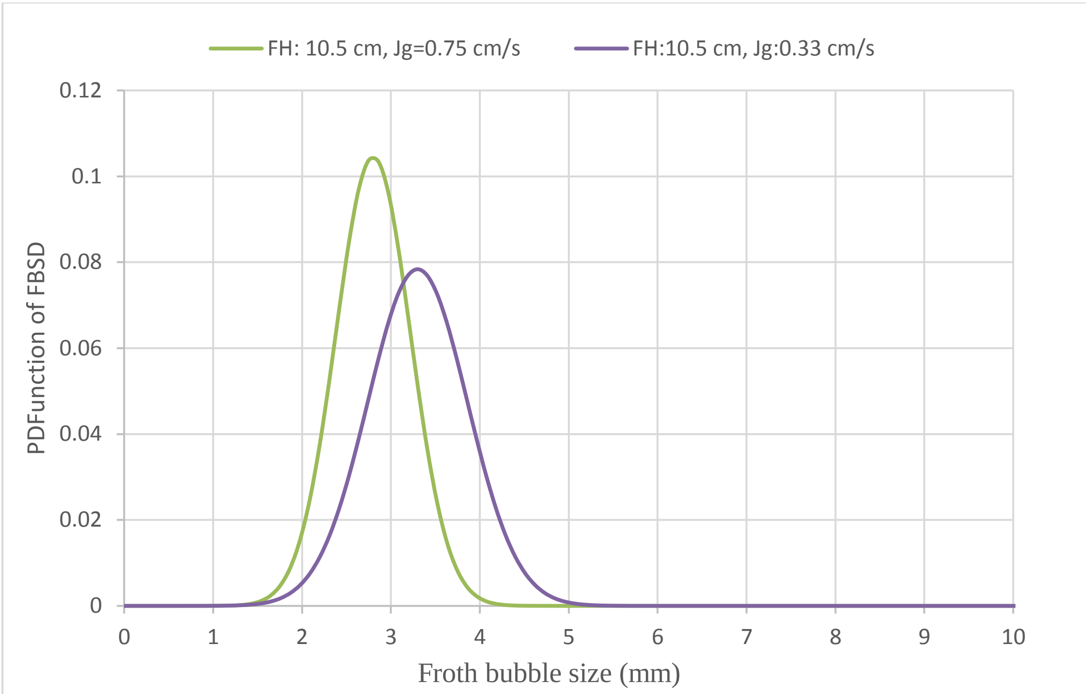

Figure 5.10: Estimation of FBSD from measured IIDDs as a function of superficial gas velocities 0.33 and 0.75 cm/s.

In Figure 5.11a and 5.11b, the model-predicted IIDDs do not deviate from the experimental IIDDs at small, medium and larger sizes. The PDF and CDF of the model-predicted IIDDs seem to be the same as experimental IIDDs. Hence, model predicted IIDDs can be regarded to be equivalent to experimental IIDDs. In other hand, the model-predicted IIDDs seem to be in agreement with the experimental IIDDs. However, we can conclude that the agreement is reasonable. Nonetheless, the present model still be a significant estimation of froth bubble size distribution FBSD. It is also observed that froth bubble size decreases with increasing in superficial gas velocity.

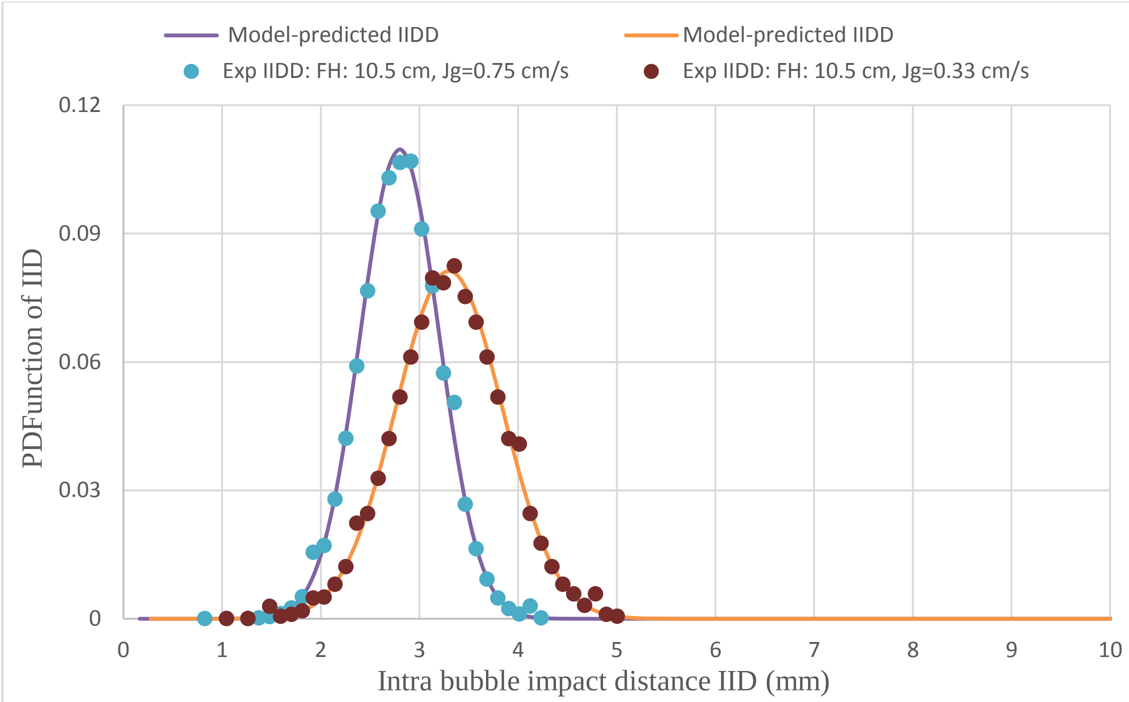

(a)

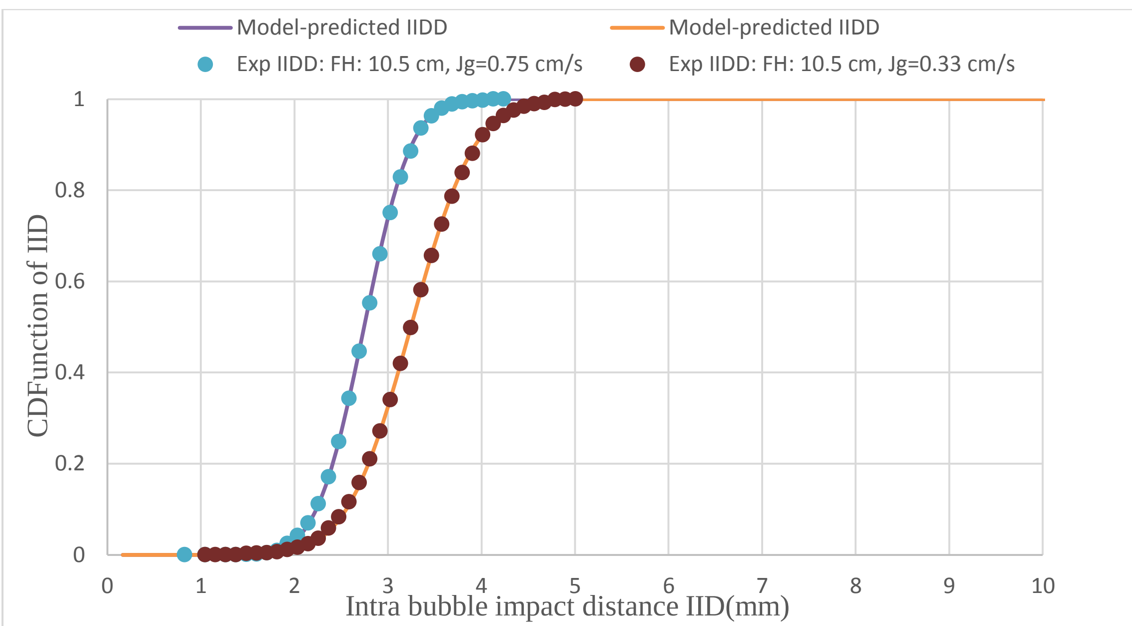

(b)

Figure 5.11: Comparison between model-calculated IIDDs with experimental measured IIDDs as a function of diverse experimental flotation conditions, respectively, (a) PDF and (b) CFD.

The validation of this current model is secondly tested against another system of froth height of 17 cm with two different superficial gas velocities Jg= 0.33 and 0.75 cm/s. A two parameter normal distribution was used to model the FBSD as a function of superficial gas velocity. The parameter values, average and standard deviation were found by fitting the discretized model calculated IIDDs with the experimental discretized IIDDs measured using Wits-BubbleSizer. A SSE value of 0.34 and 0.83 were obtained for the match which offer optimized model parameters average μ and standard deviation δ, respectively 3.8 and 0.74; 4.4 and 0.9.

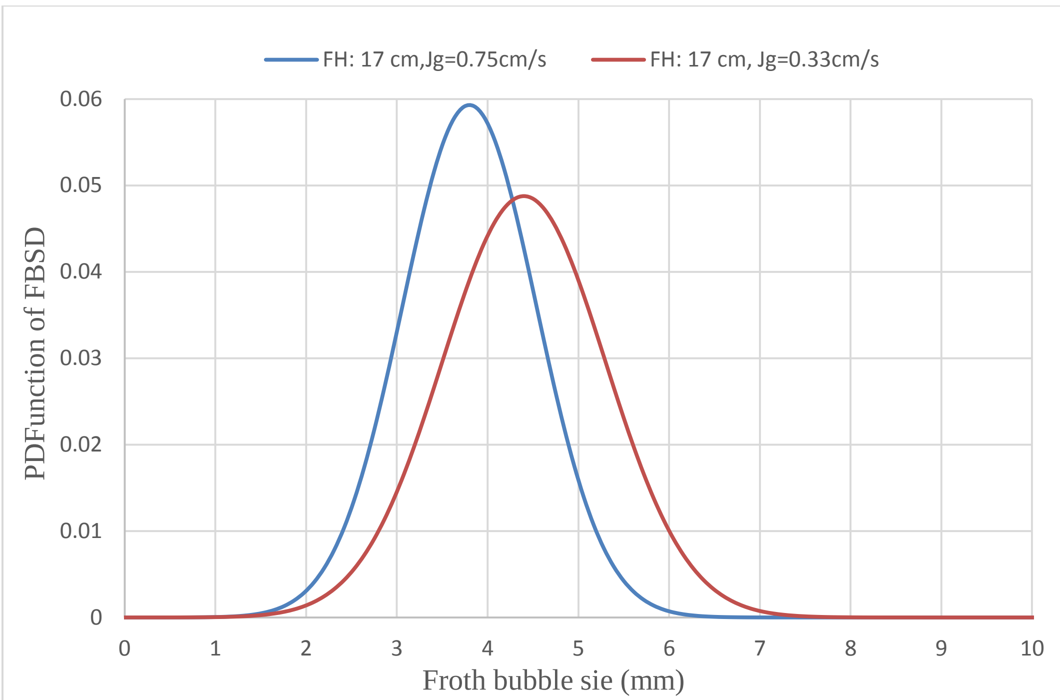

Figure 5.12: Estimation of FBSD from measured IIDD as function of superficial gas velocities 0.33 and 0.75 cm/s with froth height 17 cm.

The comparison between the discretized experimental measured IIDDs using drop of the probe and the discretized model-predicted IIDDs are shown in Figure 5.13a and 5.13b. As can be seen from these Figures, no large discrepancies are observed from the small to large sizes. The model-predicted IIDDs agree well with the experimental IIDDs. The average and standard deviation are also strongly affected by superficial gas velocity. The model was seen to adequately predict the FBSD in comparing between both the experimental and model-predicted IIDDs. The increase in superficial gas velocity increases froth bubble size distribution as shown in Figure 5.12.

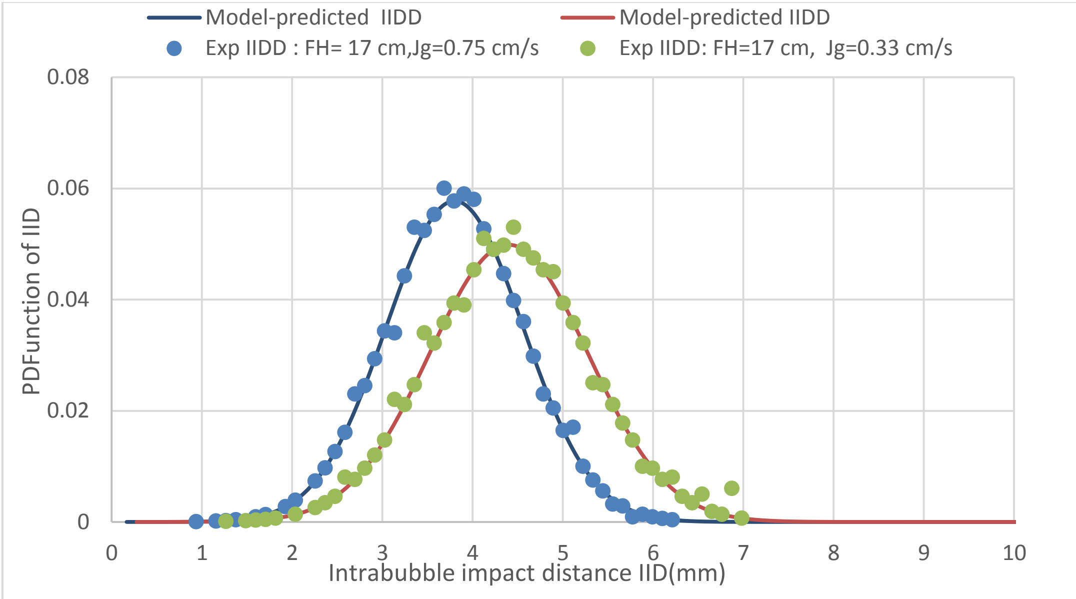

(a)

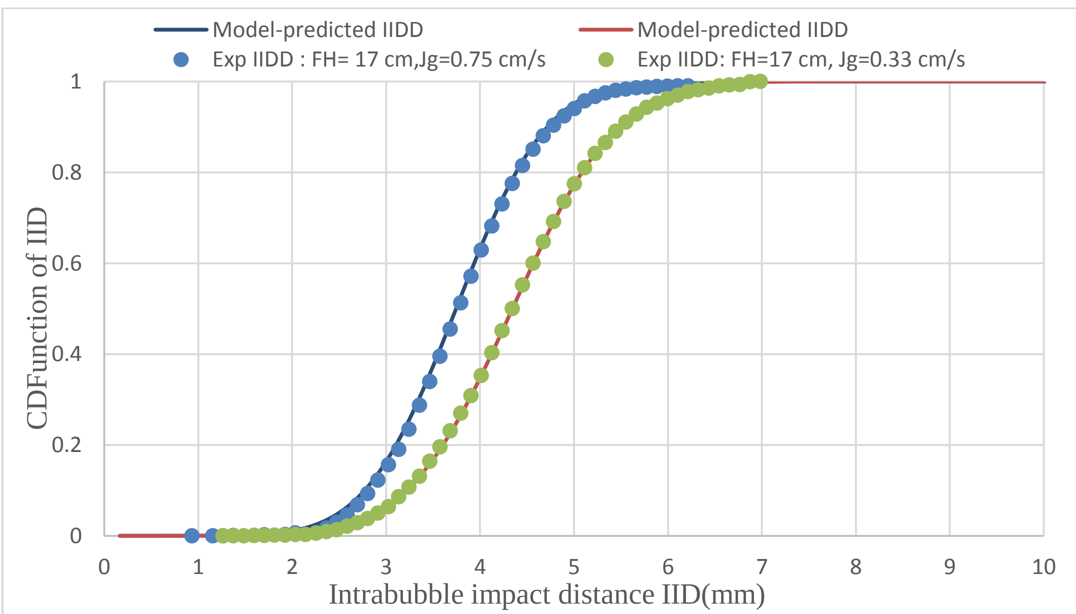

(b)

Figure 5.13: Comparison between model-calculated IIDDs with experimental measured IIDDs as a function of diverse experimental flotation conditions, respectively, (a) PDF and (b) CFD.

5.3: Conclusions

The model developed in this work was applied on IIDD experimentally measured data in Wits lab cell and Mintek pilot as fuction of froth height, frother dosage and superficial gas velocity. Estimates of froth bubble size distributions AFBSD are obtained in each case, wherein the model-predicted IIDDs accuratetly fit the experimental IIDDs. The estimates of actual FBSD and actual froth bubble size distribution AFBS data established a better agreement. The Wits-BubbleSizer can be compared to conventional photographic method.

Chapter 6

Conclusions and Recommendations

6.1 Introduction

Reattachment of desired mineral particles can take place in the froth phase if there is availability of bubble surface area, which results in mineral upgrading. The detachment of valuable particles in froth phase can be due to coalescence which leads to an inefficient flotation performance. The efficiency of flotation performance could be improved by the extra insight provided by robust measurement of froth bubble size distribution. However, no relevant method to measure bubble size in froth phase was available until Bhondayi and Moys, 2014 developed one. This is called the Wits Bubble-sizer. The Wits BubbleSizer does not measure the actual size of froth bubbles directly; it measures chord lengths per bubble and this data needs to be analysed to get an estimate of the bubble size distribution. It addresses estimating froth bubble size by providing a stereological application to estimate actual froth phase bubble sizes. In addition, stereological application allows the measurement of actual froth bubble size distribution as a function of froth height, frother concentration and superficial gas velocity. Work was done in a Wits laboratory cell and Mintek pilot environment. Overall conclusions and recommendations from this thesis are summarized in this Chapter.

6.2 Conclusions and Recommendations

Chapter 4 of this thesis is dedicated to the development of model to estimate actual froth phase bubble size distributions. This model provides valuable information on how bubble coalescence changes as a function of key parameters, height above the pulp-froth interface, frother concentration and superficial gas velocity. Estimates of froth bubble size distribution from the model can be used to control froth bubble coalescence. The model consists of simple application of a stereological method using a Normal distribution with two normal parameters (mean and standard deviation) and allows an estimation of froth bubble size distribution FBSD. The model-predicted IIDD was fitted to the experimentally measured IIDDs.Thjis was tested with and without solids, under various flotation conditions. Results reported in Chapter 5 provided confidence to conclude that a stereological application can be used to estimate froth bubble size distribution which is comparable to the photographic technique. The model was first validated for a system of flotation with variable froth height in Wits lab cell. The model was seen to accurately predict the FBSD when compared to actual FBSD data measured by conventional photographic method, wherein the model-predicted IIDDs were accurately fitted to experimental measured IIDDs. The model was used then evaluated for a system of flotation condition with variable frother dosage in the Mintek pilot plant rougher cell. The model was seen to accurately predict the FBSD when compared to actual FBSD data measured by conventional photographic method, wherein the model-predicted IIDDs were accurately fitted to experimental measured IIDDs. The model was then evaluated for a system of flotation condition with variable frother dosage in the Mintek pilot plant rougher cell. The model was seen to predict the FBSD, wherein the IIDDs were reasonably predicted compared to experimental IIDD. The matrix inversion technique (IM) was also seen to estimate the FBSD. The model validity was then tested for various systems of flotation conditions with variables superficial gas velocity and froth depth. The model was seen to estimate the FBSD for these cases.

Effects of froth height, frother concentration and superficial gas velocity on froth bubble size were tested. Results indicated that FBS increases with increasing froth height above the pulp surface. The superficial gas velocity decreases froth bubble size as superficial gas velocity was changed from 0.33 cm/s to 0.75 cm/s. Frother concentration from 3 ppm to 12 ppm resulted in a decrease in froth bubble size.

There are numerous possible extensions to the work presented in this thesis. They are addressed in the following sections,

- The froth bubble size distribution model developed in this present work is valid in the presence of spherical froth bubbles. The study on the irregular shape of froth bubbles is recommended.

- The Wits Bubble-sizer can be tested in an industrial flotation cell. The challenge here is to measure the industrial froth bubble size directly by a photographic method. This will be explored in this coming year.

References

Ahmed, N., and Jameson, G.J., 1985. The effect of bubble size on the rate of flotation of fine particles. Int. J. of Miner.Proc. 14, 195-215.

Aldrich, C., Feng, D., 2000. The effect of frothers on bubble size distributions in flotation pulp phases and surface frothers. Minerals Engineering 13, 1049-1057.

Alexander, D., Franzidis, J.-P., Manlapig, E., 2003. Froth recovery measurement in plant scale flotation cells. Minerals Engineering 16, 1197–1203.

Ata, S., Ahmed, N., Jameson, G.J., 2003. A study of bubble coalescence in flotation froths. Int. J. Miner. Process. 72, 255–266.

Ata, S., Ahmed, N., Jameson, G.J., 2003. A study of bubble coalescence in flotation froths. Int. J. Miner. Process. 72, 255–266.

Ata,S., 2012. Phenomena in the froth phase of flotation — A review. Int J. Miner. Process., (102–103) 1–12.

Atkinson C.M., Clark, N.N., 1988. Amplitude reduction and phase lag in fluidized-bed pressure measurements. Chemical Engineering Science, 1547-1557.

Aveyard, R., Binks, B.P., Fletcher, P.D.I., Peck, T.G., Rutherford, C.E., 1994. Aspects of aqueous foam stability in the presence of hydrocarbon oils and solid particles. Adv. Colloid Interface Sci. 48, 93-120.

Bhondayi, C., Moys, H.M., 2014. Measurement of a proxy for froth bubble sizes as a function of froth depth in flotation machines Part 1. Theoretical development and testing of a new technique. Int. J. Min. Proc., 130, 8-19

Brown, D.E., Pitt, K., 1972. Drop size distribution of stirred non-coalescence liquid-liquid system. Chemical Eng. Sc., 27(3), 577-583.

Buchholz, R., Schugerl, K., 1979. Bubble column bioreactors. European Journal of Applied Microbiology and biotechnology. 6(4), 301-313.

Bulatovic, S.M., 2007. Handbook of flotation reagents: chemistry, theory and practice: volume 1: Flotation of sulfide ores.

Cilliers, J.J., Sadr-Kazemi, N., 1997. An image processing algorithm for measurement of flotation froth bubble size and shape distributions. Minerals Engineering, 10(10):1075 – 1083.

Cutting G.W., Devenish, M.A., 1975. Steady-state model of froth flotation. Proceedings of the AIME Annual Meeting, New York.

Cutting, G.W., Barber, S.P., Newton, S., 1986. Effects of froth structure and mobility on the performance and simulation of continuously operated flotation cells. Int. J. Miner. Process.16: 43-61

Cutting, G.W., Watson, D., Whitehead, A., Barber, S.P., 1981. Froth structure in continuous flotation cells: relation to the prediction of plant performance from laboratory data using process models. Int. J. Miner. Process. 7 (4), 347–369.

Dahlke, C., Gomez, J.A., Finch, J.A., 2005. Operating range of a flotation cell determined from gas holdup vs. gas rate. Minerals Engineering. 18(9), 977-980.

Deglon, D., Egya-Mensah, D., Franzidis, J.P., 2000. Review of hydrodynamics and gas dispersion in flotation cells on South African platinum concentrators. Minerals Engineering 13(3), 235-244.

Dippenaar, A., 1982. The destabilization of froth by solids. I. The mechanism of film rupture. Int. J. Miner. Process. 9 (1), 1–14.

Dobby, G.S., Finch, J.A., 1986. Particle collection in columns-Gas rate and bubble size effects. Can. Metal. Quart.25, 9-13.

Drzymala, J. 1994.Characterization of materials by Hallimond tube flotation. Part 2: maximum size of floating particles and contact angle. Int. J. Miner. Process. 42: 153–167.

Falutsu, M., Dobby, G.S., 1992. Froth performance in commercial sized flotation columns. Minerals Engineering 5 (10– 12), 1207–1223.

Finch, J.A., Gomez, C.O., Hardie, C., Leichtle, G., Filipone, R., Leroux, D., 1999. Bubble surface area flux: A parameter to characterize flotation cells. In Proc. Of the 31 st Annual Operator's Conference of the Canadian Mineral Processors, 200-209.

Forbes, G., 2007. Texture and bubble size measurements for modelling concentrate grade in flotation froth systems. PhD thesis. University of Cape Town, South Africa.

Fuerstenau M.C., Jameson G.J., Yoon, R.H., 2007. Froth flotation: A century of innovation.

Gorain, B. K., Franzidis, J. P. and Manlapig, E. V. 1995. Studies on impeller type, impeller speed and air flow rate in an industrial scale flotation cell. Part 1. Effect of bubble size distribution. Miner. Eng., 8(6): 615–635.

Gorain, B. K., Franzidis, J. P. and Manlapig, E. V. 1997. Studies on impeller type, impeller speed and air flow rate in an industrial scale flotation cell. Part 4. Effect of bubble area flux on flotation performance. *Miner. Eng.*, 10, 367-379.

Grau, R., Laskowski, J.S., Heiskanen, K., 2005. Effect of Frothers on Bubble Size, Int. J. Mineral Processing 76, 225-233.

Grau, R.A., Heiskanen, K., 2002. Visual technique for measuring bubble size in flotation machines. Minerals Engineering 15, 504-513.

Guillermo, R.B., Martin, G.S., Jhon, H.P., Benedict, H., 2006. The bubblesize distribution in wheat dough. Food Research International, 39(10), 1058-1066.

Hernandez-Aguilar, J.R., Finch, J.A., Gomez, C.O., 2002. A technique for the direct measurement of bubble size distributions in industrial flotation cells. Proceedings 34th Annual Meeting of the Canadian Mineral Processors.

Jillavenkatesa, A.; Dapkunas, S. J.; Lum, L.-S., 2001. Particle size characterization. NIST Special Pub.1, 960.

King, R.P., 2001. Modelling and Simulation of mineral Processing Systems, Butterworth Heinemann, pp 290.

Klassen, V.I., Mokrousov, V.A., 1963. An Introduction to the Theory of Flotation. Butterworth, London.

Kramer, A, .Gaulocher, S, Martins, M, Leal Filho, L.S., 2012. Surface tension measurement for optimization of flotation control. Procedia Engineering 46, 111-118.

Laskowski, J.S., Tlhone, T., Williams P., Ding, K., 2003. Fundamental properties of the polyoxypropylene alkyl ether flotation frothers. International Journal of Mineral Processing 72 (1-4), 289-299.

Li, D., FitzPatrick, J., Slattery, K,. 1990. Rate of collection of particles by flotation. Ind. Eng. Chem. Res 29, 955-967.

Liu, J.J., MacGregor, J.F., Duchesne, C., Bartolacci, G., 2005. Flotation froth monitoring using multiresolution multivariate imageanalysis. Min. Eng., 18, 65-76.

Liu, W.; Clark, N. N., 1995. Relationships between distributions of chord lengths and distributions of bubble sizes including their statistical parameters. Int. J. Multiphase Flow 21, 1073.

Liu, W.; Clark, N. N.; Karamavruc, A. I., 1996. General method for the transformation of chord-length data to a local bubble-size distribution. AIChE J. 42, 2713.

Luttrell, G.H., Yoon, R.H., (1992). A hydrodynamic model for bubble-particle attachment", J. Colloid Interf. Sci., 154(1), 129-137.

Matsuura, A.; Fan, L.-S., 1984. Distribution of bubble properties in a gas-liquid-solid fluidized bed. AIChE J. 30, 894.

Moys, M.H. and Finch, J.A., 1988. Development in the control of flotation columns. Int. J. Min. Proc., 265-268.

Moys, M.H., 1979. A study of processes occurring in flotation froths. PhD thesis. University of Natal, South Africa

National Research Council (U.S.) (Ed.). 2002. Evolutionary and Revolutionary Technologies for Mining. Washington, D.C: National Academy Press.

Neethling, S.J., Cilliers, J.J., 2003. Modelling flotation froths. International Journal of Mineral Processing 72 (1–4), 267–287.

Nesset, J.A., Hermandez-Aguilar, J.R., Acuna, C., Gomez, C.O., Finch, J.A., 2006. Some gas dispersion characteristics of mechanical flotation machines. Minerals Engineering, 19, 809-815.

Preuss M., Butt, H.G., 1999. Direct measurement of forces between particles and bubbles. International Journal of Mineral Processing, 56(1–4), 99-115.

Pugh, R.J., 1996. Foaming, foam films, antifoaming and defoaming. Adv. Colloid Interface Sci. 64, 67–142.

Rodrigues, R., Rubio, J., 2003. New basis for measuring the size distribution of bubbles. Minerals Engineering, 16, 757-765.

Ross, V.E., 1990. Interpretation of froth data to study the detachment of floating particles in flotation froths. Minerals Engineering 3 (5) 525-531.

Santana, D.; Macias-Machin, V., 2000. Local bubble-size distribution in fluidized beds. AIChE J., 46, 1340.

Seaman, D.R., Manlapig, E.V., Franzidis, J.P., 2006. Selective transport of attached particles across the pulp-froth interface. Minerals Engineering 19 841-851.

Seungwoo P., 2015. Modeling of bubble coursing in froth phase from first principals. PhD thesis, Virginia Polytechnic Institute and State University. USA.

Shama, A., Ruckenstein, E., 1987. Stability, critical thickness, and the time of rupture thinning foam and emulsion films. Langmuir. 3(5), 760-768.

Subrahmanyam, T.V., Forsberg, E., 1988. Froth stability, particle entrainment and drainage in flotation — a review. Int. J. Miner. Process. 23 (1–2), 33–53.

Sung, J.S., Burgess, J.M., 1987. A laser-based method for bubble parameter measurement in two-dimensional fluidised beds. Powder Technology, 49(2), 165-175.

Schwarz, S., 2014. The relation between froth recovery and froth stability structure. PhD Thesis, University of South Australia.

Syvitski, J. P. M., 2007. Principles, methods and application of particle size analysis; Cambridge University Press: New York.

Tucker, J.P., Deglon. D.A., Franzidis, J.P., Harris, M.C., O;Connor, C.T., 1994. An evaluation of a direct method of bubble size distribution measurement in a laboratory batch flotation cell. Minerals Engineering 7 (5-6) 667-680.

Vera, M., Franzidis, J.-P., Manlapig, E., 1999. Simultaneous determination of collection zone rate constant and froth zone recovery in a mechanical flotation environment. Minerals Engineering 12 (10), 1163– 1176.

Watson, D. and Grainger-Allen, T.J.N., 1974. Study of froth flotation using a steady state technique. Trans.Soc.Min.Eng.AIME, 256: 242-247.

Weimeng H., 2014. Flotation circuit optimisation and design. Thesis.

Xu, M., Finch, J.A., Uribe-Salas, A., 1991. Maximum gas and bubble surface rates in flotation columns. International Journal of Mineral Processing, 32(3–4), 233-250.

Yang, G. Q.; Du, B.; Fan, L.-S., 2007. Bubble formation and dynamics in gas-liquid-solid fluidization - A review. Chem. Eng. Sci. 62, 2.

Yianatos, J.B., Finch, J.A., Laplante, A.R., 1986. Holdup profile and bubble size distribution of flotation column froths. Canadian Metallurgical Quarterly 25 (1), 23– 29.

Yianatos, J.B., Finch, J.A., Laplante, A.R., 1988. Selectivity in column flotation froths. Int.J. Miner. Process. 23 (3–4), 279–292.

Yoon RH, Lutterell, G.H., 1986. The Effect of Bubble Size on Fine Coal Flotation. J. Coal Preparation, 2 (3).

Yoon, R.-H. 2000. The role of hydrodynamic and surface forces in bubble-particle interaction. *Inter. J. Miner. Proces.*, 58: 128–143.

Young, P., 1982. Flotation machines. Mineralogical Magazine 145 (1), 35–39.

Wang W., Bergholm F., Yang B., 2003. Froth delineation based on image classification. Miner. Eng. 16: 1183-1192.

Appendix

Estimation of froth bubble size distribution from IIDD measured

A1: Predcition of FBSD

Model FBSD $p(D_i) = \frac{1}{\sigma\sqrt{2\pi}} e^{-(D_i-\mu)^2/2\delta^2}$

Model FBSD parametrs: μ and δ

IIDD predicted $p(L)_{pred} = \sum_{j=1}^{M} p(L_j|D)\, p(D)\, \Delta D$

$$Min-SSE(\mu,\delta) = \sum_{j}^{N} \left(p(L_j)_{pred} - p(L_j)_{meas} \right)^2$$

A2: Spread sheet for FBSD estimated from IIDD measured

Two parameter normal distribution

Average	**Standard Deviation**
3.8	0.74

Bubble size (mm)	p(D), Model FBSD
0.11	1.11425E-07
0.22	2.36426E-07
0.33	4.90694E-07
0.44	9.96162E-07
0.55	1.97812E-06
0.66	3.8422E-06
0.77	7.29979E-06
0.88	1.35658E-05
0.99	2.46594E-05
1.1	4.38454E-05

1.21	7.62551E-05
1.32	0.000129723
1.43	0.000215859
1.54	0.000351338
1.65	0.000559352
1.76	0.000871061
1.87	0.001326831
1.98	0.001976906
2.09	0.002881113
2.2	0.004107126
2.31	0.0057269
2.42	0.007810966
2.53	0.010420619
2.64	0.013598342
2.75	0.017357295
2.86	0.021671141
2.97	0.026465808
3.08	0.031614927
3.19	0.036940508
3.3	0.042219898
3.41	0.047199255
3.52	0.051612721
3.63	0.055205458
3.74	0.057757837
3.85	0.05910762
3.96	0.059167017
4.07	0.057932133
4.18	0.055483392
4.29	0.051976873
4.4	0.047627845
4.51	0.042688939
4.62	0.037426002
4.73	0.032094836
4.84	0.026921579
4.95	0.022088669
5.06	0.017727284
5.17	0.013916131
5.28	0.010685589
5.39	0.008025684
5.5	0.005896161
5.61	0.004237017
5.72	0.002978206
5.83	0.002047637

5.94	0.001377066
6.05	0.000905858
6.16	0.000582867
6.27	0.000366845
6.38	0.000225839
6.49	0.000135994
6.6	8.01018E-05
6.71	4.61498E-05
6.82	2.60076E-05
6.93	1.43362E-05
7.04	7.7299E-06
7.15	4.07676E-06
7.26	2.10311E-06
7.37	1.06123E-06
7.48	5.23797E-07
7.59	2.52883E-07
7.7	1.19421E-07
7.81	5.51625E-08
7.92	2.49236E-08
8.03	1.10149E-08
8.14	4.76165E-09
8.25	2.01343E-09
8.36	8.32756E-10
8.47	3.36902E-10
8.58	1.33319E-10
8.69	5.16043E-11
8.8	1.95381E-11
8.91	7.23573E-12
9.02	2.62112E-12
9.13	9.2874E-13
9.24	3.21888E-13
9.35	1.09124E-13
9.46	3.61858E-14
9.57	1.17371E-14
9.68	3.7238E-15
9.79	1.15562E-15
9.9	3.50792E-16
10.01	1.04156E-16

IIDD (mm)	IIDD predicted $p(L)_p$	IIDD measured $p(L)_m$	Error	Squared error
0.165	1.23057E-06	1.21832E-06	1.22483E-08	1.50021E-16
0.275	2.3829E-06	2.35918E-06	2.37178E-08	5.62532E-16
0.385	4.51862E-06	4.47365E-06	4.49753E-08	2.02278E-15
0.495	8.3909E-06	8.30738E-06	8.35173E-08	6.97514E-15
0.605	1.52585E-05	1.51067E-05	1.51873E-07	2.30655E-14
0.715	2.71719E-05	2.69014E-05	2.7045E-07	7.31434E-14
0.825	4.73836E-05	4.6912E-05	4.71624E-07	2.22429E-13
0.935	8.09168E-05	8.01114E-05	8.05391E-07	6.48655E-13
1.045	0.000135317	0.00013397	1.34685E-06	1.81401E-12
1.155	0.000221598	0.000219393	2.20564E-06	4.86485E-12
1.265	0.000355372	0.000351835	3.53713E-06	1.25113E-11
1.375	0.000558088	0.000552533	5.55483E-06	3.08561E-11
1.485	0.000858269	0.000849726	8.54263E-06	7.29765E-11
1.595	0.001292548	0.001279683	1.28651E-05	1.65512E-10
1.705	0.001906215	0.001887242	1.89732E-05	3.59981E-10
1.815	0.002752955	0.002725554	2.7401E-05	7.50817E-10
1.925	0.003893395	0.003854643	3.87522E-05	1.50173E-09
2.035	0.005392124	0.005338455	5.36695E-05	2.88042E-09
2.145	0.007312963	0.007240175	7.27883E-05	5.29813E-09
2.255	0.009712454	0.009615783	9.66712E-05	9.34532E-09
2.365	0.01263184	0.012506111	0.000125729	1.58077E-08
2.475	0.016088158	0.015928027	0.000160131	2.56418E-08
2.585	0.020065413	0.022771074	-0.00270566	7.3206E-06
2.695	0.024507103	0.024263175	0.000243927	5.95004E-08
2.805	0.02931149	0.029019743	0.000291747	8.51161E-08
2.915	0.034330956	0.033989249	0.000341707	1.16764E-07
3.025	0.039376397	0.033661587	0.00571481	3.26591E-05
3.135	0.044227065	0.043786859	0.000440206	1.93781E-07
3.245	0.048645463	0.052472474	-0.00382701	1.4646E-05
3.355	0.05239606	0.051874545	0.000521515	2.71978E-07
3.465	0.055265868	0.054715789	0.000550079	3.02587E-07
3.575	0.057084398	0.059402801	-0.0023184	5.37499E-06
3.685	0.057740419	0.05716571	0.000574709	3.3029E-07
3.795	0.057193215	0.058412754	-0.00121954	1.48728E-06
3.905	0.055476769	0.057422707	-0.00194594	3.78668E-06
4.015	0.052696271	0.052171768	0.000524503	2.75103E-07
4.125	0.049017446	0.048529559	0.000487886	2.38033E-07

4.235	0.044650214	0.044205796	0.000444418	1.97507E-07
4.345	0.039828915	0.039432485	0.00039643	1.57157E-07
4.455	0.034791687	0.03564168	-0.00084999	7.22488E-07
4.565	0.029761483	0.029465258	0.000296226	8.77496E-08
4.675	0.024930772	0.022771074	0.002159698	4.6643E-06
4.785	0.020451207	0.02024765	0.000203557	4.14356E-08
4.895	0.01642874	0.016265219	0.000163521	2.6739E-08
5.005	0.012923841	0.016830794	-0.00390695	1.52643E-05
5.115	0.009955912	0.009856818	9.90944E-05	9.8197E-09
5.225	0.007510564	0.007435809	7.47551E-05	5.58832E-09
5.335	0.00554838	0.005493155	5.52248E-05	3.04978E-09
5.445	0.004013856	0.003168149	0.000845707	7.1522E-07
5.555	0.002843541	0.002815239	2.83027E-05	8.01042E-10
5.665	0.001972692	0.000891042	0.00108165	1.16997E-06
5.775	0.001340174	0.001326835	1.33392E-05	1.77934E-10
5.885	0.00089159	0.000882716	8.87428E-06	7.87529E-11
5.995	0.00058086	0.000575078	5.78148E-06	3.34255E-11
6.105	0.000370578	0.000366889	3.68848E-06	1.36049E-11
			SSE	**9.0276E-05**

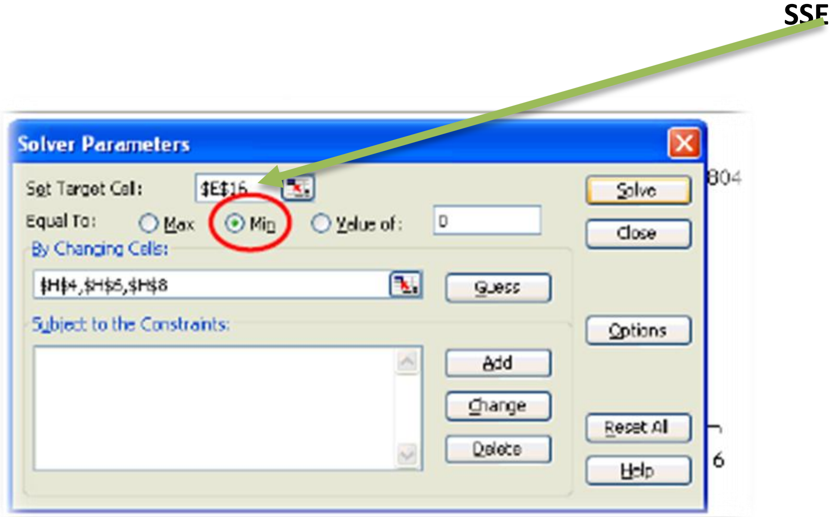

Figure A1 : Solver parameters panel for minmizing sum squared error SSE